UNIVERSITY OF CALIFORNIA, SAN DIEGO

Ventricular Dyskinesis Induced Loss of Contractile Function and Epicardial Inflammation: Role of Cellular Adhesion Molecules

A dissertation submitted in partial satisfaction

of the requirements for the degree

Doctor of Philosophy

in

Molecular Pathology

by

Katrina Go Yamazaki

Committee in charge:

Professor Francisco Villarreal, Chair
Professor Ju Chen, Co-Chair
Professor James Covell
Professor Paul Insel
Professor David Roth

2009

The Dissertation of Katrina Go Yamazaki is approved, and it is acceptable in quality and form for publication on microfilm and electronically:

Co-Chair

Chair

University of California, San Diego

2009

DEDICATION

I dedicate my thesis to my husband, Masato Yamazaki, who gave me unwavering support and love along each and every step of the way. Thank you Masato for the constant reassurance of my capabilities, for patience with my stress, frustration, and work schedule, and most importantly for always being there with open arms. You always gave me strength to keep going and provided the light at the end of the tunnel. I love you more than anything, and I cannot thank you enough for believing in me.

TABLE OF CONTENTS

LIST OF FIGURES AND TABLES

ACKNOWLEDGEMENTS

I would like to thank the many people that have made important impacts on my work. I would like to thank my mentor Dr. Francisco Villarreal for his commitment to and support of my research, education, and future goals and opportunities, and guidance in shaping me into the scientist I am today. I would also like to thank Dr. James Covell for all his guidance, training, support, discussing my research with me, and answering endless questions. Additional thanks go to committee members Dr. Ju Chen, Dr. Paul Insel, and Dr. David Roth for all their guidance and advice. Thank you to Dr. Jeffrey Omens for his helpful comments, suggestions, and advice on m project. Thanks to Ben Coppola, Elliot Howard, and Irina Ellrott for help with the animal studies and data analysis. A big thanks to Dr. Sang-Hyun Ihm for his help with the echocardiography studies. A special thanks to Maraliz Barraza-Hidalgo, and Maria Rivas for all their help with my studies and being the best support system. For all their moral support, I want to thank my Mom, Dad, Kristina Go, and the entire Yamazaki family. Thank you Monique Chambers for being a great friend and study buddy. Finally, thank you Masato for all your love, support, and understanding throughout graduate school.

Chapter 5, in part has been submitted for publication of the material as it may appear in *Circulation* 2009, Yamazaki KG, Covell JW, Ihm SH, Roth D, Villarreal FJ. The dissertation author was the primary investigator and author in this manuscript.

Chapter 6, in part has been submitted for publication of the material as it may appear in *Circulation* 2009, Yamazaki KG, Covell JW, Ihm SH, Roth D, Villarreal FJ. The dissertation author was the primary investigator and author in this manuscript.

CURRICULUM VITAE

Education:

2005-2009	University of California, San Diego Department of Molecular Pathology Ph.D. in Molecular Pathology Thesis advisor: Dr. Francisco Villarreal
2001-2004	University of California, San Diego Revelle College B.S. in Animal Physiology and Neuroscience

Research Fellowships and Awards

2007-2009	Cardiology Training Grant Fellow
2005-2007	San Diego Fellowship Award
2002	Howard Hughes Award

Publications

1. Garcia RA, Brown KL, Pavelec RS, **Go KV**, Covell JW, Villarreal FJ. Abnormal cardiac wall motion and early matrix metalloproteinase activity. *Am J Physiol,* 288:H1080-H1087, 2005

2. Garcia RA, Pantazatos DP, Gessner CR, **Go KV**, Woods VL Jr, Villarreal FJ. Molecular interactions between matrilysin and the matrix metalloproteinase inhibitor doxycycline investigated by deuterium exchange mass spectrometry. *Mol Pharmacol*, 67:1128-36, 2005

3. Garcia RA, **Go KV**, Villarreal FJ. Effects of timed administration of doxycycline or methylprednisolone on post-myocardial infarction inflammation and left ventricular remodeling in the rat heart. *Moll Cell Biochem*, 300:159-69, 2007

4. **Go K**, Horikawa Y, Garcia R, Villarreal FJ. Fluorescent method for detection of cleaved collagens using O-phthaldialdehyde (OPA). *J Biochem Biophys Methods*, 70:878-82, 2008

5. Ashikaga H, Coppola BA, **Yamazaki KG**, Villarreal FJ, Omens JH, Covell JW. Changes in myocardial tissue volume during the cardiac cycle: implications for transmural blood flow and cardiac structure. *Am J Physiol*, 295(2):H610-8,2008

6. **Yamazaki KG**, Romero-Perez D, Barraza-Hidalgo M, Cruz M, Rivas M, Cortez-Gomez B, Ceballos G, Villarreal F. Short-and long-term effects of (-)-epicatechin on myocardial ischemia-reperfusion injury. *Am J Physiol*, 295(2):H761-7, 2008.

7. Romero-Perez D, Fricovsky E, **Yamazaki KG,** Griffin M, Barraza-Hidalgo M, Dillmann W, Villarreal, F. Cardiac uptake of minocycline and mechanisms for in vivo cardioprotection. *J Am Coll Cardiol*, 52(13):1086-94, 2008.

8. Villarreal FJ, Epperson SA, Ramirez-Sanchez I, **Yamazaki KG**, Brunton LL. Regulation of cardiac fibroblast collagen synthesis by adenosine: Roles for Epac and PI3K. *Am J Physiol Cell Physiol*. 2009 Mar 11.

9. **Yamazaki KG,** Brunton L, Villarreal F. Effects of AGE and angiotensin AT_1 receptors on cardiac fibroblast function and associated signaling pathways. Submitted Am J Phys, 2009.

10. **Yamazaki KG**, Barraza-Hidalgo M, Rivas M, Witham E, Zambon A, Rajendran P, Ceballos G, Villarreal F. Amelioration of myocardial infarct size-left ventricular remodeling following permanent coronary occlusion by cocoa flavanols. Submitted Am J Phys, 2009

11. **Yamazaki KG**, Ihm S, Covell JW, Roth D, Villarreal FJ. Ventricular dyskinesis induced loss of contractile function and epicardial inflammation: Role of cellular adhesion molecules. Submitted Circ, 2009.

Abstracts and Poster Presentations

1. K. Yamazaki. Ventricular dyssynchrony induced loss of function and epicardial inflammation: Role of cellular adhesion molecules. AMPAC 2009. April 2009. Merida, Mexico.

2. K. Yamazaki. Epicardial ventricular pacing induces a local inflammatory response in the outer layers of the left ventricle. Experimental Biology 2008. April 2008. San Diego, CA.

3. K. Yamazaki. Cardioprotective effects of epicatechin in ischemia-reperfusion (IR) injury. Experimental Biology 2008. April 2008. San Diego, CA.

4. K. Yamazaki. Effects of AGE on cardiac fibroblast (CF) signaling pathways and functions. Experimental Biology 2008. April 2008. San Diego, CA.

5. K. Yamazaki. Effects of (-)-epicatechin on myocardial ischemia and reperfusion injury. American Heart Association Young Investigators Conference. Sept. 2007. La Jolla, CA.

6. K. Yamazaki. Effects of AGE on cardiac fibroblast (CF) signaling pathways and finctions. American Heart Association Young Investigators Conference. Sept. 2007. La Jolla, CA.

7. K. Go. Abnormal cardiac wall motion and early matrix metalloproteinase activity. Howard Hughes Undergraduate Research Symposium. Aug. 2003. La Jolla, CA.

ABSTRACT OF DISSERTATION

Ventricular Dyskinesis Induced Loss of Contractile Function and Epicardial Inflammation: Role of Cellular Adhesion Molecules

by

Katrina Go Yamazaki

Doctor of Philosophy in Molecular Pathology

University of California, San Diego, 2009

Professor Francisco Villarreal, Chair

Professor Ju Chen, Co-Chair

Ventricular dyssynchrony as induced by epicardial ventricular pacing has been the subject of investigations for many years. It has been shown that dyssynchrony is characterized by regions of wall thinning and hypertrophy and is detrimental to left ventricular (LV) function. The mechanisms that trigger these changes are unknown. Therefore, I hypothesize that dyskinesis, secondary to LV pacing, triggers local inflammation, reactive oxygen species (ROS) generation, and matrix metalloproteinase (MMP) activation. To gain further mechanistic insight, I wish to determine two-dimensional and/or three-dimensional changes in myocardial function and inflammation induced by myocardial dyskinesis. I also want to determine if inflammatory responses induced by dyskinesis are mediated by a vascular event via cellular adhesion molecules (CAM).

A canine model was used to determine regional and transmural differences in LV contractile function and inflammatory responses associated with local early contraction. Results investigating regional differences in LV contractile function demonstrate that local dyskinesis creates regions of early shortening at the pace site, as well as in areas immediately surrounding the pace site. Evaluation of inflammatory responses showed increases in neutrophil infiltration and in MMP-9 in regions undergoing early shortening. Results investigating the transmural differences in LV function indicate that 4 h of LV pacing results in a 30% local loss of endocardial wall thickening ($p<0.01$). Transmural assessment of neutrophil infiltration showed a significant 5 fold increase in myeloperoxidase (MPO) activity in the epicardium vs midwall/endocardium. Matrix metalloproteinase-9 (MMP- 9) activity increased ~2

fold in the epicardium and reactive oxygen species (ROS) generation ~2.5 fold. In a mouse model, results showed a significant 3 fold increase in MPO, 2 fold increase in ROS, and 3 fold increase in MMP-9 activity in dyskinetic hearts vs controls. In canine subjects anesthetized with propofol, a known cardioprotectant, and ICAM-1 or p-selectin null mice, dyskinesis failed to increase neutrophil infiltration or MMP-9 activity in early activated dyskinetic LV. Early activated dyskinetic regions demonstrate depressed endocardial contractile function, and epicardial inflammation. The upregulation of CAM appears necessary to trigger these inflammatory responses, thus suggesting inflammation is induced by vascular events. Over the long-term, these events may contribute to adverse changes in LV structure/function.

Chapter 1. General Introduction

1.1 Scope of the problem: Prevalence of CHF and ventricular dyssynchrony

Each year, 300,000 patients die from congestive heart failure (CHF) in the United States.[1] Recently, ventricular dyssynchrony is being recognized as an important risk factor in the pathophysiology of CHF. The incidence of ventricular dyssynchrony in the general population is 1-3% at the age of 65, however, this number significantly rises to 30% in patients with heart failure.[2] Left bundle branch block (LBBB) is the most common type of electrical conduction abnormality found in CHF patients. It can also occur in non-heart failure.[3] In both CHF and non-CHF patients, LBBB is associated with a high risk for mortality and morbidity.[4]

In the population of CHF patients that suffer from ventricular dyssynchrony, a large percentage can be subjected to what is termed cardiac resynchronization therapy (CRT). Patients that respond favorably to CRT demonstrate significant improvements in quality of life, diastolic and systolic function, overall cardiovascular morbidity and mortality, and reverse ventricular remodeling.[5, 6] Thus, this therapeutic tool has led, in those patients that respond, to true measurable benefits that are difficult to attain in those that suffer from CHF.

1.2 Normal Electrical Conduction System

Ventricular contraction is normally regulated by a highly coordinated electrical conduction system. Electrical signals originate in the sinus node and propagate through the atria to the atrioventricular (AV) node and into the His-Purkinje system.[7]

The bundle of His transfers the signal from the AV node to the left and right bundle branches. The bundles travel under the endocardium down the walls of the septum, and at the apex divide unto the Purkinje system.[8] The role of the specialized His-Purkinje system is to conduct the electrical impulse through the ventricular myocardium so that a highly efficient and synchronized activation (less than 40 ms) of the ventricles occurs.[9] Thus, the pacemaker and electrical conduction system is designed to maximize the efficacy of ventricular function. It follows that a perturbation of this system can have noticeable detrimental effects.

1.3 Ventricular Dyssynchrony

1.3.1 Genesis of Ventricular Dyssynchrony

An interruption of the conduction system can create regions of early and late activation (separated by as much as ~120 ms), leading to ventricular dyssynchrony.[2]There are three ways for the heart to become dyssynchronous: (1) dysfunction of the sinus node; (2) abnormal conduction of the atrioventricular node; and (3) infranodal conduction abnormalities, such as a LBBB.[1]

1.3.1.1 Right Bundle Branch Block

During a right bundle branch block (RBBB), the right ventricle is not directly activated by impulses traveling through the right bundle branch.[10] The left bundle branch, however, still normally activates the left ventricle, and these impulses travel through the LV's myocardium to the right ventricle and activate the RV. Three types of RBBB have been identified

in electrophysiological studies. Proximal, or central, RBBB occurs when a conduction block is present just distal to the bundle of His in the superior aspect of the right bundle branch. This generally occurs when the proximal bundle is injured during surgery.[10] Another type of RBBB occurs when the impulse is interrupted between the proximal and distal aspects of the right bundle branch; this type is most commonly observed after surgical division of the moderator band. Distal RBBB is observed when distal ramifications of the right bundle branch are disrupted during right ventriculotomy or resection of muscle bundles in the RV outflow tract.[10]

1.3.1.2 Left Bundle Branch Block

As opposed to RBBB, LBBB has been associated with heart diseases caused by high blood pressure, coronary artery disease, aortic valve stenosis, and cardiomyopathy.[11] As mentioned above, LBBB is the most common type of electrical conduction abnormality found in the heart. There are various types of LBBB. The first is a complete LBBB. This occurs when the electrical impulse is delayed or interrupted in either the main left bundle branch or in both anterior and posterior fascicles. In complete LBBB, conduction from the right ventricle passes first to the interventricular septum, then to the anterior and posterior portions of the left ventricle, and finally to the lateral free wall. Incomplete LBBB occurs in 2 forms, left anterior hemiblock or left posterior hemiblock. In these cases, transmission of the electrical impulse proceeds normally along the

main left bundle branch, but it is blocked or delayed in the anterior or posterior fascicle. This blockage results in delayed activation of its respective portion of the left ventricle.[12] Some risk factors for developing a LBBB are: (1) anatomic malformations and abnormalities in the conduction system; (2) hypertension; and (3) scar tissue after a myocardial infarction or surgery.[13]

1.3.2 Ventricular Dyssynchrony: Effects on LV Function

Dyssynchrony of regional contraction as induced experimentally by epicardial ventricular pacing has been the subject of investigations using increasingly sophisticated techniques for nearly a century.[14-19] In early activated areas, (i.e. at the epicardially paced site), the typical deformation pattern observed during a cardiac cycle includes early myofiber shortening followed by lengthening and subsequent shortening during systole. Late activated areas (i.e. the opposite wall) exhibit early lengthening (termed pre-stretch) followed by late shortening.[17-19] This dyssynchronous contraction pattern wastes work due to stretching of the unactivated region while the activated region contracts, thereby reducing optimal contractile efficiency.

Ventricular dyssynchrony secondary to ventricular pacing causes up to a threefold difference in myofiber work within the LV wall.[16] This difference is large enough to consider differences in myocardial work as an important determinant for abnormalities in perfusion, metabolism, structure and pump

function in the setting of ventricular dyssynchrony.[20] Ventricular dyssynchrony significantly depresses the maximal and minimal rate of increase in LV pressure, stroke volume, and stroke work.[2] Patients with ventricular dyssynchrony have larger LV end-systolic and end-diastolic volumes and smaller LV ejection fraction compared to normal patients.[21]The presence of mitral valve regurgitation has also been associated with Ventricular dyssynchrony. This is mainly due to early contraction of the septum and anterior LV wall in early systole, which results in prestretch of the still-quiescent lateral wall, delaying intracavitary pressure rise and mitral valve closure.[1]

1.3.3 Ventricular Dyssynchrony: Effects of myocardial perfusion and blood flow

During normal contraction of the ventricular myocardium (systole), the subendocardial coronary vessels (the vessels that enter the myocardium) are compressed due to the high intraventricular pressures. However, the epicardial coronary vessels (the vessels that run along the outer surface of the heart) remain patent. Because of this, blood flow in the subendocardium stops. As a result most myocardial perfusion occurs during heart relaxation (diastole) when the subendocardial coronary vessels are patent and under low pressure. Nevertheless, each part of the heart is adequately perfused.[22]

A study by Prinzen and Reneman indicated that timing of electrical activation is an important determinant for the distribution of fiber strain and

blood flow in the LV wall.[16] Previous investigations indicate that the direction of electromechanical activation matches and maintains a synchrony between the timing and direction of activation and blood flow.[23] At the tissue level, isovolumic intervals are associated with asynchronous movements of the subendocardial and subepicaridal regions. During LV isovolumic contraction, the subendocardial fibers that form a right-handed helix shorten, whereas the left-handed helically-oriented subepicardial fibers lengthen simultaneously. Conversely, during isovolumic relaxation, the subepicardial fibers that from the left-handed helix lengthen, and the right-handed helically-directed subendocardial fibers shorten briefly. Brief periods of ventricular dyssynchrony might represent a "flow-directing feature" of the myocardial wall mechanics that reverses the direction of blood flow. In a study investigating regional blood flow and contraction patterns during abnormal, asynchronous electrical activation of the LV, results showed that myocardial blood flow was ~20% lower in early activated regions and ~35% higher in late activated regions.[24]

1.3.4 Ventricular Dyssynchrony: Effects on LV Remodeling and Myocardial Energetics

It has been reported that induction of ventricular dyssynchrony in canine hearts leads to chronic LV remodeling.[15, 25] Using a 6 month chronic model of ventricular dyssynchrony induced by LV pacing, van Oosterhout demonstrated that early-activated LV regions became significantly thinner, whereas the late-activated region thickened significantly.[15] In a retrospective

study of 288 LBBB patients, the early activated septum was also significantly thinner than the late activated posterior wall.[26] Adomian and Beazell studied the effects of chronic (3 month) non-failing dyssynchrony on ventricular remodeling at the cellular level in dogs.[27] With the use of light microscopy, they demonstrated marked myofibers and myofibrils disarray at the base of the LV after 3 months of right ventricular (RV) apex pacing.[27] Van Oosterhout also showed that cardiomyocyte diameter was significantly larger in late activated regions than in early activated areas, whereas myocardial collagen fraction was unchanged in both areas in paced animals.[15]

It has been speculated that the non-homogenous remodeling processes in the LV wall causes regional differences in stress and/or strain, which in turn, may alter blood flow and the distribution of energy demands within the myocardial wall.[28] Indeed, studies have shown that while ventricular dyssynchrony decreases mechanical output in early activated regions, it either increases or does not change myocardial oxygen consumption. As a consequence, the efficiency of conversion of metabolic to mechanical energy becomes 20-30% lower in these regions.[2, 28] Other studies have shown that blood flow is reduced in early activated compared to late activated regions, and that the regional differences in blood flow and mechanical load match the asymmetry of hypertrophy during long term LV pacing.[9, 16, 26, 28]

1.3.5 Ventricular Dyssynchrony and molecular signaling

The pathophysiology of failing myocardium involves abnormalities in cellular signaling that can lead to chamber remodeling.[25] Studies in chronic models of ventricular dyssynchrony have shown that interventricular conduction delay worsens myocardial efficiency and leads to marked increases in wall stress heterogeneity, where wall stress is highest in late-activated myocardial regions.[25] Changes in wall stress are known to trigger chamber remodeling signals. However, in an animal model of non-failing dyssynchrony, Spragg et al found that sarcoplasmic reticulum CA^{2+}-ATPase, phospholamban, and gap junction protein connexin-43 expression were comparable to controls and that no transmural gradient existed.[29] However, in a rapid pacing heart failure model in the presence of dyssynchrony, late-activated myocardium demonstrated a 2-fold increase in phosphorylated *Erk* , a 30% decline in sarcoplasmic reticulum CA^{2+}-ATPase, an 80% reduction in phospholamban, and a 60% reduction in gap junction protein connexin-43, relative to neighboring myocardium with more severe decreases in endocardium vs. epicardium.[25, 30] Chakir et al demonstrated that in animals with six months of dyssynchronous heart failure, there was an increase in mitogen activated kinase p38, calcium-calmodulin-dependent kinase, tumor necrosis factor-α, apoptosis and pro-apoptotic pathways in high stress regions of the heart[30]. These results indicate that LV mechanical dyssynchrony superimposed with HF induces marked regional heterogeneity of protein expression at the site of greatest

hemodynamic load or stress[25], whereas dyssynchrony appears to do little to alter regional protein expression. Thus, the issue of dyssynchrony induced changes in cellular signaling awaits further investigation.

1.3.6 Cardiac Resynchronization Therapy as a means of treatment

Despite improvements in survival with the use of pharmacological treatments such as beta-blockers and ACE inhibitors, recurrent hospitalization for worsening heart failure or sudden cardiac death remains the fate of most patients with CHF.[21] Cardiac resynchronization therapy, a form of cardiac pacing, is an established and proven treatment for patients with intraventricular conduction abnormalities and CHF [6]. CRT intends to offset the underlying conduction delay with the goal of rendering contraction more homogenous[30]. CRT is the first nonpharmacological treatment to be tested in large scale clinical trials with placebo controls.[5] These clinical trials have shown CRT improves symptoms and the quality of life, while reducing morbidity and mortality in patients.[6] CRT has also been shown to reduce the intraventricular mechanical delay, and the end-systolic volume index, as well increase LV ejection fraction. In addition, CRT has been associated with significant LV reverse remodeling [6, 31]

The use of CRT in animal models of HF has also demonstrated beneficial effects of LV function and on the cellular signaling pathways in the myocardium. In an animal model of dyssynchronous heart failure, animals

underwent LBBB radioablation and either 6 weeks of dyssynchronous heart failure (DHF) or 3 weeks of DHF followed by 3 weeks of CRT. At 6 weeks, ejection fraction improved in CRT compared with DHF animals, although both groups remained in failure with similarly elevated diastolic pressures and reduced dP/dt_{max}.[30] The use of CRT normalized mitogen activated kinase p38, calcium-calmodulin-dependent kinase, and tumor necrosis factor-α levels similar to controls.[30]They also demonstrated a reduction in apoptosis and enhanced antiapoptotic signaling molecules such as phosphorylated BAD levels. These results demonstrate that CRT normalizes myocardial cellular signaling pathways. Such changes may yield important benefits from CRT that likely benefit cardiac structure/function and long-term outcomes.[30] Whereas, most studies have focused on long-term changes in heart structure/function, little is known about those that occur immediately upon ventricular dyssynchrony. These changes may precede and trigger long term consequences.

1.4 Published Study

To gain insight into early changes in heart structure/function that may be induced by ventricular dyskinesis, abnormal wall motion at a target site on the anterior lateral wall of the LV was induced by pacing atrial and ventricular sites. Changes in shortening at the LV pacing site and at a remote site at the anterior base of the LV were monitored with sonomicrometer crystals [32] Simultaneous atrial and ventricular

pacing resulted in abnormal motion at the LV pacing site, yielding early shortening and late systolic lengthening, whereas the shortening pattern at the remote site remained unaffected. In this study, we reported that short term ventricular dyssynchrony (< 4 h) as a result of LV pacing, significantly increased neutrophil infiltration (i.e. inflammation), as determined by myeloperoxidase (MPO) activity, by 2-fold at the LV paced site relative to a remote site. Increases in MPO activity correlated with significant 20-fold increase in nitrotyrosine levels, a marker for oxidative stress [32]. Furthermore, local dyskinesis yielded a sevenfold increase in global MMP activity, more specifically ~40 fold and ~100-fold increases in 92 kDa and 86 kDa MMP-9 activity, respectively. Results also demonstrated a twofold increase in collagen degradation at the pacing site compared to the remote site [32]. Altogether, these unique and novel results indicate that early activated regions demonstrate a localized inflammatory response likely mediated by neutrophil infiltration, which ultimately trigger collagen damage. These events, if expressed long term, may explain the long term remodeling observed with ventricular dyssynchrony.

1.5 Myocardial structure

1.5.1 Muscle

The myocardium consists of cardiac myocytes, which are relatively small and branched, with a single nucleus, and are rich in mitochondria.[8] Cardiac myocytes are interconnected as a network through intercalated discs. These intercalated discs provide both a structural attachment by ‘glueing’ the

myocytes together at desmosomes, and an electrical connection through gap junctions formed of pores made up of proteins called connexons.[8] As a result, the myocardium acts as a single functional unit, even though the individual cells are still separate. The gap junctions play a vital role in conduction of the electrical impulse through the myocardium.[8]

The myocytes contain actin and myosin filaments, which form the contractile apparatus, and exhibit the classical M and Z lines, and A, H, and I bands. The intercalated discs always coincide with a Z line, as it is here that the actin filaments are anchored to the cytoskeleton. At the Z lines, the sarcolemma forms tubular invaginations into the cells known as transverse (T) tubules. The sarcoplasmic reticulum (SR) runs generally in parallel with the length of the cells. Close to the T tubules the SR forms terminal cisternae that with the T tubule make up diads, an important component of excitation-contraction coupling.[8]

1.5.2 Extracellular Matrix

The organization and function of the myocardium is also highly dependent on the cardiac extracellular matrix (ECM). The ECM is a complex mixture of collagen fibrils, elastin, cells including fibroblasts and macrophages, marcomolecules such as glycoproteins, and glycosaminoglycans together with other molecules such as growth factors, cytokines, and extracellular proteases.[33] Collagen is the predominant structural component of

the ECM and has been classified in three components: epimysium, surrounding the entire muscle; endomysium, surrounding and interconnecting individual myocytes and capillaries; and perimysium, surrounding and interconnecting groups of myocytes.[34] The complex physiological role of the ECM includes connecting myocytes, aligning contractile elements, preventing overextending and disruption of myocytes, transmitting force, and providing tensile strength to prevent rupture.[33] Alterations or damage to the collagen structure from various cardiac events, such as myocardial infarction, is known to lead to adverse ventricular remodeling.

1.5.3 Vasculature

The blood vessels of the cardiovascular system are classified into arteries, resistance vessels, capillaries, venules, and veins. Blood is supplied to the heart by its own coronary circulation. The aorta branches off into two main coronary arteries. These coronary arteries branch off into smaller arteries, which supply oxygen-rich blood to the entire heart muscle. The vessels that remove the deoxygenated blood from the heart muscle are the coronary veins.[8]

The coronary arteries that run on the surface of the heart are called epicardial coronary arteries. These arteries, when healthy, are capable of autoregulation to maintain coronary blood flow at levels appropriate to the needs of the heart muscle. The coronary arteries that run deep within the myocardium are referred to as subendocardial. The coronary arteries are

classified as “end circulation”, since they represent the only source of blood supply to the myocardium: there is very little redundant blood supply, which is why blockage of these vessels can be so critical.[22]

The microvasculature comprises the smallest arterioles, and the exchange vessels, including the capillaries and the post-capillary venules. Blood enters the microcirculation via small arterioles, which then divide to give rise to sets of capillaries. The capillaries then join to postcapillary venules, which then merge to form venules.[8] Capillaries contain a large portion of the blood volume in the coronary system. In a dog, capillary volume is 4-6% of myocardial wall volume and exhibits a significant transmural gradient, increasing from epicardium to endocardium, which is primarily attributed to a transmural increase in microvessel diameter.[35] In the myocyte sheets, true capillaries are packed in densely stacked parallel arrays neighboring closely on the myocytes (~three capillaries to one myocyte by sharing a capillary among two or three myocytes) with numerous short anastomotic connections between them.[36]

1.6 Triggering of Acute Inflammation

In the setting of acute inflammation, the recruitment of neutrophils into tissue is dependent upon their ability to respond to chemoattractant molecules and the expression of cell adhesion molecules (CAM) on their surface, as well as in the vascular endothelium. During an inflammatory response, neutrophils roll onto and

attach to the endothelial walls prior to squeezing through gaps between adjacent endothelial cells (EC) to migrate into tissues following chemoattractant concentration gradients.[37] This process requires two different sets of adhesion receptors expressed on neutrophils and endothelium. Three groups of adhesion molecules are involved: selectins, integrins and the immunoglobulin (Ig) superfamily.[37] Three types of selectins are responsible for the attachment of neutrophils to the endothelium and include L-selectin, which is mostly expressed on the neutrophil, E-selectin, and P-selectin, both of which are expressed on ECs.[37] The major groups of integrins present on neutrophils are LFA-1 (CD11a/CD18), Mac-1 (CD11b/CD18), and CR3 (CD11b/CD18). Immunoglobulins include ICAM-1, ICAM-2, VCAM1 and PECAM-1 all expressed in ECs.[37]

1.6.1 Selectins

The selectin family of adhesion molecules mediates the initial trapping of neutrophils from the rapidly flowing bloodstream to the blood vessel endothelium, before their firm adhesion and diapedesis at sites of tissue injury and inflammation.[38] The selectin family consists of three closely related cell-surface molecules: L-selectin, E-selectin, and P-selectin. One important property of the selectins is that they promote leukocyte attachment and rolling at shear stresses characteristic of post-capillary venules.[39] P-selectin rapidly increases on endothelial cells after exposure to reactive oxygen, and appears to play a more important role that E-selectin in neutrophil extravasation with cardiac ischemia-

reperfusion (IR) injury.[40]

1.6.2 Integrins and Immunoglobulins

Firm adhesion of neutrophils is dependent primarily on the leukocyte β_2 (CD11/CD18) integrins and endothelial intercellular adhesion molecule-1 (ICAM-1).[40] ICAM-1 is constitutively expressed at low levels on the endothelial surface and is markedly upregulated by cytokine stimulation.[40] Recent studies have also shown cardiac myocyte ICAM-1 protein expression within 6 h of reperfusion after ischemia.[40] The rapid induction of ICAM-1 occurs in viable myocytes immediately adjacent to nonviable myocardial cells, which coincides with the region of maximal neutrophil infiltration.[40]

1.6.3 Vascular Flows and Inflammation

In the microcirculation, the concept of laminar or streamlined blood flow has existed since the nineteenth century. In this concept, the cells and the molecules of the plasma are considered to flow in a series of laminas parallel to the vessel wall[41] so that they move at approximately the same speed and in the same direction. By definition, the microvasculature system becomes pathological when cells adhere to each other or to the vessel walls.[41] This may occur when there is disruption to laminar flow leading to turbulent flow or altered patterns of flow. It has been speculated that alterations in regional myocardial perfusion associated with ventricular pacing can be associated with abnormalities of microvascular flow.[42] Smith and Kassab demonstrated that as

heart rate increases, small-vessel epicardial flow increases due to higher average arterial inflow pressure and intramyocardial vessels show a decrease in flow particularly in the LV endocardium.[43] These hemodynamic changes may potentially alter shear stress in the coronary microvasculature system and therefore lead to an inflammatory response.

The effects that mechanical forces exert on EC gene expression and protein production have gained vast attention due to its relationship with atherogenesis.[44] One of the initial events that occur with atherogenesis is the adherence of neutrophils.[44] Hemodynamic forces are known to regulate vascular wall structure/function including EC cell shape, NO and prostacycin production and EC proliferation [45-48]. Studies have shown that exposure of EC to laminar flow produces low levels of CAM expression and enhances the production of anti-adhesive factors, such as NO.[44] When EC are exposed to altered flow patterns, such as oscillatory flows, CAM expression/production significantly increases [45, 49, 50]. Emerging studies have now highlighted the importance of complex hemodynamics in modulating EC structure/function. Blood vessel ECs *in vivo* are subjected to simultaneous pulsatile shear stress and circumferential strain. In a study by Dancu et al, the effects of asynchronous circumferential strain and fluid shear stress on EC gene expression was investigated *in vitro* .[51] Results indicated that highly asynchronous mechanical force patterns could by 5 h elicit decreases in NO synthase and COX-2 gene expression while upregulating endothelin-1, thus yielding a proatherogenic profile.[51]

1.7 Neutrophils, ROS, and the heart

Neutrophils contain an abundance of membrane-bound organelles referred to as granules, which contain an array of antimicrobial proteins.[37] These granules are classified on the basis of their contents.[52] Granules that contain myeloperoxidase (MPO) are characterized as peroxidase positive, whereas peroxidase negative do not contain MPO. Peroxidase negative granules contain matrix metalloproteinase (MMP)-8 and -9, and cytochrome b_{558}. Cytchrome b_{558} plays an important role in the generation of ROS by functioning as the terminal electron carrier of NADPH oxidase.[53] Activation of the NADPH oxidase system initiates a respiratory burst characterized by increased oxygen consumption and generation of superoxide anions, which are converted to hydrogen peroxide by superoxide dismutase.[54] MPO released from the peroxidase positive granules reacts with the hydrogen peroxide to form the neutrophil specific byproduct, hypochlorous acid (HOCl) [37, 52, 53]. HOCl is a highly reactive ROS that can act to damage/destroy foreign objects and tag them for phagocytosis by macrophages.[54] Ultimately, many types of ROS can be generated by neutrophils; however, ~70% of generated ROS is HOCl.[37]

1.8 Inflammation, MMPs, and cardiac remodeling

Matrix metalloproteinases (MMPs) are a family of zinc-containing endoproteinases that share structural domains, but differ in substrate specificity, cellular sources, and inducibility.[55] MMPs share the following functional features: (1) they degrade ECM components; (2) they are secreted in a latent proform and require

activation for proteolytic activity; and (3) they contain Zn^{2+} at their active site.[56] Based on their substrate specificity and primary structure, the MMP family can be divided into interstitial collagenases, gelatinases, stromelysins and membrane type MMPs.[56] Collagenases, which include MMP-1, -8, and -13, cleave fibrillar collagens I, II, and III. The gelatinases MMP-2 and -9 can degrade a variety of ECM proteins. The cellular source of MMPs in the myocardium has been identified as myocytes, fibroblasts, and other cell types such as macrophages and neutrophils[57-60].The propeptide region contains a cysteine residue that suppresses MMP action. MMP expression and activity is regulated at the following three levels: transcription, activation of the latent pro-enzymes and inhibition by their endogenous inhibitors, the tissue inhibitors of MMPs (TIMPs).[55]

Two direct mechanisms have been proposed for MMP activation. The first involves proteinases such as plasmin, trypsin, chymase, elastase and kallikrein.[55] These proteinases cleave the propeptide domain of MMPs exposing the catalytic site yielding a lower molecular weight active product. A second mechanism of MMP activation is known as the cysteine switch activation. This process occurs when ROS modifies the cysteine residue on the conserved prodomain without cleavage of this domain.[55] Exposure to ROS, such as HOCl, will convert the sulfhydryl of cysteine to sulfinic acid exposing the catalytic site.[54] Full enzymatic activity is gained in the absence of a change in molecular weight.

The inflammatory process is tightly coupled to the induction and release of MMPs within the myocardium. Inflammatory cells, such as neutrophils, contain MMPs and other proteases (i.e. elastase) in their granules and are released upon activation. These proteases released from the granules can participate directly or indirectly (by activating MMPs) in fibrillar collagen damage.[61] There are two types of MMPs, MMP-8 and MMP-9 that are only found in neutrophils. MMP-8 is a collagenase, which can degrade fibrillar collagen yielding gelatin that is further degraded by the MMP-9. While MMP-9 is produced by a variety of cells, neutrophils produce a unique truncation variant that lacks 8 aminoterminal residues yielding an enzyme with a 91 kDa molecular weight compared to the normal 92 kDa molecular weight [58, 61, 62] Thus, MMPs participate in the inflammatory cascade and the ensuing injury events.

1.9 Objectives of Dissertation

In our initial published study, pairs of sonomicrometer crystals assessed ventricular function and inflammation was evaluated by utilizing transmural samples of myocardium. To further understand short-term functional consequences of ventricular dyssynchrony, a detailed assessment of 2D and 3D LV function over time is required (short and long-term). Similarly, in order to identify the molecular mechanism possibly involved in the development of long-term structural changes, a detailed regional and transmural assessment of inflammatory responses is required. Although ventricular dyssynchrony is known to induce adverse changes in LV

diastolic and systolic function, most of the published studies have focused on long-term changes. Thus, in this study, we have focused on the acute changes induced by ventricular dyskinesis on 2D and 3D LV function and regional and transmural distribution of inflammatory responses. By pursuing these objectives we intend to gain insight into their possible role in long term changes in structure/function. Our hypothesis is explained in detail in Figure 1.11.

To address these objectives, we examined the following aims: (1) investigate the effects of LV pacing on 2D myocardial deformation and regional myocardial inflammatory responses (discussed in Chapter 2), (2) assess the effects of local dyskinesis, secondary to LV pacing, on LV function and inflammation in the presence of propofol, a known cardioprotectant (discussed in Chapter 3), (3) examine the effects of transmural bead implantation on LV function and inflammatory responses induced by dyskinesis (discussed in Chapter 4), (4) evaluate 3D myocardial deformation and transmural distribution of dyskinesis induced inflammatory responses (discussed in Chapter 5), and (5) assess the role played by CAM (specifically, ICAM-1 and p-selectin) in the development of ventricular dyssynchrony induced inflammation (discussed in Chapter 6). A summary and discussion of the data is presented in Chapter 7.

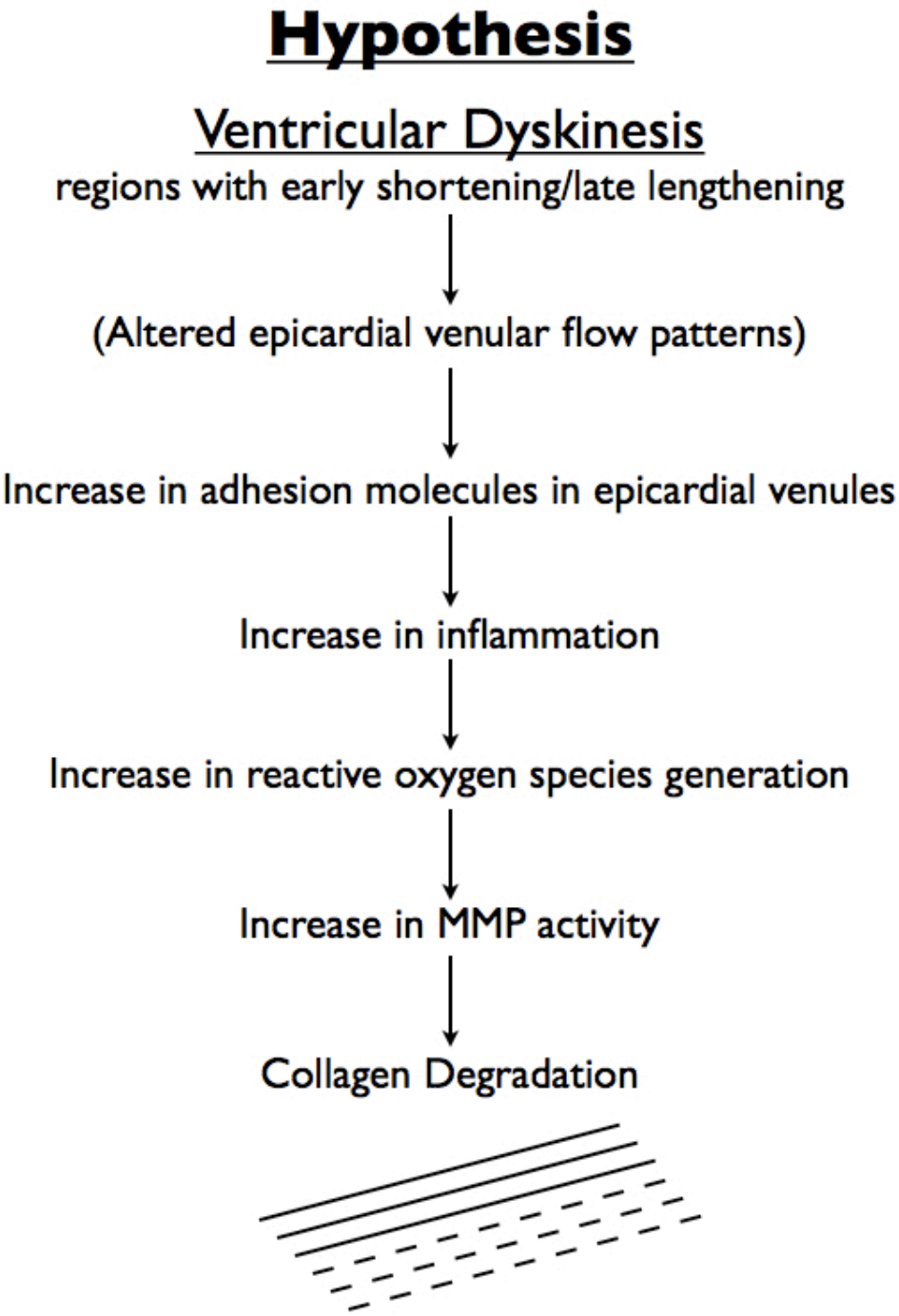

Figure 1.10.1. Flow diagram of our proposed hypothesis. We propose that heart wall abnormalities secondary to local epicardial pacing, (which are characterized by areas of early shortening), trigger local inflammation, reactive oxygen species generation, matrix metalloproteinase activation and fibrillar collagen degradation.

Chapter 2. Effects of myocardial dyskinesis on two-dimensional myocardial deformation and inflammation

2.1 Introduction

The normal electrical activation of the LV initiated from the atrium and traveling through the His-Purkinje system via the AV node, provides for almost synchronous endocardial to epicardial activation of ventricular muscle[16]. The use of epicardial ventricular pacing changes the sequence and rate of electrical activation[18], generating a heterogeneous pattern of ventricular contraction with areas of early activation-contraction and late activation-contraction known as ventricular dyssynchrony.

Data from published literature indicate that impaired electrical activation in the setting of epicardial ventricular pacing are determined by at least four myocardial properties: (1) Poor coupling of the ectopically generated impulse to the rapid conduction system due to the slow conduction through the normal myocardium, away from the pacing site, (2) Because conduction through the myocardium is up to four times slower than conduction through the Purkinje system, activation of the entire ventricular wall is more dyssynchronous than normal sinus rhythm and atrial pacing, (3) Conduction is approximately two times faster along the muscle fibers than perpendicular to them. Because fiber orientation changes by more than 90 degrees across the LV wall, and because impulses are also conducted in a transmural direction,

an abnormal and complex three-dimensional electrical activation occurs in the LV wall, and (4) Myocardial fibers in the most endocardial layer, even though not part of the Purkinje system, conduct impulses faster than the fibers in the rest of the LV wall.[7] How changes in the electrical activation of the myocardium translate into the mechanical activation sequence is important and has been the subject of investigation.

Badke et al. were the first to observe early onset and rapid shortening in early activated regions and lengthening in late activated regions.[18] As early activated muscle fibers contract rapidly with a high shortening velocity, then stretching the serially connected, as yet non-activated muscle fibers occurs. This prestretch induces an increase in contractile force of these fibers. When finally activated, these late activated fibers shorten vigorously, counteracting any further contraction of the early activated fibers.[63] Therefore, during ventricular pacing, local contraction patterns do not only differ in the onset of contraction, but also in the pattern of contraction and they vary as a function of the pacing site and distribution of electrical and mechanical events over the ventricular chambers. The mapping of epicardial deformation using various methods, such as MRI and ultrasound, has shown that the pattern of myocardial deformation gradually changes with increasing distance from the pacing site.[20, 64]. These correlate with epicardial electrical activation maps in that isochrone lines are close to each other in the vicinity of the site of pacing, and larger distances between the isochrone lines more remote from the pacing site [20, 64].

We previously reported that short term LV pacing (4 h), significantly increased

neutrophil infiltration (i.e. inflammation), as determined by myeloperoxidase (MPO) activity, at the early activated dyskinetic site relative to a remote site [32]. Increases in MPO activity correlated with significant increases in reactive oxygen species (ROS) generation, matrix metalloproteinase (MMP) activity and collagen degradation[32]. However, little is known about the mechanistic link between early myofiber contraction and late systolic stretching present locally at epicardial paced sites with the inflammatory responses seen in our study. Thus, this group of studies was intended to establish a correlation between epicardial 2D strain patterns near and around the site of early epicardial activation with the inflammatory responses. For this purpose, an epicardial bead array was placed on the free wall of the LV and 2D strain patterns and inflammatory responses were documented.

2.2 Methods

All procedures were approved by the Institutional Animal Care and Use Committee and conform to published NIH guidelines for animal research.

2.2.1 Surgical Preparation

A total of two adult male dogs weighing ~25kg were used. Animals were anesthetized with pentobarbital sodium (25-30 mg/kg iv), intubated, and mechanically ventilated using a Harvard respirator. Continuous intravenous infusion of pentobarbital sodium (0.15-0.25 mg/kg hr) was used to maintain a surgical plane of anesthesia. The femoral veins were catherized and used as infusion lines. The heart was exposed via a medial sternotomy and left thoracotomy at the fifth intercostal space and supported in a pericardial cradle. LV pressure (LVP) was recorded with a pigtail micromanometer catheter (Millar Instruments, Houston, TX) inserted into the left femoral artery and advanced into the LV. Aortic pressure (AoP) was measured with a fluid-filled catheter placed in the aortic arch. Aortic pressure, LV pressure, and surface electrocardiograms (ECG) were monitored throughout the study.

2.2.2 Epicardial surface bead array

To measure the 2D LV epicardial deformation, gold beads (1.2 or 2 mm) beads were sutured to the surface of the anterolateral wall in a rectangular pattern (Fig 2.5.1). Gold beads (2mm diameter) were sutured to the apical dimple (apex bead) and on the epicardium at the bifurcation of the LAD and left

circumflex coronary artery (base bead) to provide reference endpoints for the determination of the LV long axis.

2.2.3 Study Design

Pacing electrodes were sutured to the left or right atrium, and a second set was sutured to the epicardium of the LV within the bead set site. Atrial pacing was performed by stimulating the atrial electrodes and atrioventricular sequential pacing by stimulating both atrial and LV pacing electrodes with an A-V delay of 40-60 ms. All pacing protocols were conducted using a square-wave, constant-voltage electronic stimulator (Grass Instruments, Quincy, MA) at a frequency 10-20% above baseline heart rate to suppress native sinus rhythm. Stimulation parameters (voltage 10% above threshold, duration 8ms, and frequency) were kept constant in each animal. Zetabradine (0.5 mg/kg) was administered to dogs with heart rates >110 beats/min to reduce intrinsic heart rate. Each animal was positioned in a biplane radiography system, and synchronous biplane cineradiographic images of bead displacement were digitally acquired with mechanical ventilation suspended at end expiration. LVP, AoP, and ECG were recorded simultaneously. Baseline measurements were obtained during atrial electrical stimulation. During LV pacing, electromechanical dyssynchrony was verified by the widening of the QRS complex and depression of + dP/dt. After 4 h of LV pacing, the ventricular stimulator was turned off, and a final reading of physiological parameters with atrial pacing was recorded.

2.2.4 Sacrifice protocol and tissue collection

Animals were euthanized with pentobarbital sodium (200 mg/kg), hearts excised, and myocardial sections (see below) were rapidly cooled and frozen. Myocardium was taken from the pace site (~1 cm^2 area around the pacing electrodes) and areas surrounding it (~15-20 1 cm^2 samples), as well as from the posterior wall. In order to examine transmural differences in inflammatory responses, each of these regions were sectioned in half to obtain samples from the epicardium and endocardium. Samples were stored at -80°C.

Initial evaluations of the inflammatory responses were performed to compare responses in the 15-20 samples from around the pace site. Results indicate no statistical differences in any of the measured inflammatory parameters (MPO activity, glutathione levels, and MMP-9 activity), thus biochemical results from these two regions were combined and referred to as areas around the pace site.

2.2.6 Epicardial surface bead array analysis

3D coordinates of markers were reconstructed from the cineradiography images. The basic data analysis uses a homogenous strain calculation based on a triad of markers. This technique assumes a homogenous distribution of strain within a triangle formed by three material markers. Myocardial markers were grouped automatically to form triangles with minimum height of 2.5 mm and maximum area of 60 mm^2. Additional triangles of larger area were then added

manually in areas of low bead density to ensure coverage of the array. A single marker was often used in multiple adjacent triangles. These constraints resulted in ~50 triangles (functional data points) per array. The coordinate axes were defined individually in each triangle, using the following method. First, the outward-facing normal vector (local radial direction) of the triangle was determined. Next, the circumferential direction was determined by finding a vector perpendicular to both the radial direction and the LV long axis, pointing toward the septum. Finally, the longitudinal direction was determined by finding a vector perpendicular to the radial and circumferential directions pointing toward the apex. This process ensures that the circumferential and longitudinal directions lie in the plane of the triangle.[17]

2D Lagrangian finite strains could then be calculated with respect to cardiac coordinates at the centroid of each triangle, as reported previously. 3D triangle centroids were then projected on a two-dimensional grid such that the plane of the grid was perpendicular to the radial direction of an arbitrary triangle located near the center of the array. By representing all the strains from a single time point at their respective centroid locations on the grid, a spatial distribution of strain could then be fit using the Matlab function grid data (The Mathworks, Natick, MA) and visualized as a color map. Cubic interpolation was used to ensure smooth gradients between adjacent strain measurements.

2.2.7 Myeloperoxidase Activity

Tissue samples were homogenized in ice-cold buffer (50mM KH_2PO_4 and 0.5% hexadecyltrimethylammonium bromide, pH 6.0). Homogenates were incubated on ice for 30 min and centrifuged at 4°C for 5 min. Following centrifugation, the supernatants were reacted with 0.8mM tetramethylbenzidine (Sigma; St. Louis, MO) and 0.006% H_2O_2 in 50mM KH_2PO_4.Kinetic absorbance measurements of MPO activity were immediately monitored at 655 nm (readings every 40s for ~20 min). Substrate cleavage rates were determined from the linear regions of the kinetic curve. Data were normalized to protein concentrations determined the BCA protein assay kit (Pierce, Rockford, IL).

2.2.8 Gelatin Zymography

Samples were homogenized in 10mM HEPES, pH 7.5, 150mM NaCl, 0.2mM EDTA, 25% glycerol, with protease inhibitor cocktail (Sigma). Samples (10g of protein) was loaded onto a 10% SDS-PAGE gel substituted with 0.1% gelatin and then stained with 0.5% coomassie blue. Bands of gelatinolytic activity were digitally quantified with Image J.

2.2.9 Data analyses and statistics

Results were expressed as mean ± SEM. Comparisons between means were analyzed, as appropriate, by student's *t*-test, one-way ANOVA, or two-way ANOVA followed by Bonferroni post-hoc analysis. A value of $p<0.05$ was considered statistically significant.

2.3 Results

2.3.1 Ventricular Function

Figure 2.5.2 shows a representative time course of circumferential strain (E_{11}) and longitudinal strain (E_{22}) in one triangle at the epicardial surface located at the pace site in an animal subjected to LV pacing. At the beginning atrial period (Figure 2.5.2), E_{11} and E_{22} demonstrate a typical contraction-relaxation pattern with peak shortening near end systole. Epicardial pacing markedly changes the time course of E_{11} and E_{22} where there is early shortening during diastole and also during late systole (Figure 2.5.2). The peak early shortening E_{11} and E_{22} strain data computed from the array of a representative experiment are shown in Figure 2.5.3. The strain maps shown in Figure 2.5.3 were obtained at end diastole during the beginning atrial period and at peak early shortening during the 4 h ventricular pace period (marked by vertical lines in Figure 2.5.2). The strain map represents the spatial distribution of circumferential strains, where blue indicates shortening and red indicate stretching. As seen, areas around the pace site demonstrate early shortening with epicardial LV pacing.

2.3.2 Neutrophil Infiltration

Neutrophil infiltration, as assessed by MPO activity, was significantly increased by ~4-fold in the epicardium vs. endocardium (5.1±1.4 vs. 1.4±0.3; $p<0.05$; paired t-test; Figure 2.5.4) at the pace site in animals undergoing LV pacing. Results also demonstrate a 4-fold increase in epicardial vs. endocardial

MPO activity in areas around the pace site (6.4±2.2 vs. 1.6±0.2; $p<0.05$; paired t-test). No significant differences were seen between the epicardium and endocardium in the posterior wall.

2.3.3 92 kDa MMP-9 activity

Gelatin zymography of tissue homogenates only revealed bands corresponding to 92 kDa MMP-9 and 72 kDa MMP-2. The 86 kDa MMP-9 was not visible. Densitometric analysis revealed significant increases in 92 kDa MMP-9 activity in the epicardium vs. endocardium (146±29 vs. 63±13; $p<0.01$; paired t-test; Figure 2.5.5) in areas around the pace site in animals undergoing LV pace. No statistical differences were found in the pace site or in the posterior wall. No notable differences were identified in 72 kDa MMP-2 activity (data not shown).

2.4 Discussion

Our previously published study evidenced local dyskinesis induced inflammation early after LV pacing [32]. Local dyskinesis was induced by pacing atrial and ventricular sites in open-chest anesthetized animals. Changes in shortening at the LV pacing site and at a remote site at the anterior base of the LV were monitored with sonomicrometer crystals. Simultaneous atrial and ventricular pacing resulted in abnormal motion at the LV pacing site, yielding early shortening and late systolic lengthening, whereas the shortening pattern at the remote site remained unaffected. Results from this study demonstrated that short term dykinesis induced by epicardial LV pacing is associated with increases in neutrophil infiltration as measured by MPO, which correlated with increases in nitrotyrosine levels (a marker for oxidative stress), and enhanced 92 kDa MMP-9 activity only at the pacing site/early shortening site. Results also revealed increases in local collagen degradation at this site. However, little is known about the regional and transmural distribution of inflammatory responses associated with dyskinesis. Thus, the objectives of the current study were to establish a wider correlation between regions of early shortening and the distribution of inflammatory responses induced by local dyskinesis.

To gain insight into regional patterns of abnormal contraction associated with epicardial LV pacing, an epicardial surface bead array covering an area of ~20 cm^2 was used. Results demonstrate that LV epicardial pacing induced early shortening at the pacing site and in most of the areas adjacent during diastole. As seen in the computed strain maps (Figure 2.5.3), the degree of early shortening declines with

distances further from the site of pacing. This finding is supported by previous similar studies that demonstrated the pattern of deformation gradually decreases with increasing distance from the pacing site[20, 64].

In order to establish a correlation between early shortening and inflammation, tissue samples were obtained from various regions within the bead array, as well as from the posterior wall. Our findings demonstrate that in early shortening regions (at the pacing site and areas around it), there is increased neutrophil infiltration and MMP-9 activity. More interestingly, theses inflammatory responses were localized to the epicardial half of the LV. However, in the posterior wall, where early lengthening occurs during diastole[17], no transmural differences in inflammatory responses were observed. Thus, inflammatory responses correlate with early shortening regions and are focused to the outer half of the LV wall. Early lengthening regions do not demonstrate this inflammatory response. Thus, early shortening appears to be a unique trigger of myocardial inflammation.

In conclusion, these data demonstrated that local dyskinesis induced early shortening at the epicardial pace site, as well as in the areas around the pace site. More importantly, inflammation occurred in the epicardial half in all these early activated sites.

Figure 2.5.1. Schematic diagram of bead array and experimental design. Cineradiographic images are also shown. Top: anterior-posterior view; Bottom: Lateral view.

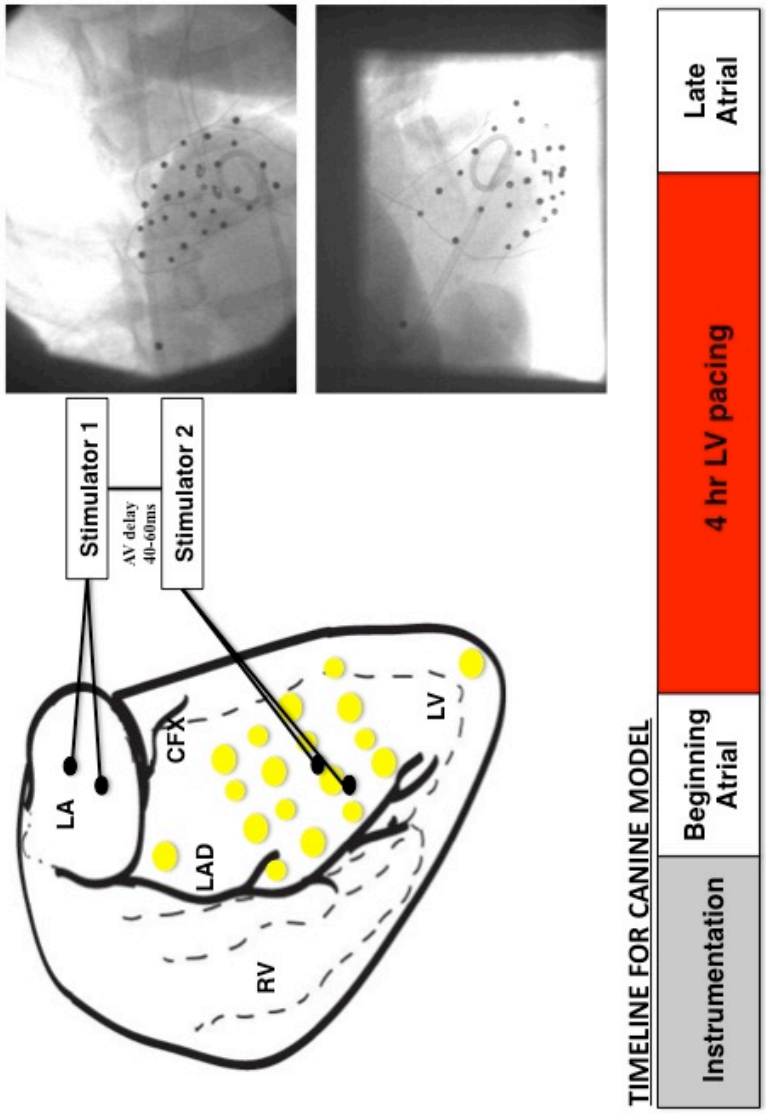
Stimulator 1
AV delay
40-60ms
Stimulator 2
LA
CFX
LAD
RV
LV
TIMELINE FOR CANINE MODEL
Instrumentation
Beginning Atrial
4 hr LV pacing
Late Atrial

Figure 2.5.2. Representative time course of epicardial circumferential strain (E_{11}) and longitudinal strain (E_{22}) in one triangle close to the pacing site. Left ventricular pressure is also noted. The reference frame for strain calculation was end-diastole for atrial pacing or the timing of the stimulus artifact for LV pacing. *A*: beginning atrial; *B*: 4 h ventricular run. Vertical lines=peak early shortening.

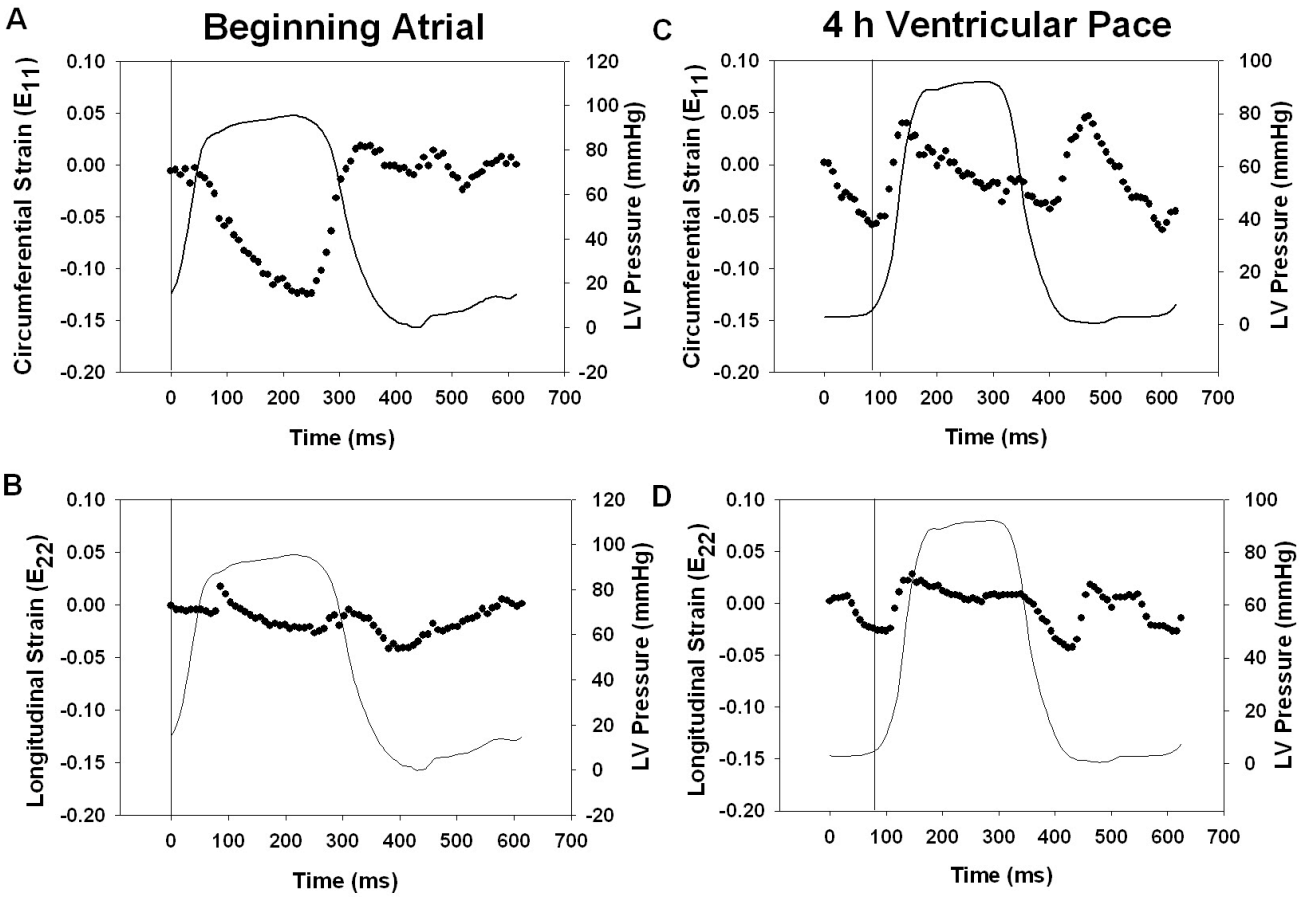
A
Beginning Atrial
C
4 h Ventricular Pace
B
D
Circumferential Strain (E_{11})
Longitudinal Strain (E_{22})
LV Pressure (mmHg)
Time (ms)
0.10
0.05
0.00
-0.05
-0.10
-0.15
-0.20
120
100
80
60
40
20
0
-20
0
100
200
300
400
500
600
700

Figure 2.5.3. Spatial distribution of peak early shortening circumferential strain (E_{11}), and longitudinal strain (E_{22}) in a representative animal during the beginning atrial and 4 h ventricular pace period. Red (positive) strains indicate stretching, whereas blue (negative) strains indicate shortening. Small x's represent locations of beads. Black circles represent pacing electrodes.

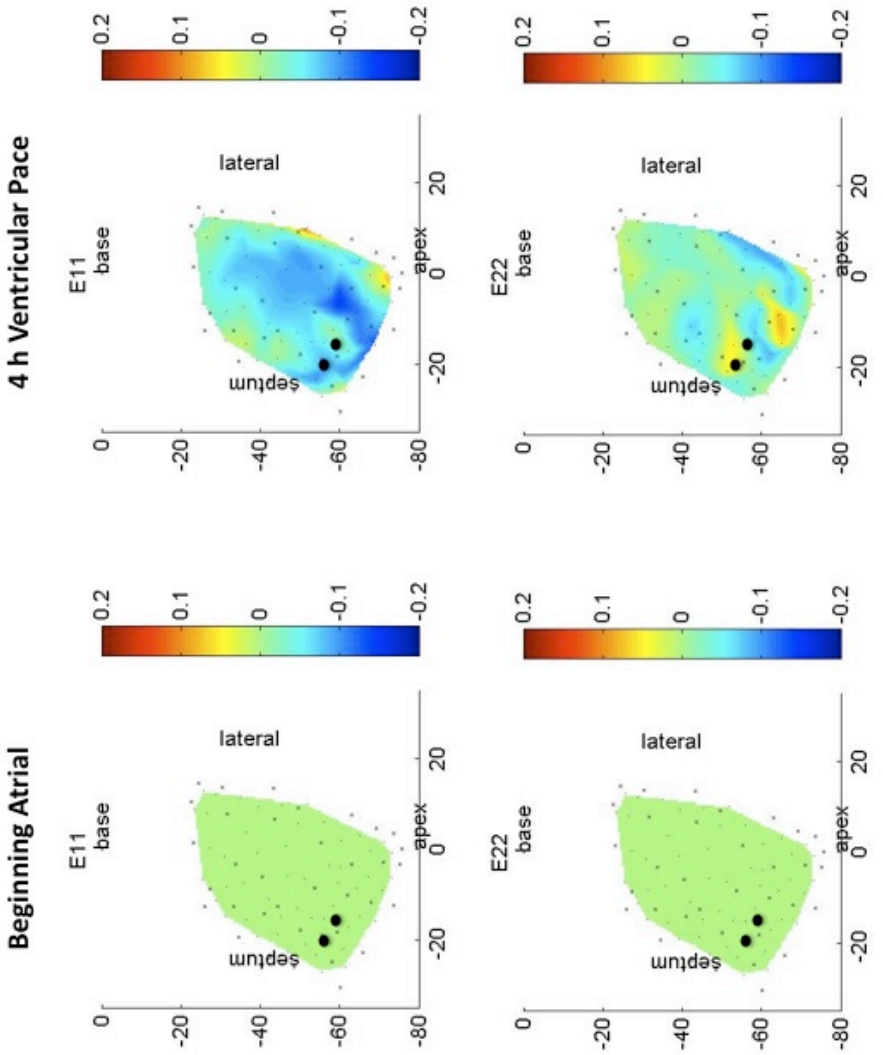
4 h Ventricular Pace
Beginning Atrial
E11
E22
base
apex
lateral
septum
0.2
0.1
0
-0.1
-0.2
0
-20
-40
-60
-80
20

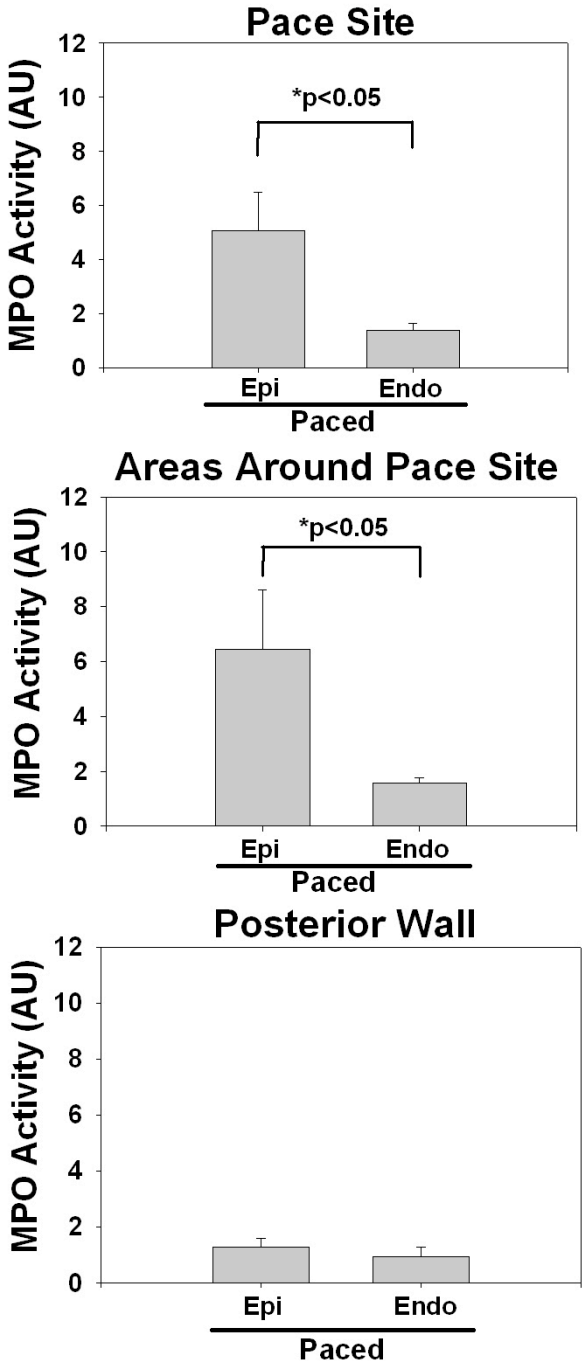

Figure 2.5.4. Acute neutrophil infiltration induced by local dyskinesis in paced hearts (n=2) at the pace site, areas around the pace site, and posterior wall. Values are means±sem.

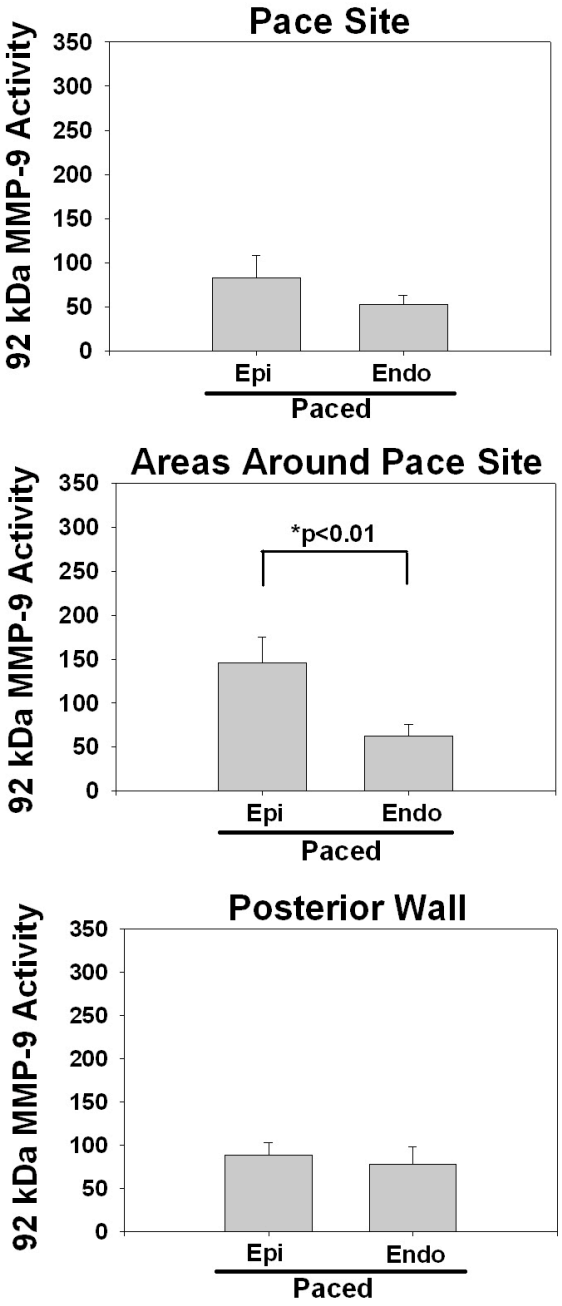

Figure 2.5.5. Acute 92 kDa MMP-9 activity induced by local dyskinesis in paced hearts (n=2) at the pace site, areas around the pace site, and posterior wall. Values are means±sem.

Chapter 3. Effects of Propofol on inflammatory responses induced by myocardial dyskinesis

3.1 Introduction

Results from chapter 2 studies demonstrate the triggering of an inflammatory response at early activated sites in the setting of LV pacing. It is interesting to speculate that agents known to suppress the activation of an inflammatory response may mitigate dyskinesis induced inflammation. Ischemic preconditioning is an adaptational response of briefly ischemic tissues, which serves to protect against subsequent prolonged ischemic insults and reperfusion injury.[65] It can be brought on by pharmacological or mechanical interventions.[65] In principle, the cellular signals generated by brief periods of ischemia in ischemic preconditioning must be passed to, and preserved in, intracellular component(s). This memory should be retrieved, at the time of ischemia, resulting in forwarding of signals to the effector(s) that can mitigate IR injury.[66]

Previous studies, by and large, led to identify the constituents of a series of preconditioning induced cellular events in the heart. In preconditioning, a brief direct ischemic insult to the target organ followed by reperfusion results in tolerance to subsequent insults of ischemia. Ischemic tolerance is induced by regulation of endothelial function, blood flow, and decreased parenchymal injury.[65] Recent studies have shown that various triggering substances like NO, adenosine, bradykinin, calcitonin gene-related peptide, PKCε, manganese superoxide dismutase,

COX-2, oxygen free radicals, and mitochondrial ATP sensitive potassium channels (K_{ATP}) induce similar cardioprotection as afforded by ischemic preconditioning.[67] These triggering substances amplify their signals inside the cell to activate numerous downstream mediators like ERK/Akt, PKC, tyrosine kinase, PI-3K, and MAPK.[67] These signaling events lead to myocardial protection by opening mitochondrial K_{ATP} channels, blocking mitochondrial permeability transition pore (MPTP), upregulating HSPs, activating antioxidant defense system, improving myocardial energy balance and inhibiting the release of proapoptotic substances, which are collectively known as end-effectors in ischemic preconditioning induced cardioprotection.[67]

Investigators have reported that certain analgesics and/or anesthetic agents have cardioprotective effects.[66] There is accumulating evidence that halothane, isoflurane, and sevoflurane improves postischemic functional recovery.[66] Shultz et al recently found that ischemic preconditioning, a powerful prevention to reduce IR injury, is at least in part mediated by opioid receptors.[68] More recently, the cardioprotective properties of propofol have been described.

Propofol has a chemical structure similar to that of phenol-based free radical scavengers, such as vitamin E, and has been shown to reduce free radicals during IR injury.[66, 69, 70] Studies have demonstrated the effects of propofol are present in the same range as the anesthetic concentrations used clinically, thus it is possible that propofol may act as an antioxidant during anesthesia.[69] In a pig model of cardiopulmonary bypass, typical clinical concentrations of propofol improved

functional recovery of the heart, reduced troponin I release, and maintained higher tissue ATP levels.[71] It has also been shown that propofol decreases postischemic myocardial mechanical dysfunction, infarct size, histological degeneration, intracellular Ca^{2+}levels, and neutrophil infiltration.[66] Propofol has also been shown to protect the Langendorff-perfused heart from IR injury, damage caused by H_2O_2-induced oxidative stress, as well as MPTP.[66]

In our study, we hypothesized that epicardial pacing induced dyskinesis induced inflammation is largely mediated by neutrophil infiltration and reactive oxygen species generation. The use of propofol in our study during anesthesia should ameliorate these inflammatory associated responses.

3.2 Methods

All procedures were approved by the Institutional Animal Care and Use Committee and conform to published NIH guidelines for animal research.

3.2.1 Surgical Preparations

A total of three adult male mongrel dogs weighing between 25 and 28 kg were used. Animals were induced with propofol (10 mg/kg IV), intubated, mechanically ventilated with isoflurane (0.5%-2.5%), and medical oxygen (2l/min) to maintain a surgical plane of anesthesia during the duration of the study. The femoral veins were catherized and used as infusion lines. The heart was exposed via a medial sternotomy and left thoracotomy at the fifth intercostal space and supported in a pericardial cradle. LV pressure (LVP) was recorded with a pigtail micromanometer catheter (Millar Instruments, Houston, TX) inserted into the left femoral artery and advanced into the LV. AoP was measured with a fluid-filled catheter placed in the aortic arch. AoP, LVP, and ECG were monitored throughout the study.

3.2.2 Epicardial surface bead array

To measure 2D LV mechanics, gold beads (1.2 or 2 mm) beads were sutured to the surface of the anterolateral wall in a rectangular pattern (Fig 3). Gold beads (2mm diameter) were sutured to the apical dimple (apex bead) and on the epicardium at the bifurcation of the LAD and left circumflex coronary artery (base bead) to provide endpoints for the identification of the LV long axis.

3.2.3 Study Design

Pacing electrodes were sutured to the left or right atrium, and a second set was sutured to the epicardium of the LV within the bead set site. Atrial pacing was performed by stimulating the atrial electrodes and AV sequential pacing by stimulating both atrial and LV pacing electrodes with an A-V delay of 40-60 ms. All pacing protocols were conducted using a square-wave, constant-voltage electronic stimulator (Grass Instruments, Quincy, MA) at a frequency 10-20% above baseline heart rate to suppress native sinus rhythm. Stimulation parameters (voltage 10% above threshold, duration 8ms, and frequency) were kept constant in each animal. Zetabradine (0.5 mg/kg) was administered to dogs with heart rates >110 beats/min to reduce intrinsic heart rate. Each animal was positioned in a biplane radiography system, and synchronous biplane cineradiographic images of bead displacement were digitally acquired with mechanical ventilation suspended at end expiration. LVP, AoP, and ECG were recorded simultaneously. Baseline measurements were obtained during atrial electrical stimulation. During LV pacing, electromechanical dyssynchrony was verified by the widening of the QRS complex and depression of + dP/dt. After 4 h of LV pacing, the ventricular stimulator was turned off, and a final reading of physiological parameters with atrial pacing was recorded.

3.2.4 Sacrifice protocol and tissue collection

Animals were euthanized with pentobarbital sodium (200 mg/kg),

hearts excised, and myocardial sections (see below) were rapidly cooled and frozen. Myocardium was taken from the pace site (~1 cm^2 area around the pacing electrodes) and areas surrounding it (~15-20 1 cm^2 samples), as well as from the posterior wall. In order to examine transmural differences in inflammatory responses, each of these regions were sectioned in half to obtain samples from the epicardium and endocardium. Samples were stored at -80°C.

Initial evaluations of the inflammatory responses were performed to compare responses in the 15-20 samples from around the pace site. Results indicate no statistical differences in any of the measured inflammatory parameters (MPO activity, glutathione levels, and MMP-9 activity), thus biochemical results from these two regions were combined and referred to as areas around the pace site.

3.2.5 Epicardial surface bead array analysis

3D coordinates of markers were reconstructed from the cineradiography images. The basic data analysis uses a homogenous strain calculation based on a triad of markers. This technique assumes a homogenous distribution of strain within a triangle formed by three material markers. Myocardial markers were grouped automatically to form triangles with minimum height of 2.5 mm and maximum area of 60 mm^2. Additional triangles of larger area were then added manually in areas of low bead density to ensure coverage of the array. A single marker was often used in multiple adjacent triangles. These constraints resulted

in ~50 triangles (functional data points) per array. The coordinate axes were defined individually in each triangle, using the following method. First, the outward-facing normal vector (local radial direction) of the triangle was determined. Next, the circumferential direction was determined by finding a vector perpendicular to both the radial direction and the LV long axis, pointing toward the septum. Finally, the longitudinal direction was determined by finding a vector perpendicular to the radial and circumferential directions pointing toward the apex. This process ensures that the circumferential and longitudinal directions lie in the plane of the triangle.[17]

2D Lagrangian finite strains could then be calculated with respect to cardiac coordinates at the centroid of each triangle, as reported previously.[17] 3D triangle centroids were then projected on a two-dimensional grid such that the plane of the grid was perpendicular to the radial direction of an arbitrary triangle located near the center of the array. By representing all the strains from a single time point at their respective centroid locations on the grid, a spatial distribution of strain could then be fit using the Matlab function grid data (The Mathworks, Natick, MA) and visualized as a color map. Cubic interpolation was used to ensure smooth gradients between adjacent strain measurements.[17]

3.2.6 Myeloperoxidase Activity

Tissue samples were homogenized in ice-cold buffer (50mM KH_2PO_4 and 0.5% hexadecyltrimethylammonium bromide, pH 6.0). Homogenates were

incubated on ice for 30 min and centrifuged at 4°C for 5 min. Following centrifugation, the supernatants were reacted with 0.8mM tetramethylbenzidine (Sigma; St. Louis, MO) and 0.006% H_2O_2 in 50mM KH_2PO_4.Kinetic absorbance measurements of MPO activity were immediately monitored at 655 nm (readings every 40s for ~20 min). Substrate cleavage rates were determined from the linear regions of the kinetic curve. Data were normalized to protein concentrations determined the BCA protein assay kit (Pierce, Rockford, IL).

3.2.7 Gelatin Zymography

Samples were homogenized in 10mM HEPES, pH 7.5, 150mM NaCl, 0.2mM EDTA, 25% glycerol, with protease inhibitor cocktail (Sigma). Samples (10g of protein) was loaded onto a 10% SDS-PAGE gel substituted with 0.1% gelatin and then stained with 0.5% coomassie blue. Bands of gelatinolytic activity were digitally quantified with Image J.

3.2.8 Data analyses and statistics

Results were expressed as mean ± SEM. Comparisons between means were analyzed, as appropriate, by student's *t*-test, one-way ANOVA, or two-way ANOVA followed by Bonferroni post-hoc analysis. A value of $p<0.05$ was considered statistically significant.

3.3 Results

3.3.1 Ventricular Function

Figure 3.5.1 shows a representative time course of circumferential strain (E_{11}) and longitudinal strain (E_{22}) in one triangle at the epicardial surface located at the pace site in an animal subjected to atrial or 4 h LV pacing. At the beginning atrial period (Figure 3.5.1), E_{11} and E_{22} demonstrates a typical contraction-relaxation pattern with peak shortening near end systole. Epicardial LV pacing markedly changed the time course of E_{11} and E_{22} where there is early shortening during diastole and also during late systole (Figure 3.5.1). E_{11} and E_{22} strain data from the whole array of a representative animal are shown in Figure 3.5.2. The strain maps shown in Figure 3.5.2 were obtained at the time of end diastole or peak early shortening as marked by vertical lines in Figure 3.5.1. The strain map represents the spatial distribution of circumferential strains, where blue indicates shortening and red indicate stretching. As seen, areas around the pace site demonstrate early shortening with epicardial LV pacing.

3.3.2 Myocardial Inflammatory responses

Acute myocardial inflammatory responses measured in paced animals (n=2) are seen in Figure 3.5.3. Neutrophil infiltration, as measured by MPO activity, in the presence of epicardial LV pacing was mitigated in the presence of propofol at the pace site, and areas around the pace site. As expected, no

changes were observed in the posterior wall. 92 kDa MMP-9 activity was not different in any of these sites as well. These results suggest that propofol, indeed, acts as a preconditioning agent to protect the myocardium from dyskinesis-induced inflammation.

3.4 Discussion

We previously reported that 4 h of epicardial LV pacing led to increases in epicardial MPO activity and 92 kDa MMP-9 activity in regions of early shortening. These findings suggest that a mechanistic link between early shortening patterns and inflammation exists. Results from this present study demonstrated that the use of the "preconditioning like" agent, propofol, abrogated dyskinesis induced increases in MPO and MMP-9 activity.

The suppression of measured myocardial inflammatory responses may be attributable in part to the antioxidant properties of propofol, and suggest that propofol may have a protective role in disorders where free radical mediated injury promotes leukocyte-endothelium adhesive interactions (Corocoran influence of propofol 2006). These features suggest that propofol may directly intervene at the critical phase of inflammation-induced injury by reducing free radicals, Ca^{2+} influx, and neutrophil activity.[72] If an inflammatory response is to be secondary to a vascular dependent event, an upregulation of CAM in the involved region needs to occur. Free radical production and endothelial activation promote leukocyte-endothelium interactions via endothelial expression of VCAM-1 and ICAM-1, which augment these processes, as well documented in the setting of reperfusion injury. In cultured human umbilical vein endothelial cells undergoing 20 min of hypoxia, propofol prevented the increase in ICAM-1/VCAM-1 expression during reoxygenation.[72] Another study demonstrated that propofol inhibited the inflammatory reaction (TNF-α, IL-1, and ICAM-1

expression) by inhibiting the NFκB activation during transient focal cerebral IR.[73] In an *in vivo* rat model of intestinal IR injury, early treatment of propofol (10 mi prior to ischemia) followed by continuous infusion of this agent significantly decreased TNF-α content, ICAM-1 expression, and MPO activity in lung tissue.[74]

Thus, propofol has various "protective features that lead to a suppression of early shortening triggering inflammatory responses.

Figure 3.5.1 Representative time course of epicardial circumferential strain (E_{11}) and longitudinal strain (E_{22}) in one triangle. Left ventricular pressure is also noted. The reference frame for strain calculation was end-diastole for atrial pacing or the timing of the stimulus artifact for LV pacing. *A*: beginning atrial; *B*: 4 h ventricular run. Vertical lines=peak early shortening.

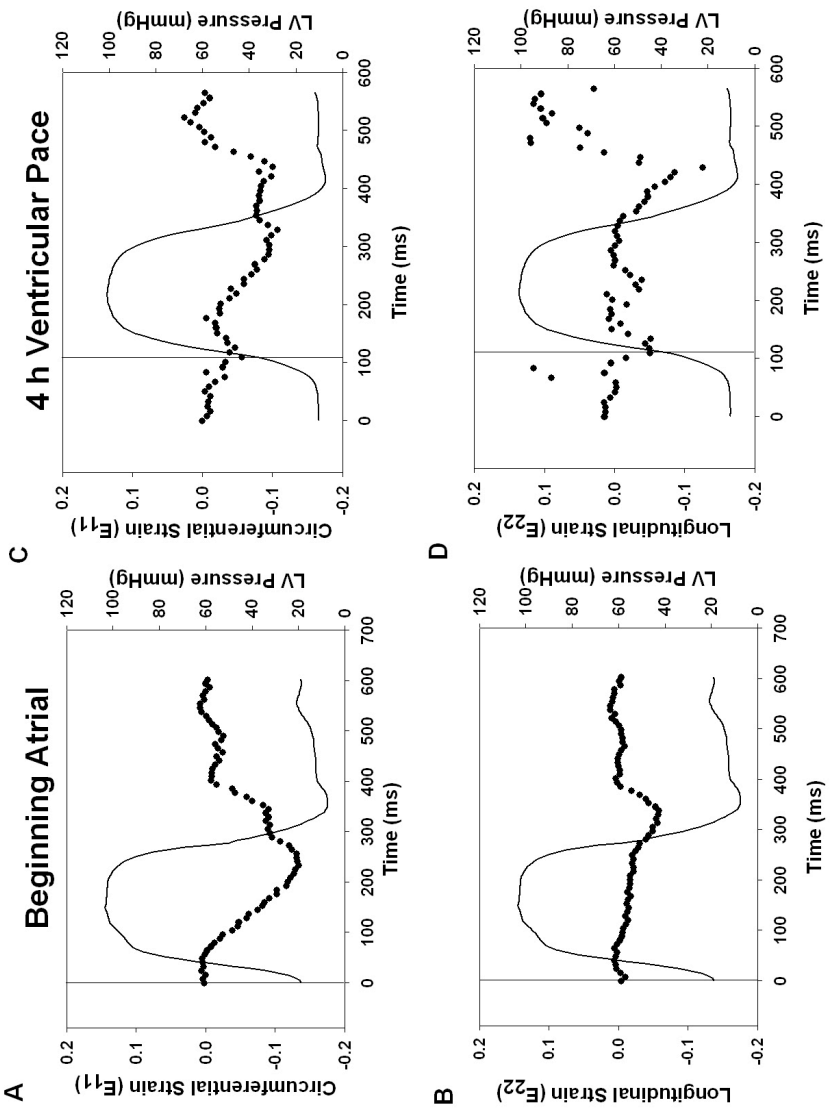
A
Beginning Atrial
Circumferential Strain (E_{11})
LV Pressure (mmHg)
Time (ms)
B
Longitudinal Strain (E_{22})
LV Pressure (mmHg)
Time (ms)
C
4 h Ventricular Pace
Circumferential Strain (E_{11})
LV Pressure (mmHg)
Time (ms)
D
Longitudinal Strain (E_{22})
LV Pressure (mmHg)
Time (ms)

Figure 3.5.2 Spatial distribution of peak early shortening circumferential strain (E_{11}) and longitudinal strain (E_{22}) in a representative animal during the beginning atrial and 4 h ventricular run. Red (positive) strains indicate stretching, whereas blue (negative) strains indicate shortening. Small x's represent locations of beads. Black circles represent pacing electrodes.

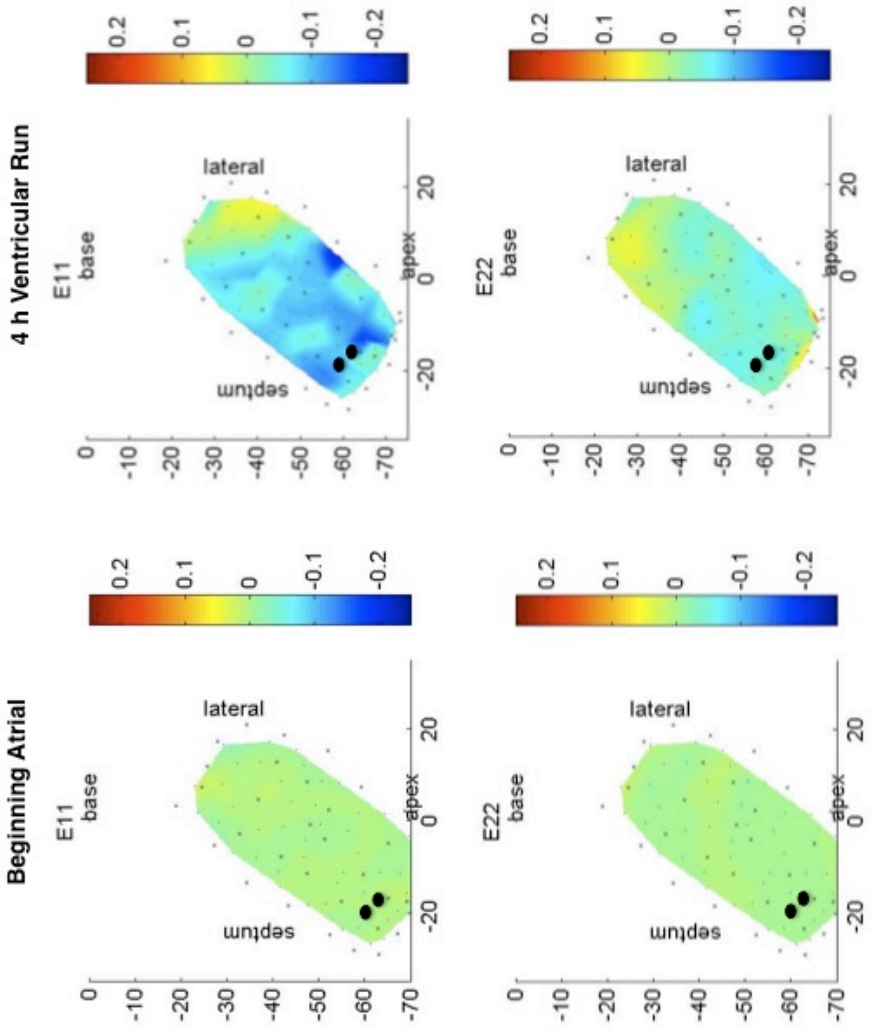
4 h Ventricular Run
Beginning Atrial
E11
E22
base
apex
lateral
septum
0.2
0.1
0
-0.1
-0.2
0
-10
-20
-30
-40
-50
-60
-70
20
0
-20

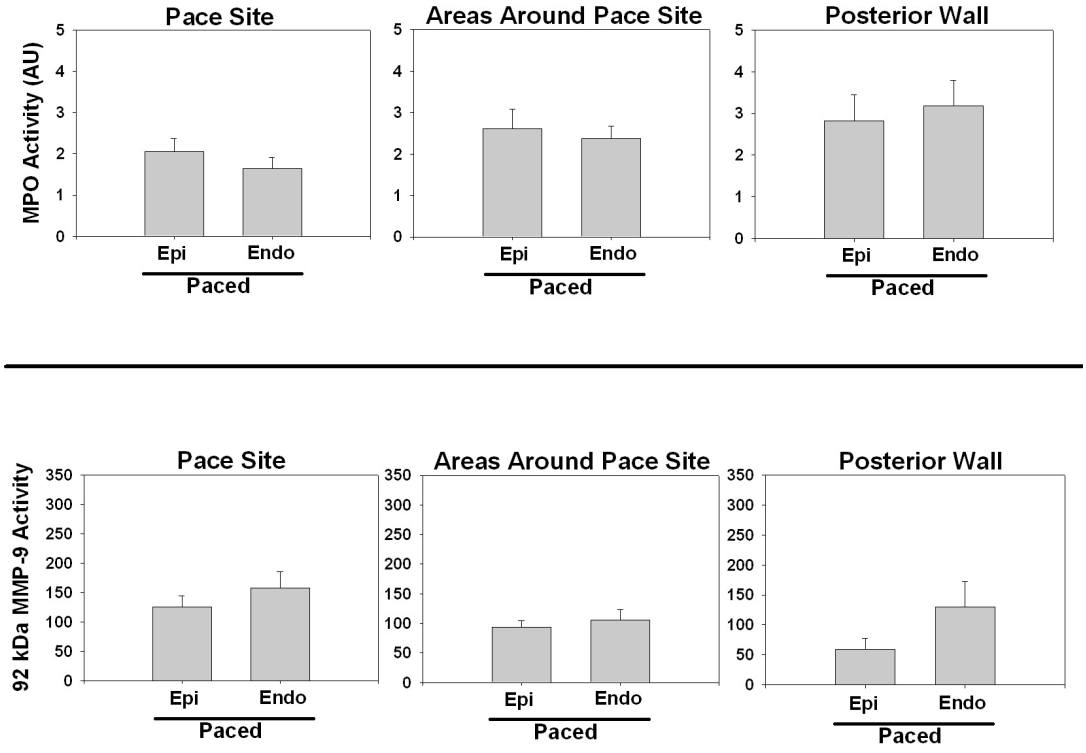

Figure 3.5.3. Myocardial inflammatory responses induced by local dyskinesis in paced animals (n=2). *A*: MPO activity; *B*: 92 kDa MMP-9 activity in the pace site, areas around the pace site and the posterior wall. Values are mean±sem.

Chapter 4. Effects of transmural bead implantation

4.1 Introduction

Our previous studies have demonstrated that early shortening, secondary to LV pacing, induces an inflammatory response. More interesting, the inflammatory responses appear to be localized to the epicardial half of the myocardium. However, the cause of this epicardial inflammation is unknown. To further understand the nature of ventricular dyskinesis-induced acute changes in cardiac structure/function, a detailed assessment of 3D LV function is required. Similarly, in order to identify the molecular mechanism possibly involved in the development of structural changes, a detailed transmural assessment of inflammatory responses is required.

Dyssynchrony of regional contraction as induced by epicardial ventricular pacing has been the subject of investigations using increasingly sophisticated techniques for nearly a century. [14-19] Techniques used in our laboratories, which use permanent radiopaque material markers implanted in the myocardium, allows us to accurately describe 3D finite deformation.[14, 75, 76] Techniques that rely on the use of permanent markers are the only methods that can be used to demonstrate short and long-term tissue remodeling in a region of interest. Other imaging techniques such as MRI can provide high resolution information of shape and dimensions, but because they do not track the same material points over long periods of time they cannot reveal specific changes in structure within a given region. This technique would be advantageous to our objectives in that we will be able to accurately document the

character of transmural changes in LV mechanics that might partly explain to the epicardial localization of inflammatory responses.

To our knowledge, little is known about the effects of radiopaque markers implantation on acute changes in LV structure/function. It can be speculated that the implantation of gold beads damages the myocardium in a way that depresses LV function, as well as blunts the development of inflammatory responses associated with ventricular dyskinesis. Thus, the objective of this study is to determine the acute effects of bead inflammation on LV function and myocardial inflammatory responses in the presence of ventricular dyskinesis.

4.2 Methods

All procedures were approved by the Institutional Animal Care and Use Committee and conform to published NIH guidelines for animal research.

4.2.1 Surgical Preparations: Acute Study

A total of four adult male dogs (two mongrel; two beagles) weighing between 12 and 28 kg were used. Animals were anesthetized with pentobarbital sodium (25-30 mg/kg iv), intubated, and mechanically ventilated using a Harvard respirator. Continuous intravenous infusion of pentobarbital sodium (0.15-0.25 mg/kg hr) was used to maintain a surgical plane of anesthesia. The femoral veins were catherized and used as infusion lines. The heart was exposed via a medial sternotomy and left thoracotomy at the fifth intercostal space and supported in a pericardial cradle. LV pressure (LVP) was recorded with a pigtail micromanometer catheter (Millar Instruments, Houston, TX) inserted into the left femoral artery and advanced into the LV. AoP was measured with a fluid-filled catheter placed in the aortic arch. AoP, LVP, and ECG were monitored throughout the study.

4.2.2 Surgical Preparations: Chronic Study

In another group (n=2), animals underwent a thoracotomy 2 weeks prior to the initiation of LV pacing. In this group, animals were anesthetized with intravenous propofol (6 mg/kg), intubated, and mechanically ventilated with isoflurane (0.5-2.5%), and medical oxygen (2 L/min) to maintain a surgical

plane of anesthesia. The heart was exposed via a left thoracotomy at the fifth intercostal space. After a pericardial dissection, a transmural bead array was implanted (see below). The chest was closed and the animals were allowed to recover. Two weeks post-thoracotomy, the animals underwent the surgical preparation and LV pacing protocol as described below.

4.2.3 Transmural bead array

To assess transmural LV mechanics, three columns of three to four 0.8-mm-diameter-gold beads were inserted into the anterior wall between the first and second diagonal branches of the left anterior descending (LAD) coronary artery. After bead implantation, 1.7-mm-diameter surface gold beads were sewn on the epicardium above each column. Gold beads (2mm diameter) were sutured to the apical dimple (apex bead) and on the epicardium at the bifurcation of the LAD and left circumflex coronary artery (base bead) to provide endpoints for the LV long axis.

4.2.4 Study Design and Groups

Pacing electrodes were sutured to the left or right atrium, and a second set was sutured to the epicardium of the LV within the bead set site. Atrial pacing was performed by stimulating the atrial electrodes and LV pacing by stimulating both atrial and LV pacing electrodes with an A-V delay of 40-60 ms. All pacing protocols were conducted using a square-wave, constant-voltage electronic stimulator (Grass Instruments, Quincy, MA) at a frequency 10-20% above

baseline heart rate to suppress native sinus rhythm. Stimulation parameters (voltage 10% above threshold, duration 8ms, and frequency) were kept constant in each animal. Zetabradine (0.5 mg/kg) was administered to dogs with heart rates >110 beats/min to reduce intrinsic heart rate. Each animal was positioned in a biplane radiography system, and synchronous biplane cineradiographic images of bead displacement were digitally acquired with mechanical ventilation suspended at end expiration. LVP, AoP, and ECG were recorded simultaneously. Baseline measurements were obtained during atrial electrical stimulation. During LV pacing, electromechanical dyssynchrony was verified by the widening of the QRS complex and depression of + dP/dt. After 4 h of LV pacing, the ventricular stimulator was turned off, and a final reading of physiological parameters with atrial pacing was recorded. Table 4.5.1 summarizes the study groups utilized in this section.

4.2.5 Sacrifice protocol and tissue collection

Animals were euthanized with pentobarbital sodium (200 mg/kg), hearts excised, and myocardial sections (see below) were rapidly cooled and frozen. Myocardium was taken from the site were beads were implanted and two regions surrounding it, as well as from the posterior wall. These sites were basal to the bead set, and lateral to the bead set. In order to examine transmural differences in inflammatory responses, each of these four regions were sectioned into 2 mm slices from the epicardium to the endocardium and samples were

stored at -80°C.

Comparisons were made within each study group comparing transmural responses of inflammatory parameters. Samples encompassed in the outer third of the LV wall were defined as epicardial samples, middle third is midwall, and inner third was endocardial. Results indicated no statistical differences between midwall and endocardial samples in any of the measured inflammatory parameters, thus results are combined and referred to as Mid/Endo.

4.2.6 Transmural bead array analysis

The 3D coordinates of the implanted markers were obtained from the spherically corrected data set for an entire cardiac cycle selected in each animal. In principle, continuous, nonhomogenous transmural distributions of 3D finite strains were computed.[76] Six independent finite strains were computed in the cardiac coordinate system (X_1, X_2, X_3). The three normal strain components reflect myocardial stretch or shortening along the circumferential (E_{11}), longitudinal (E_{22}), or radial (E_{33}) cardiac axes.[77] Finite strains were calculated for each frame (125 frames/sec) as a deformed configuration with end diastole as the reference state at three wall depths: 25% (subepicardium), 50% (midwall),and 75% (subendocardium) wall depth from the epicardial surface. End diastole was defined as the time of the peak of the ECG R-wave for atrial pacing and the ventricular pacing artifact for the LV epicardial pacing. We chose the V-spike rather than the peak of the R-wave as the reference state for LV

epicardial pacing because the former reflects the timing of the activation of the pacing site, as opposed to the latter, which represents the timing of activation of the whole ventricle.[75]

4.2.7 Myeloperoxidase activity

Tissue samples were homogenized in ice-cold buffer (50mM KH_2PO_4 and 0.5% hexadecyltrimethylammonium bromide, pH 6.0). Homogenates were incubated on ice for 30 min and centrifuged at 4°C for 5 min. Following centrifugation, the supernatants were reacted with 0.8mM tetramethylbenzidine (Sigma; St. Louis, MO) and 0.006% H_2O_2 in 50mM KH_2PO_4.Kinetic absorbance measurements of MPO activity were immediately monitored at 655 nm (readings every 40s for ~20 min). Substrate cleavage rates were determined from the linear regions of the kinetic curve. Data were normalized to protein concentrations determined the BCA protein assay kit (Pierce, Rockford, IL).

4.2.8 Glutathione (GSSG/GSH) Assay

Reduced and oxidized glutathione, GSH and GSSG respectively, levels were determined as previously described by Senft et al.[78] Briefly, tissue samples were homogenized in ice cold homogenization buffer (154mM KCL, 5mM diethylenetriaminepentaacetic acid (DPTA), and 0.1M potassium phosphate, pH 6.8). After centrifugation, an aliquot was removed for protein determination using the BCA protein assay kit. Immediately after an aliquot was taken, one volume of cold acid buffer (40mM HCl, 10mM DPTA, 20mM ascorbic acid,

and 10% trichloroacetic acid (TCA) was added to the homogenate. The suspension was centrifuged and the resulting supernatant solution was centrifuged through a 0.45m microcentrifuge filter (Millipore Corp., Bedford, MA). GSH and GSSG levels were determined using the fluorophore *o*-phtaladehyde.

4.2.9 Gelatin Zymography

Samples were homogenized in 10mM HEPES, pH 7.5, 150mM NaCl, 0.2mM EDTA, 25% glycerol, with protease inhibitor cocktail (Sigma). Samples (10g of protein) was loaded onto a 10% SDS-PAGE gel substituted with 0.1% gelatin and then stained with 0.5% coomassie blue. Bands of gelatinolytic activity were digitally quantified with Image J.

4.2.10 Data analyses and statistics

Results were expressed as mean ± SEM. Comparisons between means were analyzed, as appropriate, by student's *t*-test, one-way ANOVA, or two-way ANOVA followed by Bonferroni post-hoc analysis. A value of $p<0.05$ was considered statistically significant.

4.3 Results

Group 1 (n=4) evaluated the transmural effects of 4 h ventricular dyssynchrony on LV function and inflammatory responses. Group 2 (n=2) assessed dyskinesis induced inflammatory response in the absence of beads. Group 3 (n=2) was used to determine if bead implantation on the day of LV pacing preconditions or stuns the myocardium, which in turn may suppress LV function and inflammatory responses at the bead site. Initial evaluations of hemodynamic and inflammatory parameters were performed to compare these responses in groups 2 and 3. Results indicate no statistical differences in any of the measured parameters, thus groups 2+3 were combined for all hemodynamic and biochemical parameters and are referred to as chronic/no beads group (n=4).

4.3.1 Hemodynamics

Comparisons of data measured during beginning atrial, 4 h LV pacing and late atrial between acute and chronic/no beads animals did not reveal any significant changes in heart rate, LV systolic pressure, or LV end-diastolic pressure, or ±dP/dt (p=ns, paired t-test; Table 4.5.2).

4.3.2 Ventricular Function

Figure 4.5.3 shows 3D end-systolic normal strains (E_{11}, E_{22}, E_{33}) at the pacing site. End systolic E_{11}, E_{22}, and E_{33} demonstrate a non-significant progressive loss of function over time with LV pacing, as seen with strains

shifting towards in the positive direction for E_{11} and E_{22}, and in the negative direction for E_{33} for both the acute and chronic animals. The early activated site only partially recovered with late atrial pacing for all strain components. This apparent loss of function is seen more clearly in Figure 4.5.4. Figure 4.5.4 compares end-systolic normal strains during beginning atrial, 1 min LV pacing, 4 h LV pacing and late atrial. No significant differences in the strain patterns were observed between the acute animals (Group 1) and the chronic animals (Group 3).

4.3.3 Neutrophil Infiltration

Figure 4.5.5 shows MPO activity results from acute and chronic/no beads animals. Data demonstrates no differences in MPO activity in the bead site and in the posterior wall for acute animals. However, there is a significant 3-fold increase in MPO activity in the epi vs. mid/endo (2.0±0.5 vs. 0.69±0.11; $p<0.05$; paired t-test; Figure 4.5.5.A) in the areas surrounding the bead set. In the chronic/no beads group (Figure 4.5.5.B), there was a significant 4-fold increase in MPO activity in the epi compared to the mid/endo (2.4±0.4 vs. 0.61±0.39; $p<0.05$; paired t-test) at the bead set site, as well as in the areas around the bead set (2.1±0.6 vs. 0.05±0.03; $p<0.05$; paired t-test). No significant differences were found in the posterior wall. Analysis of results suggest that bead implantation performed the day of LV pacing, may stun or precondition the myocardium to diminish the upregulation of MPO activity.

4.3.4 Oxidative Stress

Figure 4.5.6 summarizes oxidative stress results from myocardium of acute and chronic/no beads animals. Results are shown as GSSG/GSH, which is a measure of total tissue oxidative stress. Figure 4.5.6.A demonstrates that results from acute animals fail to increase oxidative stress levels at the bead set site. A 3-fold increase in oxidative stress was seen in the epi vs. the mid/endo in areas around the bead set (1.5±0.5 vs. 0.53±0.25; $p<0.05$; paired t-test). No differences were seen in the posterior wall. Combined results from group 2 and 3 suggest increased oxidative stress in the epi vs. the mid/endo (3.2±1.3 vs. 1.9±0.6; p=NS; paired t-test; Figure 4.5.6.B) at the bead set site and in the posterior wall (2.1±1.3 vs. 0.77±0.5; p=NS; paired t-test). There was a significant 2 fold increase in oxidative stress in areas around the bead set (3.6±0.9 epi vs. 1.6±0.3 mid/endo; $p<0.05$; paired t-test).

4.3.5 MMP Activity

Gelatin zymography of tissue homogenates only revealed bands corresponding to 92 kDa MMP-9 and 72 kDa MMP-2. The 86 kDa MMP-9 was not visible. Densitometric analysis demonstrate no significant differences in 92 kDa MMP-9 activity in the epi vs. mid/endo at the bead set site (44±5 vs. 26±2; p=NS; paired t-test; Figure 4.5.7.A) and in the posterior wall (78±16 vs. 48±16; p=NS; paired t-test; Figure 4.5.7.A) in acute animals. In this group of animals, 92 kDa MMP-9 activity significantly increased by 2-fold in areas

around the bead set (101±12.6 epi vs. 50±6 mid/endo; $p<0.01$; paired t-test). Combined results from group 2 and 3 showed a significant 2-fold increase in 92 kDa MMP-9 activity in the epi vs. mid/endo (72+5 vs. 33+6; $p<0.01$; paired t-test; Figure 4.5.7.B) at the bead set site, as well as in the areas around the bead site (104±13 vs. 54±4; $p<0.01$; paired t-test). No significant differences were observed in the posterior wall. Densitometric analysis, no notable differences were noted in 72 kDa MMP-2 levels.

4.4 Discussion

Results from this study demonstrate that acute bead implantation had no effect on LV hemodynamics and 3D myocardial deformation. However, results show that ventricular dyskinesis failed to initiate an inflammatory response at the bead set/pace site in acute animals, whereas there is significant transmural upregulation of MPO activity, oxidative stress, and MMP-9 activity at the bead set/pace site in the chronic/no beads group.

Previous studies demonstrated that in preconditioning, a brief direct ischemic insult to the target organ followed by reperfusion results in tolerance to subsequent insults of ischemia.[65] It can be speculated that bead implantation preconditions the myocardium against further injury induced by ventricular dyskinesis. The fact that inflammatory responses associated with dyskinesis were clearly blunted in acute animals, but seen in a "healed" bead set, i.e. chronic animals, supports this notion of temporary preconditioning.

In conclusion, bead implantation causes acute injury to the myocardium, which inhibits the upregulation of myocardial inflammatory responses induced by ventricular dyskinesis. This finding prompted us to in the next chapter to present results only from areas around the bead set, which also undergo early shortening when subjected to local LV pacing (chapter 2). Data from this chapter is also used as material for chapter 5.

Table 4.5.1 Study Groups

Acute Studies				**Final Groups**
Groups	***n***	**Procedure**	**Reason**	
1	4	Instrumentation Beads/ 4 h LV Pace	To determine the transmural effects of 4hr pacing on LV function and inflammatory responses	**Acute Beads Group**
2	2	Instrumentation No beads/ 4 h LV Pace	To assess pacing induced inflammatory responses in the absence of beads	**Groups 2 and 3 were combined to form the Chronic/No bead group.**
Chronic Studies				
Groups	***n***	**Procedure**	**Reason**	
3	2	Bead implantation 2 wks prior to 4 h LV Pace	To determine if bead implantation on the day of LV pacing preconditions or stuns myocardium, which in turn diminishes the inflammatory response	

Table 4.5.2. Hemodynamic parameters. Hemodynamic values (means±sem); HR=heart rate, LVSP=left ventricular systolic pressure; LVEDP=left ventricular end diastolic pressure, ±dP/dt, increase (+) or decrease (-) of left ventricular pressure.

Acute Group (n=4)			
	Beginning Atrial	**4 h LV Pace**	**Late Atrial**
HR, beats/min	108±6	113±6	112±6
LVSP, mmHg	130±9	123±5	131±7
LVEDP, mmHg	9±2	9±1	9±1
+ dP/dt, mmHg/s	2228±441	1978±341	1832±161
-dP/dt, mmHg/s	-2213±333	-2122±286	-2120±144
Chronic/No Beads Group (n=4)			
	Beginning Atrial	**4 h LV Pace**	**Late Atrial**
HR, beats/min	108±8	115±3	115±3
LVSP, mmHg	129±9	112±3	123±3
LVEDP, mmHg	9±2	7±1	6±2
+ dP/dt, mmHg/s	2952±774	2060±321	2296±664
-dP/dt, mmHg/s	-3210±468	-2241±221	-2620±191

Figure 4.5.3. Time course of end-systolic strains at the early activated site in acute (n=4) and chronic studies(n=2). Subepicardial, midwall, and subendocardial represent 25%, 50%, and 75% wall depth. Values are mean± sem.

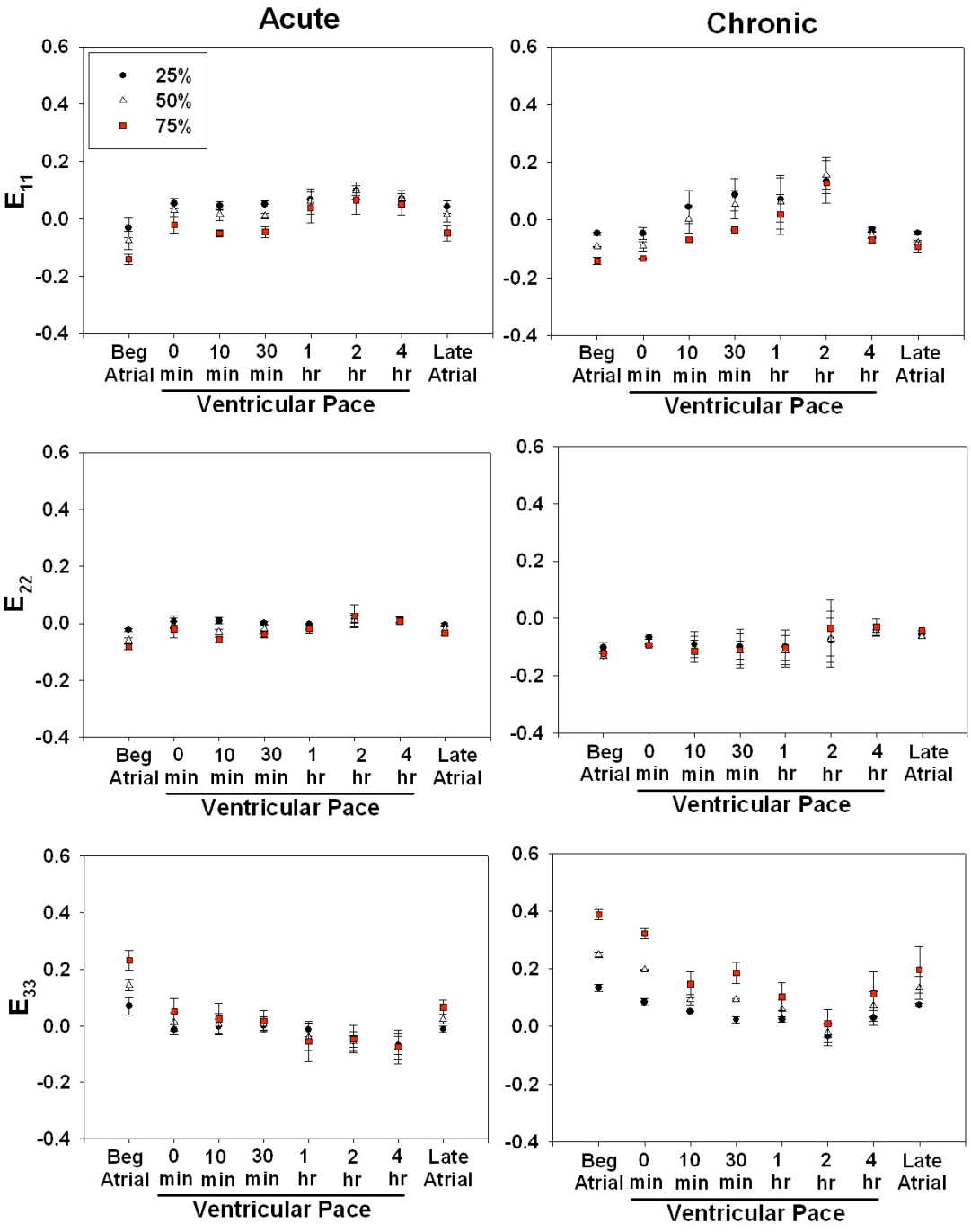
Acute
Chronic
25%
50%
75%
E_{11}
E_{22}
E_{33}
0.6
0.4
0.2
0.0
-0.2
-0.4
Beg Atrial
0 min
10 min
30 min
1 hr
2 hr
4 hr
Late Atrial
Ventricular Pace

Figure 4.5.4. End systolic normal strains in acute (n=4) and chronic (n=2) studies at beginning atrial, 1 min LV pace, 4 h LV pace and late atrial periods. Subepicardial, midwall, and subendocardial represent 25%, 50%, and 75% wall depth. Values are mean± sem (n=6).

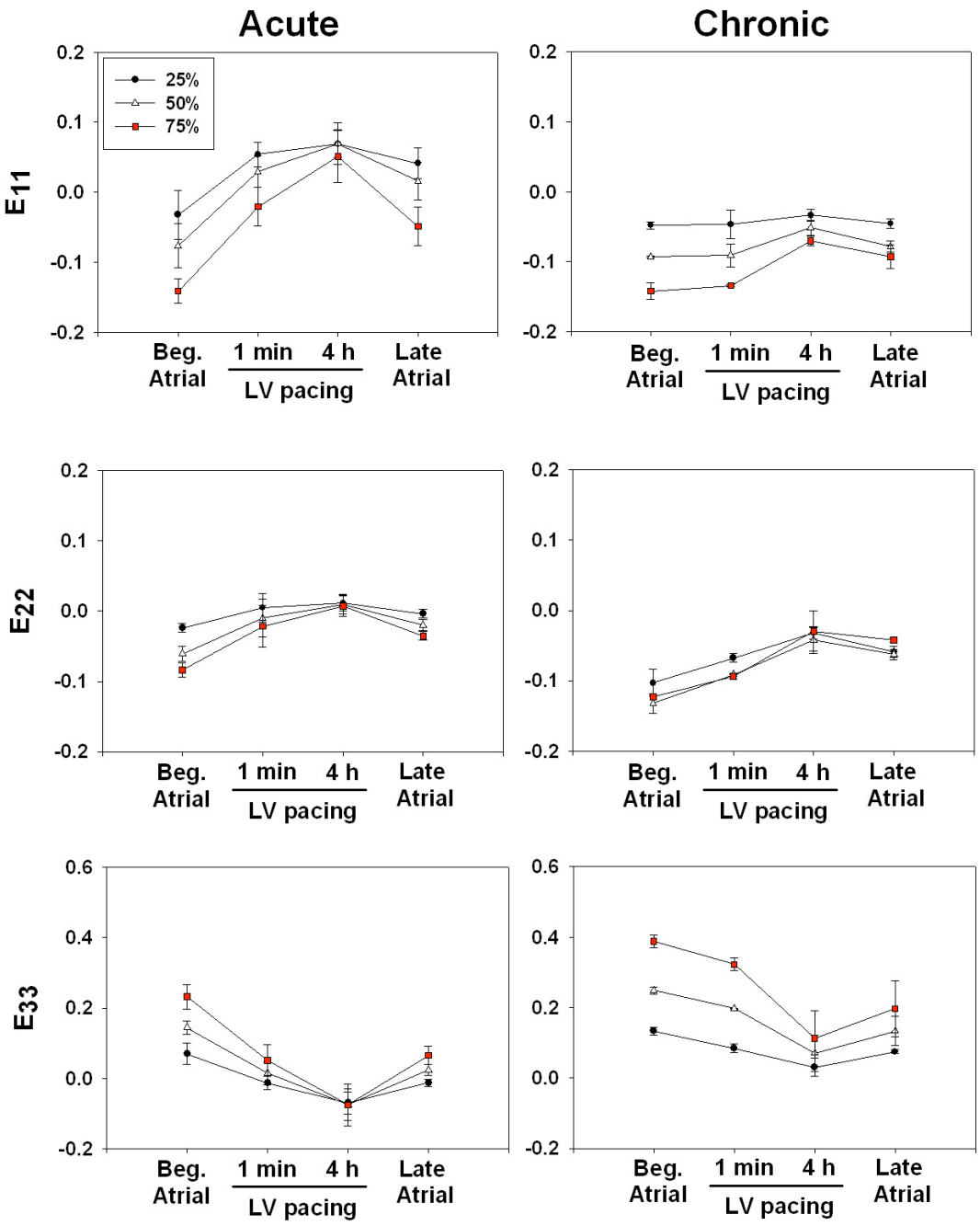
Acute
Chronic
25%
50%
75%
E11
E22
E33
0.2
0.1
0.0
-0.1
-0.2
0.6
0.4
Beg. Atrial
1 min
4 h
Late Atrial
LV pacing

Figure 4.5.4 Effects of bead implantation on neutrophil infiltration in paced animals. MPO activity at the bead set, areas around the bead set and posterior wall in acute (n=4) or chronic/no beads (n=4) animals. Values are means ± sem. AU=arbitrary units.

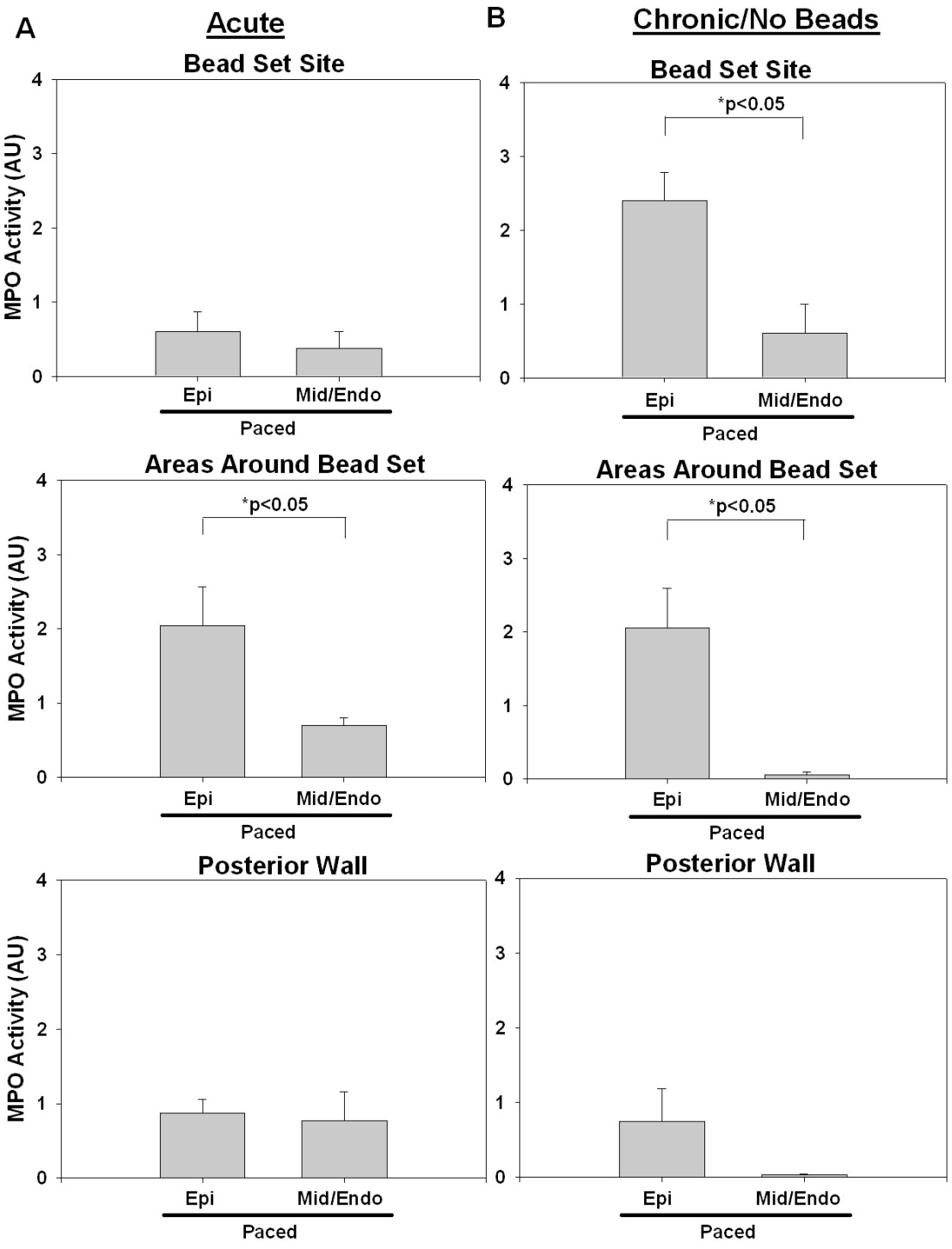
A
Acute
B
Chronic/No Beads
Bead Set Site
Bead Set Site
*p<0.05
MPO Activity (AU)
0
1
2
3
4
Epi
Mid/Endo
Paced
Areas Around Bead Set
Areas Around Bead Set
*p<0.05
*p<0.05
Posterior Wall
Posterior Wall

Figure 4.5.5 Effects of bead implantation on oxidative stress at the bead set, areas around the bead set and posterior wall in acute (n=4) or chronic/no beads (n=4) animals. Values are means ± sem.

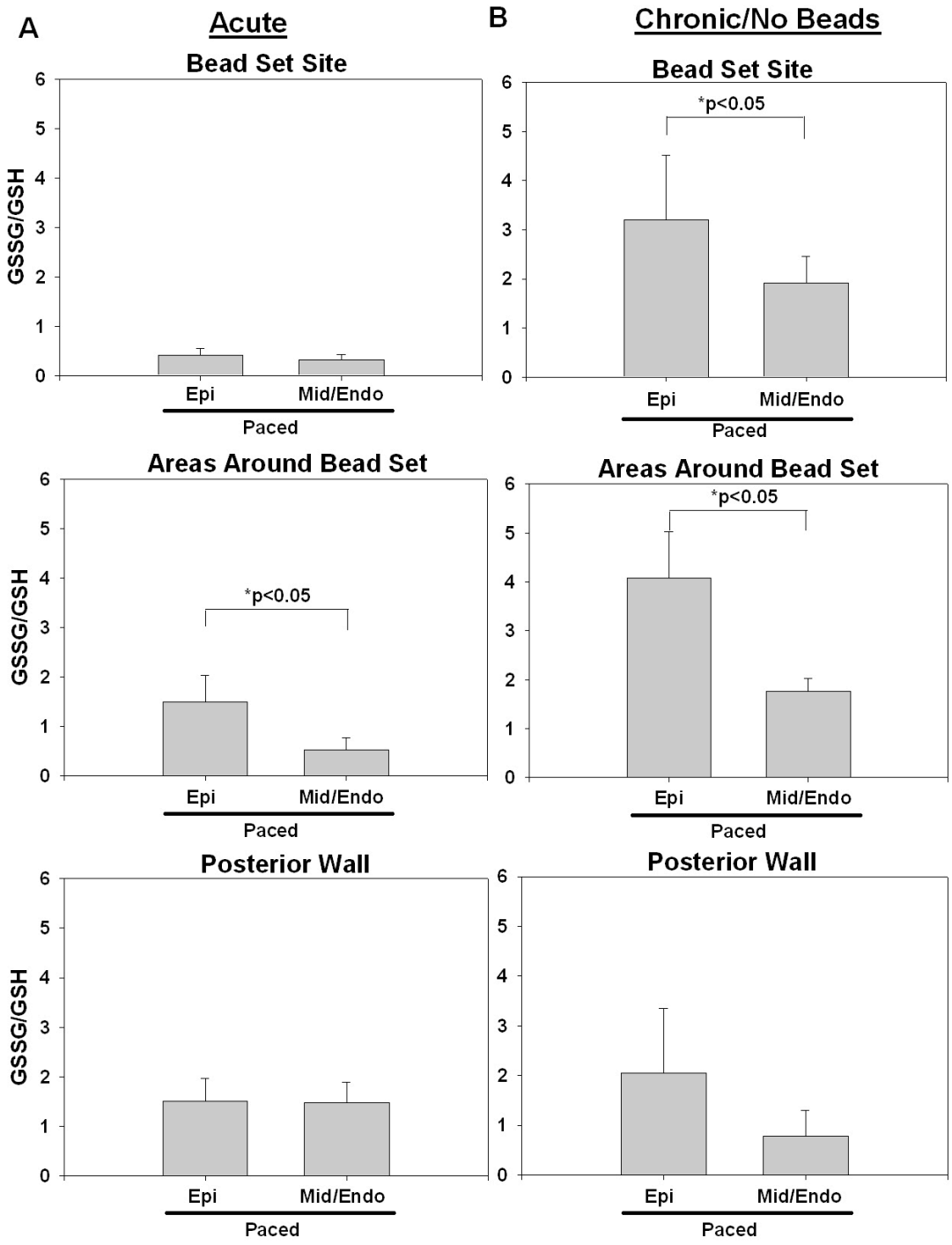
A
Acute
B
Chronic/No Beads
Bead Set Site
Areas Around Bead Set
Posterior Wall
GSSG/GSH
0
1
2
3
4
5
6
*p<0.05
Epi
Mid/Endo
Paced

Figure 4.5.6 Effects of bead implantation on 92 kDa MMP-9 activity in paced animals. 92 kDa MMP-9 activity at the bead set, areas around the bead set and posterior wall in acute (n=4) or chronic/no beads (n=4) animals. Values are means ± sem. ADU=arbitrary density units.

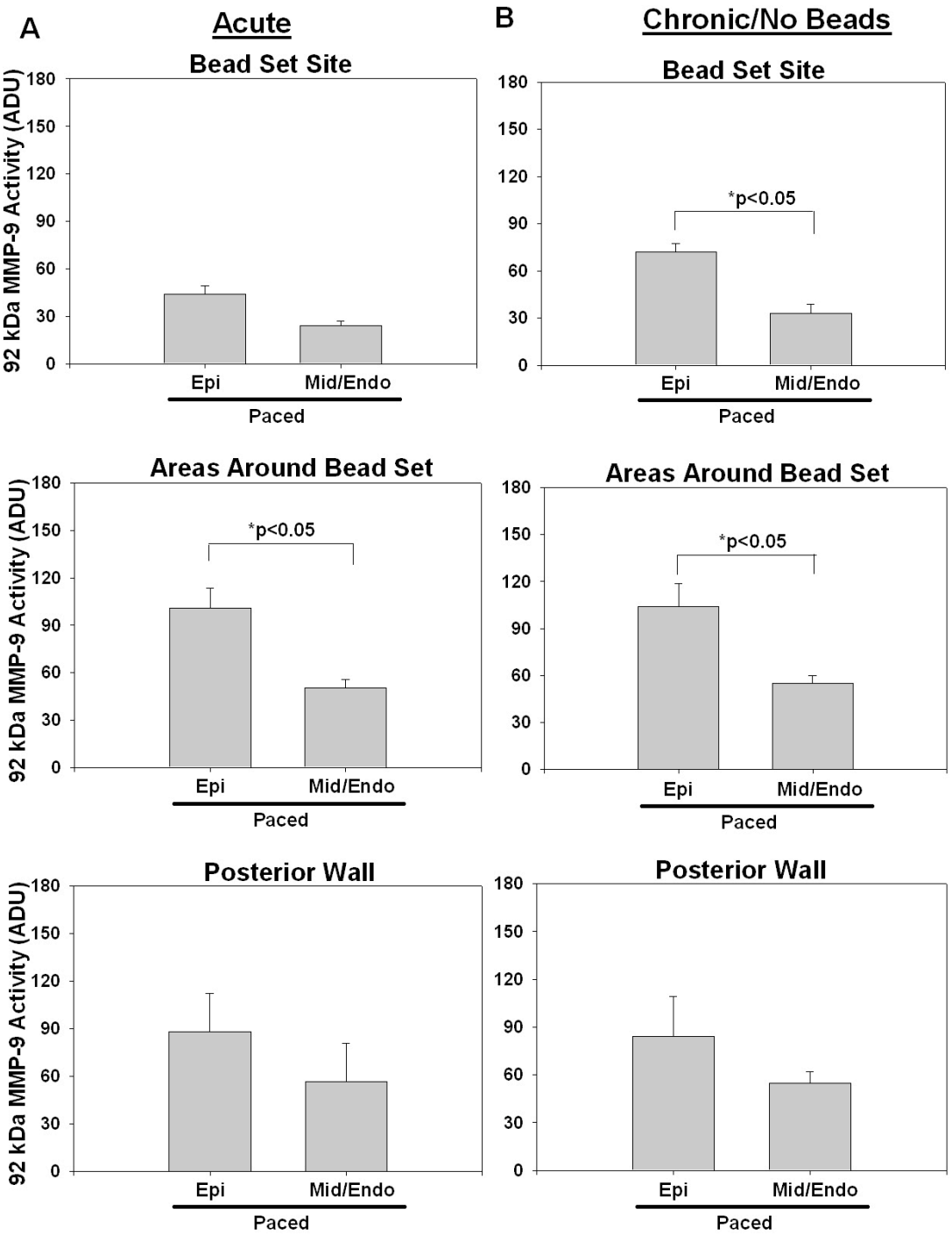
A
Acute
B
Chronic/No Beads
Bead Set Site
Bead Set Site
92 kDa MMP-9 Activity (ADU)
180
150
120
90
60
30
0
*p<0.05
Epi
Mid/Endo
Paced
Areas Around Bead Set
Areas Around Bead Set
Posterior Wall
Posterior Wall

Chapter 5. Changes in transmural LV function and inflammatory responses associated with myocardial dyskinesis

5.1 Introduction

Electrical pacemaker impulses originate in the sinus node and propagate through the atria reaching the atrioventricular node and the His-Purkinje system.[7] The role of the His-Purkinje system is to efficiently conduct the electrical impulses so that a highly synchronized activation (< 40 ms) of the ventricles occur,[9] thus, maximizing the efficacy of ventricular contraction. An interruption in the electrical conduction system can create regions of early and late activation, leading to local dyskinesis and a dyssynchronous contraction pattern referred to as ventricular dyssynchrony.[2]

Approximately 30% of CHF patients have abnormal electrical conduction, which leads to ventricular dyssynchrony.[1] LBBB is the most common type of electrical conduction abnormality found in CHF patients and can also occur in apparently healthy individuals.[3] Risk factors for developing a LBBB are: (1) anatomic malformations in the conduction system; (2) hypertension; (3) scar tissue; and (4) myocarditis.[13]A significant percentage of CHF patients that suffer from asynchronous LV contraction, are subjected to CRT with the aim of eliminating ventricular dyssynchrony. Patients that respond favorably to CRT demonstrate significant improvements in quality of life, diastolic and systolic function, overall cardiovascular morbidity and mortality, and reverse ventricular remodeling.[5, 6, 31]

It has been reported that the induction of ventricular dyssynchrony in canine hearts leads to LV remodeling. Using a chronic model of ventricular dyssynchrony induced by LV pacing, van Oosterhout demonstrated that early-activated LV regions became significantly thinner, whereas the late-activated region thickened significantly.[15] We previously reported that short term LV pacing (4 h), significantly increased neutrophil infiltration (i.e. inflammation), as determined by MPO activity, at the early activated dyskinetic site relative to a remote site.[32] Increases in MPO activity correlated with significant increases in ROS generation, MMP activity and collagen degradation.[32] These events, if sustained long term, may partly explain LV remodeling observed with myocardial dyskinesis. To gain further insight into the mechanisms that trigger ventricular dyssynchrony induced changes in LV structure/function a 3D assessment of LV function and of the transmural distribution of inflammatory responses is needed.

Thus, the major objectives of this study are to: (1) assess dyskinesis induced changes in 3D LV function in early activated regions, and (2) evaluate the transmural distribution of local dyskinesis induced inflammatory responses. For this purpose, we implemented a canine model to determine transmural differences in LV function and inflammatory responses.

5.2 Methods

5.2.1 Animal Studies

All procedures were approved by the Institutional Animal Care and Use Committee and conform to published NIH guidelines for animal research.

5.2.2 Surgical Preparations

A total of fifteen adult male dogs (seven mongrel; eight beagles) weighing between 12-28 kg were used. All animals used in chapter four are included in these studies. For terminal studies, animals were anesthetized with pentobarbital sodium (25-30 mg/kg IV), intubated, and mechanically ventilated using a Harvard respirator. Continuous IV infusion of pentobarbital sodium (0.15-0.25 mg/kg hr) was used to maintain a surgical plane of anesthesia. The heart was exposed via a medial sternotomy and left thoracotomy at the 5^{th} intercostal space and supported in a pericardial cradle. LVP was recorded with a pigtail micromanometer catheter (Millar Instruments, Houston, TX) inserted into the left femoral artery and advanced into the LV. AoP was measured with a fluid-filled catheter placed in the aortic arch. AoP, LV pressure, and surface ECG were monitored throughout the study.

5.2.3 Transmural Bead Array Implantation

To assess 3D finite strains, three columns of three to four 0.8-mm-diameter-gold beads were inserted across the LV anterior wall between the first

and second diagonal branches of the LAD coronary artery. After bead implantation, 1.7-mm-diameter surface gold beads were sewn on the epicardium above each column. Gold beads (2mm diameter) were sutured to the apical dimple (apex bead) and on the epicardium at the bifurcation of the LAD and left circumflex coronary artery (base bead) to provide endpoints for the LV long axis. Figure 5.5.1 shows a schematic diagram of the surgical preparation.

5.2.4 Study groups and study design

To assess the effects of instrumentation and anesthesia on LV function and inflammatory responses, three dogs served as shams that were instrumented, but not paced. In another group (n=4), animals underwent instrumentation and bead implantation, but no pacing and served as controls. There were no statistical differences between these two groups in all measured parameters (hemodynamics, MPO activity, oxidative stress levels, and MMP-9 activity), and therefore the results were combined to generate our control group (n=7).

Four animals were instrumented, underwent bead implantation and 4 h LV pacing. Another group (n=2) underwent instrumentation and 4 h of LV pacing induced dyssynchrony in the absence of beads. In an additional sub-group of animals (n=2), animals underwent a thoracotomy 2 weeks prior to the initiation of LV pacing. In this group, animals were anesthetized with intravenous propofol (6 mg/kg), intubated, and mechanically ventilated with isoflurane (0.5-2.5%), and medical oxygen (2 L/min) to maintain a surgical plane of anesthesia.

The heart was exposed via a left thoracotomy at the fifth intercostal space. After a pericardial dissection, a transmural bead array was implanted. The chest was closed and the animals were allowed to recover. Two weeks post-thoracotomy, the animals underwent a terminal study as described above. Comparisons between the three groups yielded no statistical difference in any of the measured parameters, and therefore results were combined to generate the paced group (n=8).

Bipolar pacing electrodes were sutured to the left or right atrium, and a second set was sutured to the epicardium of the LV within the bead set site. Atrial pacing was performed using atrial electrodes. LV pacing by using atrial and LV electrodes with an A-V delay of 40-60 ms. All pacing protocols were conducted using a square-wave, constant-voltage electronic stimulator (Grass Instruments, Quincy, MA) at a frequency 10-20% above baseline heart rate to suppress native sinus rhythm. Stimulation parameters (voltage 10% above threshold, duration 8ms, and frequency) were kept constant in each animal. Zetabradine (0.5 mg/kg) was administered to dogs with heart rates >110 beats/min to reduce intrinsic heart rate. Each animal was positioned in a biplane X-ray system, and synchronous biplane cineradiographic images of bead displacement were digitally acquired with mechanical ventilation suspended at end expiration. LVP, AoP, and ECG were recorded simultaneously. During LV pacing, electromechanical dyssynchrony was verified by the widening of the QRS complex and depression of +dP/dt.

The recordings of physiological parameters in the control group (atrial pace group) took place immediately after instrumentation (beginning atrial), at 4 h, and immediately after (late atrial). In the paced group, recordings took place immediately after instrumentation with atrial pacing (beginning atrial), 4 h under LV pacing, and then immediately after under atrial pacing (late atrial). Additional recordings took place in all animals between the beginning atrial and 4 h timepoints. For practical purposes, only a select sampling of such data may be shown.

5.2.5 Sacrifice protocol and tissue collection

After 4 h of atrial or LV pacing animals were euthanized with pentobarbital sodium (200 mg/kg), the hearts excised, and myocardial sections (see below) were rapidly cooled and semi-frozen. Myocardial samples were taken from the bead site and two adjacent regions, as well as from the posterior wall. Adjacent sites were basal to the bead set, and lateral to the bead set (Figure 5.5.1). In order to examine transmural differences in inflammatory responses, each of these four regions were sectioned into 2 mm slices from the epicardium to the endocardium (typically 6-9 slices per region) and samples were stored at -80°C.

Initial evaluations of inflammatory parameters were performed to compare responses in basal vs. lateral regions. Results indicate no statistical differences in any of the measured inflammatory parameters, thus biochemical

results from these two regions were combined and referred to as areas around the bead set. Similar comparisons were made within each study group comparing transmural responses of inflammatory parameters. Samples encompassed within the outer third of the LV wall were defined as epicardial, middle third=midwall, and inner third=endocardial. Results indicated no statistical differences between midwall and endocardial samples in any of the measured inflammatory parameters, thus results are combined and referred to as Mid/Endo.

5.2.6 Transmural Bead Array Analysis

The 3D coordinates of the implanted gold beads were obtained from the spherically corrected data set for an entire cardiac cycle selected in each animal.[77] In principle, continuous, nonhomogenous transmural distributions of 3D finite strains were computed.[76] Six independent finite strains [circumferential strain (E_{11}), longitudinal strain (E_{22}), radial strain (E_{33}), circumferential-longitudinal shear (E_{12}), longitudinal-radial shear (E_{23}), and circumferential-radial shear (E_{13})] were computed in the local cardiac coordinate axis (circumferential, longitudinal, and radial, respectively) system (X1, X2, X3) .The three normal strain components reflect myocardial stretch or shortening along the circumferential (E_{11}), longitudinal (E_{22}), or radial (E_{33}) cardiac axes.[77] Finite strains were calculated for each frame (125 frames/sec) as a deformed configuration with end diastole as the reference state at three wall depths: 25% (subepicardium), 50% (midwall),and 75% (subendocardium) wall depth from

the epicardial surface. End diastole was defined as the time of the peak of the ECG R-wave for atrial pacing and the ventricular pacing artifact for the LV epicardial pacing. We chose the V-spike rather than the peak of the R-wave as the reference state for LV epicardial pacing because the former reflects the timing of the activation of the pacing site, as opposed to the latter, which represents the timing of activation of the whole ventricle.[75] End systole was derived from the dichrotic notch of the central aortic pressure.

5.2.7 Myeloperoxidase activity

Tissue samples were homogenized in ice-cold buffer (50mM KH_2PO_4 and 0.5% hexadecyltrimethylammonium bromide, pH 6.0). Homogenates were incubated on ice for 30 min and centrifuged at 4°C for 5 min. Following centrifugation, the supernatants were reacted with 0.8mM tetramethylbenzidine (Sigma; St. Louis, MO) and 0.006% H_2O_2 in 50mM KH_2PO_4.Kinetic absorbance measurements of MPO activity were immediately monitored at 655 nm (readings every 40s for ~20 min). Substrate cleavage rates were determined from the linear regions of the kinetic curve. Data were normalized to protein concentrations determined the BCA protein assay kit (Pierce, Rockford, IL).

5.2.8 Glutathione (GSSG/GSH) Assay

Reduced and oxidized glutathione, GSH and GSSG respectively, levels were determined as previously described.[78] Briefly, tissue samples were homogenized in ice cold homogenization buffer (154mM KCL, 5mM

diethylenetriaminepentaacetic acid (DPTA), and 0.1M potassium phosphate, pH 6.8). After centrifugation, an aliquot was removed for protein determination using the BCA protein assay kit. Immediately after an aliquot was taken, one volume of cold acid buffer (40mM HCl, 10mM DPTA, 20mM ascorbic acid, and 10% trichloroacetic acid (TCA) was added to the homogenate. The suspension was centrifuged and the resulting supernatant solution was centrifuged through a 0.45m microcentrifuge filter (Millipore Corp., Bedford, MA). GSH and GSSG levels were determined using the fluorophore *o*-phtaladehyde.

5.2.9 Gelatin Zymography

Samples were homogenized in 10mM HEPES, pH 7.5, 150mM NaCl, 0.2mM EDTA, 25% glycerol, with protease inhibitor cocktail (Sigma). Samples (10g of protein) was loaded onto a 10% SDS-PAGE gel substituted with 0.1% gelatin and then stained with 0.5% coomassie blue. Bands of MMP-2 and/or MMP-9 gelatinolytic activity were digitally quantified with Image J.

5.2.10 Westerns

Western blots were used to determine increases in MMP-9 protein levels. Briefly, equal amounts of total protein were separated by 10% SDS-PAGE gels under reducing conditions and transferred onto a polyvinylidene difluoride membrane. Membranes were blocked in 5% nonfat milk in tris-buffered saline that contained 0.1% Tween 20 (TTBS) and were exposed to MMP-9 primary

antibody. Membranes were incubated for 1 h at room temperature with the respective secondary horseradish peroxidase-labeled antibody and then developed using an ECL Plus detection system (Amersham Pharmacia Biotech; Buckinghamshire, UK).

5.2.11 Data analyses and statistics

Results were expressed as mean ± SEM. Comparisons between means were analyzed, as appropriate, by student's *t*-test, one-way ANOVA, or two-way ANOVA followed by Bonferroni post-hoc analysis. A value of $p<0.05$ was considered statistically significant.

5.3 Results

5.3.1 Hemodynamics

Comparisons of data measured during beginning atrial, and late atrial in control animals did not reveal any significant changes in heart rate, LVP, LV end-diastolic pressure, or ±dP/dt. In the LV paced group, no significant changes were observed in heart rate, LV systolic pressure, or LV end-diastolic pressure at beginning atrial compared to 4 h LV pacing or late atrial. However, peak +dP/d*t* was significantly depressed at 4 h LV pacing and late atrial (*$p<0.05$, paired t-test; Table 5.5.2).

5.3.2 Ventricular function

Figure 5.5.3 shows a representative time course of normal strains (E_{11}, E_{22}, and E_{33}) at 25, 50, and 75% depth in an animal subjected to LV pacing. At the beginning atrial period E_{11}, E_{22}, and E_{33} demonstrates a simple contraction-relaxation pattern with peak strains near end systole. With LV pacing, E_{11} and E_{22} demonstrated early shortening during diastole, while E_{33} demonstrated early wall thickening during diastole and also during late systole. However, LV contractile function decreases notably at 4 of h LV pacing at all depths. As seen during late atrial pacing, the early activated site partly recovered a normal contractile pattern.

Figure 5.5.4 compares averaged end-systolic normal strains from control and paced animals. All other strain components are in Table 5.5.6 and 5.5.7. Data demonstrates a significant loss of E_{11} and E_{33} from 1 min to 4 h of LV pace. Loss of circumferential shortening and wall thickening was more severe in the endocardium than in the epicardium (E_{11}, $p<0.02$; E_{33}, $p<0.01$; 2-way ANOVA). Results also show significant loss of E_{33} during the late atrial timepoint ($p<0.01$; 2-way ANOVA) suggesting wall thickening only partly recovers after 4 of h LV pacing. These results contrast with those observed in control animals, where contraction patterns observed during the beginning atrial period remained essentially unaltered as a function of time (Figure 5.5.4). Endocardial loss of E_{33} is unrelated to the effects of instrumentation and anesthesia as there is a significant difference between control (group B) and paced animals ($p<0.01$; 2 way ANOVA; Figure 5.5.5).

5.3.3 Neutrophil infiltration

We assessed the capacity of local dyskinesis to alter inflammatory cell infiltration across the myocardium by measuring MPO activity. A significant 3-fold increase in MPO activity was observed in areas around the bead set in paced vs. control animals (2.1±0.4 vs. 0.72±0.21 AU; $p<0.01$; t-test; Figure 5.5.8.A). Results also demonstrate a 5-fold increase in epicardial vs. mid/endo MPO activity in areas around the bead set (2.1±0.4 vs. 0.39±0.1 AU; $p<0.01$; paired t-test). Posterior wall samples from paced animals had comparable MPO

activity to controls, and no significant differences were seen between the epicardium (epi) and mid/endo.

5.3.4 Oxidative stress

Figure 5.5.8.B summarizes oxidative stress results from myocardium of control and paced animals. Results are shown as GSSG/GSH, which is a measure of total tissue oxidative stress. Oxidative stress was significantly increased by ~5-fold in the epicardium of paced vs. control animals (2.5 ± 0.6 vs. 0.47±0.1; $p<0.01$; t-test) in areas around the bead set (Figure 6-I). There was also a significant 2-fold difference in the epi vs. mid/endo (2.5± 0.6 vs. 1.1±0.2; $p<0.01$; paired t-test) of paced animals in these areas.

5.3.5 MMP Activity

Gelatin zymography of tissue homogenates only revealed bands corresponding to 92 kDa MMP-9 and 72 kDa MMP-2. The 86 kDa MMP-9 was not visible. Densitometric analysis revealed significant increases in 92 kDa MMP-9 activity in paced vs. control animals in areas around the bead set (103±9 vs. 63±5 ADU; $p<0.01$; t-test; Figure 5.5.8.C). Moreover, 92 kDa MMP-9 activity was significantly increased two-fold in the epi vs. the mid/endo samples from the paced group in areas around the bead set (103±9 vs. 52±4 ADU; $p<0.01$; paired t-test). No statistical significance was found in

the posterior wall. As observed by densitometric analysis, no notable differences were identified in 72 kDa MMP-2 levels.

5.3.6 MMP-9 protein expression

Western blot analysis (Figure 5.5.8.D) demonstrated that there were no differences 92 kDa MMP-9 protein levels between control and paced animals in areas around the bead set (82±21 vs. 83±13 AU; p=ns; t-test), or in the posterior wall (51±14 vs. 63±15; p=ns; t-test). No significant transmural differences were found in either region.

5.4 Discussion

The present study demonstrated that 4 h of local epicardial activation induced local dyskinesis at the site of early activation and progressively depressed endocardial wall thickening, which did not recover upon discontinuation of LV pacing. In addition, an inflammatory response was localized to the epicardium.

Results from this study indicate that LV pacing leads to a progressive loss of systolic endocardial wall thickening. The loss of wall thickening was unrelated to the consequences of surgical instrumentation or implantation of columns of beads since no differences were observed in the control group, thus it occurred as a function of local dyskinesis. The loss of endocardial function may be secondary to the inflammatory response triggered by LV pacing. In our previous study where LV dyskinesis was induced by pacing, we demonstrated that inflammation induced MMP activity and collagen degradation[32]. Studies have demonstrated that regional damage to collagen resulting from MMP-mediated proteolysis can yield loss of ECM superstructure leading to myocyte slippage and loss of contractile function.[32, 56] However, the inflammatory response was limited to the outer third of the LV, thus the loss of the endocardial function must arise from an independent mechanism. There is evidence that metabolism and blood flow is altered in chronically early activated regions.[16] Prinzen and Reneman proposed that the reduction of blood flow is directly proportional to reduced local work in early activated regions. Their studies demonstrated an epicardial or global reduction in blood flow of about 20%. However,

no data is available on the transmural distribution of blood flow. The reduction in regional work estimated from the use of a mathematical model of ventricular contraction was found to be proportional to the reduction in blood flow.[79] Thus, the authors concluded that a no flow-function (i.e. ischemia driven) mis-match occurs in early activated regions. This conclusion is not supported by our findings on the progressive decrease in endocardial function during LV pacing and in particular, by the persistent depression following the return to normal activation.

It has been demonstrated that epicardial pacing induces the reversal of the transmural mechanical activation sequence, which depresses sheet extension and wall thickening early in the cardiac cycle [75]. It can be speculated that the reversal of the mechanical activation sequence can lead to reduced endocardial perfusion. Goto et al showed that cardiac contraction predominantly affects subendocardial vessels and impedes subendocardial more than subepicardial flow.[80] Thus, during early contraction, endocardial blood flow may be further impeded leading to brief periods of ischemia. Therefore, it can be speculated that the loss of endocardial function seen in our study mimics the "repetitive stunning" hypothesis, in which the subendocardium is subjected to repetitive brief episodes of ischemia during early contraction leading to stunning, which trigger a "sustained" depression of contractile function.[81] The elucidation of this issue awaits further investigation.

Studies in chronic models of dyssynchrony have shown that interventricular conduction delay worsens myocardial efficiency and leads to marked increases in wall

stress heterogeneity, where wall stress is highest in late-activated myocardial regions.[25, 30] In an animal model of non-failing dyssynchrony, Spragg et al found that sarcoplasmic reticulum CA^{2+}-ATPase, phospholamban, and gap junction protein connexin-43 expression were comparable to controls and that no transmural gradient existed.[29] However, in a rapid pacing heart failure model in the presence of dyssynchrony, late-activated myocardium demonstrated a 2-fold increase in phosphorylated *Erk* , a 30% decline in sarcoplasmic reticulum CA^{2+}-ATPase, an 80% reduction in phospholamban, and a 60% reduction in gap junction protein connexin-43, relative to neighboring myocardium with more severe decreases in endocardium vs. epicardium.[25, 30] Chakir et al demonstrated that in animals with six months of dyssynchronous heart failure, there was an increase in mitogen activated kinase p38, calcium-calmodulin-dependent kinase, tumor necrosis factor-α, apoptosis and pro-apoptotic pathways in high stress regions of the heart.[30] These results indicate that LV mechanical dyssynchrony superimposed with HF induces marked regional heterogeneity of protein expression at the site of greatest hemodynamic load or stress[25], whereas long-term dyssynchrony appears to do little to alter a select group of remodeling markers. In a previous study. We hypothesized that at sites of early activation (as induced by ventricular dyssynchrony), an inflammatory response may be triggered. Initial supportive evidence was generated to this effect. However, obtaining greater insight into the transmural distribution of the inflammatory process may allow us to better identify the mechanism responsible for ventricular dyssynchrony induced changes in cardiac structure/function.

To investigate the inflammatory responses in a transmural fashion, we developed a tissue slicer that allowed us to take serial 2 mm sections from the epicardium to the endocardium. Our results are similar to our previous study, in that there were 2-3 fold increases in neutrophil infiltration at the early activated site. Increases in 92 kDa MMP-9 activity were more pronounced in the previous study (~40-fold) compared to the present study (~2-fold). It is not clear why MMP activity was greater in our previous study, but sample size, location, and the differences in instrumentation (columns of beads vs. sonomicrometer crystals) may explain the differences. A surprising finding of this study is that the inflammatory responses are localized to the epicardial (outer 1/3) layer of the LV wall. If acute inflammatory responses are to act as initial triggers for long-term structural changes in the remodeled LV, it is reasonable to speculate that the remodeling of the LV is to differ transmurally. In a canine model, animals were paced from the base of the LV free wall for 6 months at physiological heart rates.[15] Results from this study showed that the early activated LV free wall became significantly thinner (~17%), whereas the late activated septum thickened significantly (~23%) compared to control animals. They also found that cardiomyocyte diameter was significantly larger (~18%) in the septum than in the LV free wall of paced hearts. However, no studies have examined the transmural distribution by layers of the remodeling responses. If the inflammatory events were initially responsible for localized remodeling, then long-term studies assessing the transmural distribution of LV remodeling would predict that thinning of the LV wall would be mostly localized to the outer 1/3 of the chamber.

In conclusion, our results demonstrate that local dyskinesis causes a loss in endocardial wall thickening over time. More importantly, our results show an epicardial localization of inflammatory responses. The apparent lack of relationship between these observations and the underlying mechanisms awaits further investigation.

5.5 Acknowledgements

Chapter 5, in part, has been submitted for publication as it might appear as Yamazaki KG, Covell JW, Ihm SH, Roth D, Villarreal FJ. *Circulation*. 2009. The dissertation author was the primary author on this manuscript.

Figure 5.6.1.Schematic diagram of transmural bead array and experimental design. Cineradiographic images are also shown. Top: anterior-posterior view; Bottom: lateral view. Yellow box=bead set site; Blue boxes; areas around bead set for sampling protocol.

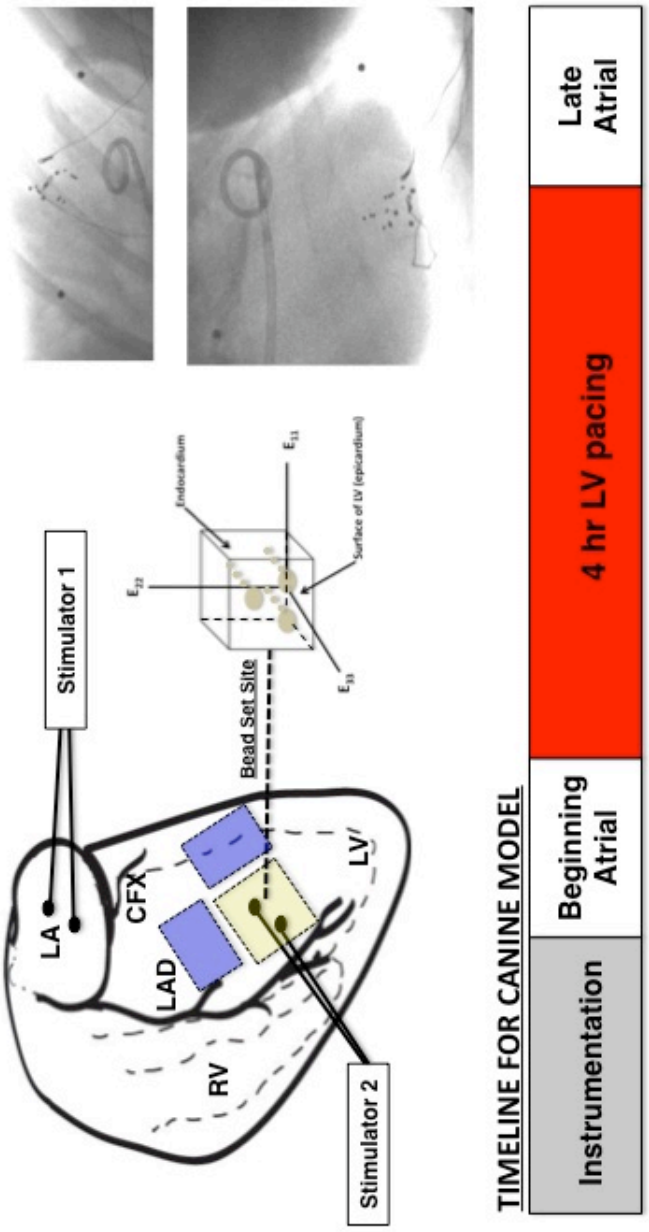
Stimulator 1
LA
CFX
LAD
RV
LV
Bead Set Site
Stimulator 2
Endocardium
Surface of LV (epicardium)
TIMELINE FOR CANINE MODEL
Instrumentation
Beginning Atrial
4 hr LV pacing
Late Atrial

Table 5.6.2. Hemodynamic measurements. Values are means±sem; Control group n=7; Paced Group n=8;HR, heart rate, LVS.P, left ventricular systolic pressure; LVEDP, left ventricular end diastolic pressure, ±dP/dt, increase (+) or decrease (-) of left ventricular pressure.*$p<0.05$ vs. Beginning atrial. na=non-applicable

Control Group			
	Beginning Atrial	**4 h LV pacing**	**Late Atrial**
HR, beats/min	120±5	Na	121+5
LVSP, mmHg	137±6	Na	121±6
LVEDP, mmHg	13±2	Na	10±3
+ dP/dt, mmHg/s	2632±354	Na	2617±191
-dP/dt, mmHg/s	-2524.2±234	Na	-2410±283
Paced Group			
	Beginning Atrial	**4 h LV pacing**	**Late Atrial**
HR, beats/min	108±5	114±3	113±3
LVSP, mmHg	129±6	118±4	127±4
LVEDP, mmHg	9±1	8±1	8±1
+ dP/dt, mmHg/s	2538±403	2013±220*	2030±281*
-dP/dt, mmHg/s	-2640±322	-2173±176	-2334±146

Figure 5.6.3. Representative time course of normal strains at the early activated site. Circumferential strain (E_{11}), longitudinal strain (E_{22}), and wall thickness (E_{33}) are shown. Subepicardial, midwall, and subendocardial represent 25%, 50%, and 75% wall depth. Left ventricular pressures (LVP) are noted. The reference frame for strain calculation was end-diastole for atrial pacing or the timing of the stimulus artifact for LV pacing.

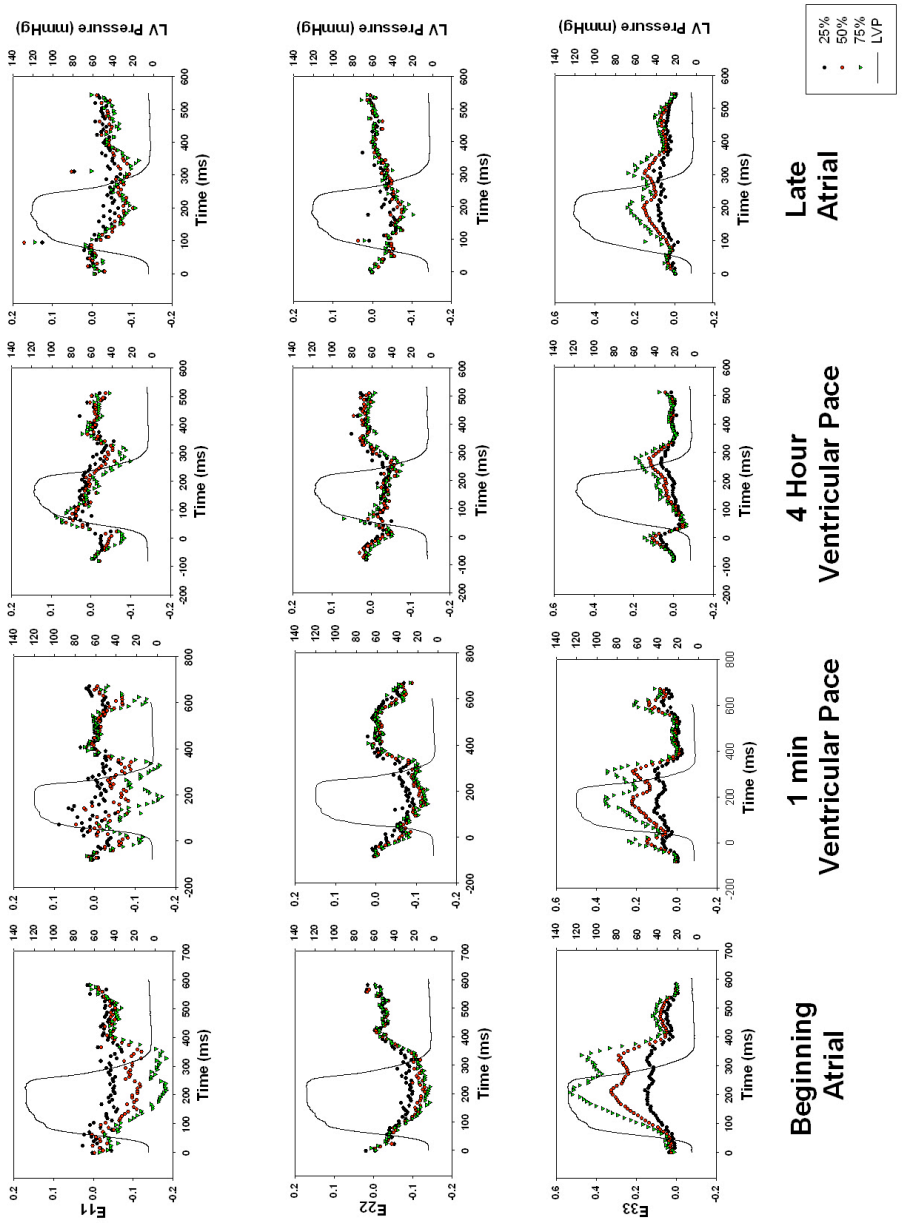
Beginning Atrial
1 min Ventricular Pace
4 Hour Ventricular Pace
Late Atrial
LV Pressure (mmHg)
Time (ms)
E11
E22
E33
25%
50%
75%
LVP

Figure 5.6.4. End systolic E_{11}, E_{22}, and E_{33} strains in control (n=4) and paced animals (n=6) at beginning atrial, 1 min LV pace, 4 h LV pace and late atrial periods. circumferential strain (E_{11}), longitudinal strain (E_{22}), and wall thickness (E_{33}) are shown. Subepicardial, midwall, and subendocardial represent 25%, 50%, and 75% wall depth. Values are mean± sem.

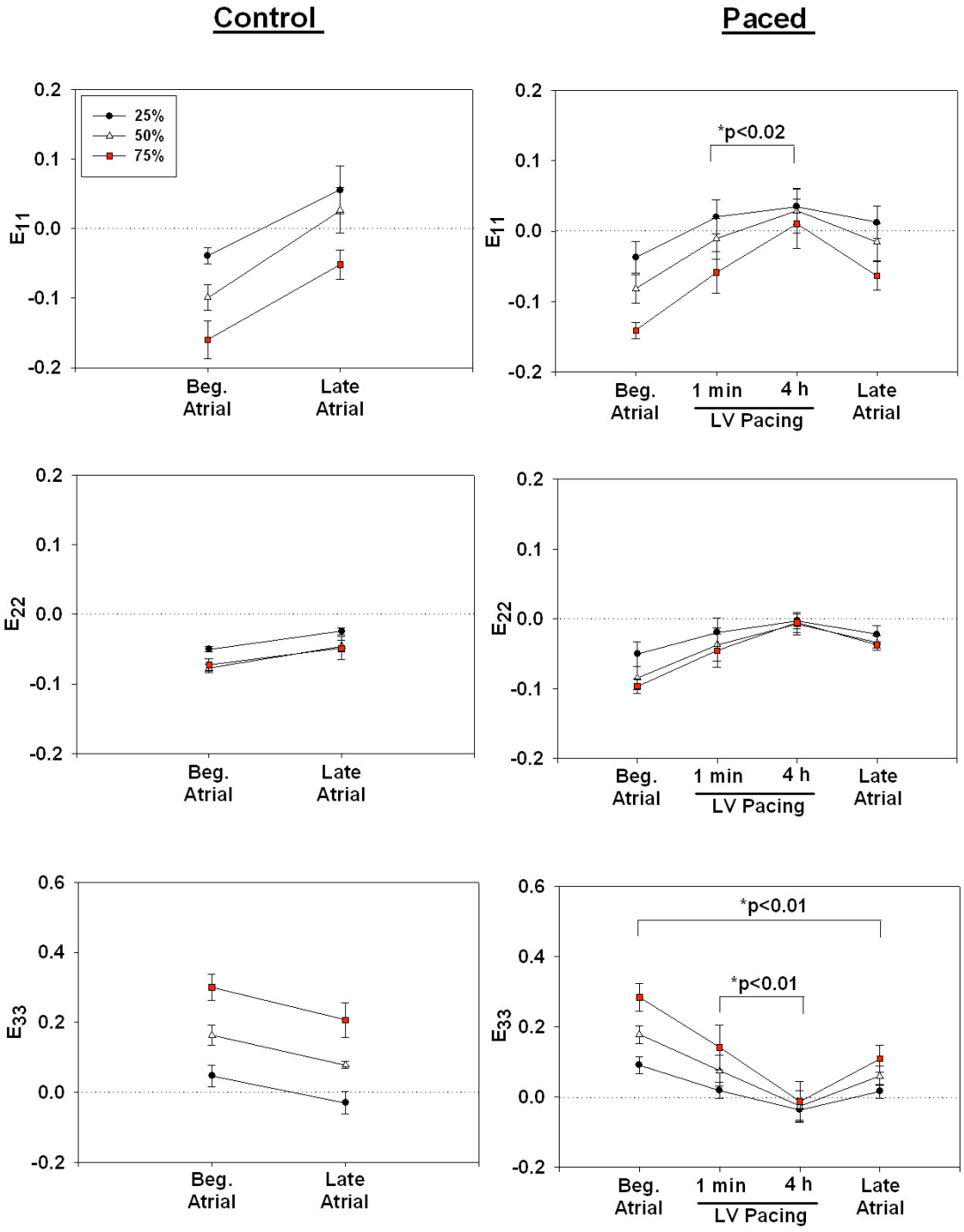
Control
Paced
25%
50%
75%
E_{11}
E_{22}
E_{33}
0.2
0.1
0.0
-0.1
-0.2
0.6
0.4
*p<0.02
*p<0.01
*p<0.01
Beg. Atrial
Late Atrial
1 min
4 h
LV Pacing

Figure 5.6.5. End systolic normal strains in control (n=4) and paced (n=6) animals at the beginning atrial and late atrial periods. Circumferential strain (E_{11}), longitudinal strain (E_{22}), and wall thickness (E_{33}) are shown. Subepicardial, midwall, and subendocardial represent 25%, 50%, and 75% wall depth. Values are mean±sem. *$p<0.01$ Beg vs. late atrial; 2 way ANOVA.

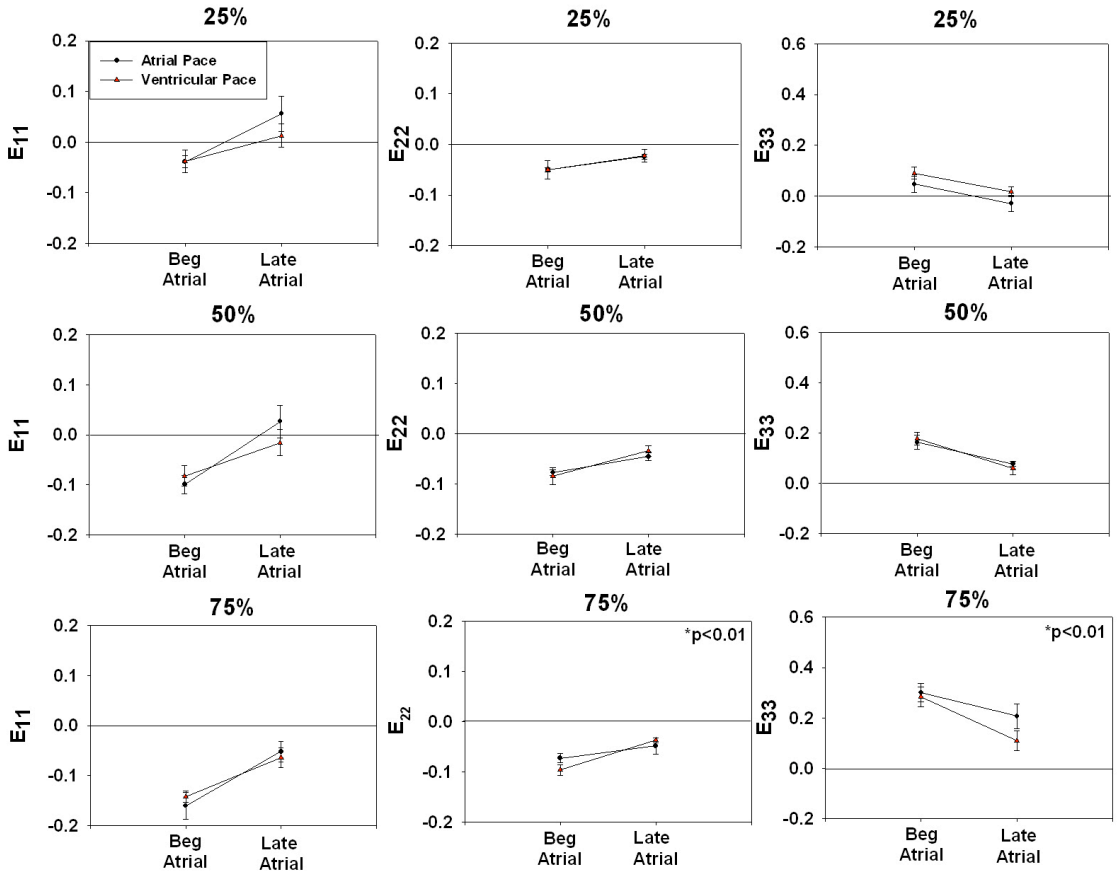
25%
50%
75%
Atrial Pace
Ventricular Pace
E11
E22
E33
0.2
0.1
0.0
-0.1
-0.2
0.6
0.4
Beg Atrial
Late Atrial
*p<0.01

Table 5.6.6 Three dimensional end systolic strains in control animals (n=4). Average three-dimensional end systolic strains for controls (mean ± sem). 25%= subepicardium; 50%= midwall; 75%= subendocardium. E_{11}= circumferential strain= E_{22}, longitudinal strain; E_{33}= radial strain; E_{12}=circumferential-longitudinal shear strain; E_{23}= longitudinal-radial shear strain; E_{13}=circumferential-radial shear strain. na=not applicable.

Control Group (n=4)				
25%	**Beginning Atrial**	**1 min LV Pace**	**4 h LV Pace**	**Late Atrial**
E_{11}	-0.039±0.012	na	na	0.056±0.035
E_{22}	-0.050±0.004	na	na	-0.024±0.005
E_{33}	0.047±0.031	na	na	-0.030±0.032
E_{12}	-0.016±0.025	na	na	0.013±0.027
E_{23}	-0.028±0.023	na	na	-0.015±0.018
E_{13}	0.021±0.019	na	na	0.030±0.007
50%	**Beginning Atrial**	**1 min LV Pace**	**4 h LV Pace**	**Late Atrial**
E_{11}	-0.099±0.019	na	na	0.026±0.033
E_{22}	-0.078±0.006	na	na	-0.046±0.008
E_{33}	0.163±0.029	na	na	0.078±0.010
E_{12}	-0.016±0.025	na	na	0.016±0.025
E_{23}	-0.007±0.020	na	na	-0.008±0.015
E_{13}	0.024±0.032	na	na	0.040±0.025
75%	**Beginning Atrial**	**1 min LV Pace**	**4 h LV Pace**	**Late Atrial**
E_{11}	-0.160±0.027	na	na	-0.052±0.021
E_{22}	-0.073+0.009	na	na	-0.049±0.017
E_{33}	0.300±0.037	na	na	0.207±0.050
E_{12}	-0.007±0.020	na	na	0.014±0.013
E_{23}	0.038±0.029	na	na	0.006±0.012
E_{13}	0.044±0.041	na	na	0.048±0.036

Table 5.6.7. Three dimensional end systolic strains for paced animals (n=6). Average three-dimensional end systolic strains for paced (mean ± sem). 25%= subepicardium; 50%= midwall; 75%= subendocardium. E_{11}= circumferential strain= E_{22}, longitudinal strain; E_{33}= radial strain; E_{12}=circumferential-longitudinal shear strain; E_{23}= longitudinal-radial shear strain; E_{13}=circumferential-radial shear strain. *$p<0.02$ vs. 1 min LV pace; **$p<0.01$ vs. Beginning Atrial.

Paced Group (n=6)				
25%	**Beginning Atrial**	**1 min LV Pace**	**4 h LV Pace**	**Late Atrial**
E_{11}	-0.038±0.022	0.020±0.0244	0.035±0.025*	0.012±0.023
E_{22}	-0.050±0.018	-0.019±0.020	-0.003±0.011	-0.022±0.012
E_{33}	0.091±0.024	0.020±0.024	-0.036±0.030*	0.016±0.020**
E_{12}	0.011±0.016	0.002±0.009	-0.017±0.014	0.002±0.009
E_{23}	0.012±0.019	-0.025±0.013	-0.032±0.016	-0.005±0.011
E_{13}	-0.002±0.008	-0.002±0.011	0.003±0.015	0.006±0.011
50%	**Beginning Atrial**	**1 min LV Pace**	**4 h LV Pace**	**Late Atrial**
E_{11}	-0.082±0.020	-0.011±0.029	0.029±0.032*	-0.016±0.026
E_{22}	-0.085±0.017	-0.037±0.024	-0.008±0.015	-0.034±0.010
E_{33}	0.179±0.025	0.075±0.044	-0.026±0.044*	0.060±0.027
E_{12}	0.009±0.015	0.005±0.008	-0.011±0.011	0.002±0.007**
E_{23}	0.033±0.018	-0.008±0.015	-0.033±0.016	0.010±0.013
E_{13}	0.008±0.020	0.003±0.009	0.009±0.020	0.020±0.018
75%	**Beginning Atrial**	**1 min LV Pace**	**4 h LV Pace**	**Late Atrial**
E_{11}	-0.142±0.011	-0.059±0.030	0.011±0.035*	-0.064±0.020
E_{22}	-0.097±0.010	-0.046±0.024	-0.005±0.014	-0.038±0.004
E_{33}	0.284±0.040	0.141±0.064	-0.013±0.058*	0.109±0.038**
E_{12}	0.002±0.013	0.008±0.008	0.003±0.006	0.001±0.011
E_{23}	0.054±0.028	0.003±0.023	-0.037±0.020	0.024±0.025
E_{13}	0.005±0.040	0.006±0.017	0.018±0.031	0.029±0.031

Figure 5.6.8 Acute myocardial inflammatory responses induced by ventricular dyssynchrony in control (n=7) and paced (n=8) hearts. *A*: Myeloperoxidase (MPO) activity; *B*: Oxidized stress (GSSG/GSH) levels; *C*: 92 kDa MMP-9 activity in areas around the beads set and posterior wall of control or LV paced animals. Values are means±sem.

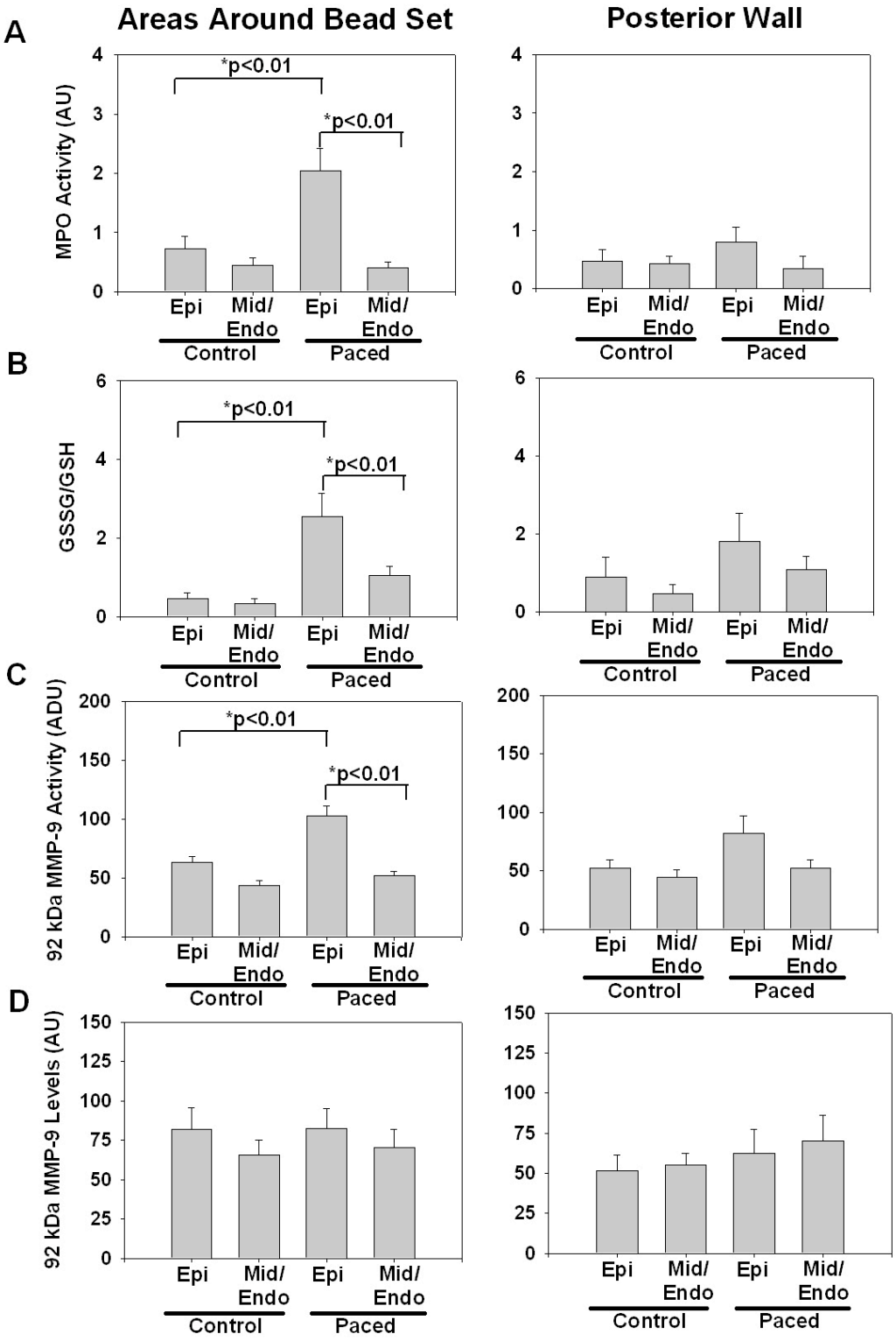
A
Areas Around Bead Set
Posterior Wall
MPO Activity (AU)
*p<0.01
*p<0.01
B
GSSG/GSH
*p<0.01
*p<0.01
C
92 kDa MMP-9 Activity (ADU)
*p<0.01
*p<0.01
D
92 kDa MMP-9 Levels (AU)
Epi
Mid/ Endo
Epi
Mid/ Endo
Control
Paced

Chapter 6. Mediation of myocardial dyskinesis induced inflammatory responses by cellular adhesion molecules

6.1 Introduction

Previous chapter 5 results from the canine model of dyskinesis demonstrated that 4 h of LV pacing led to an inflammatory response, characterized by increased neutrophil infiltration, ROS generation, and 92 kDa MMP-9 activity. We have also demonstrated that the use of propofol mitigates these responses, possibly due to a vascular event. However, propofol is known to exert its cardioprotective effects in a variety of ways, thus it is important to more clearly define the link between early shortening and associated inflammation. If an inflammatory response is to be secondary to a vascular dependent event, an upregulation of CAM in the involved region needs to occur. A mouse model of ventricular dyssynchrony can be a useful tool to better understand the role of CAM in the setting of dyskinesis due to the availability of mice deficient in CAM.

In the setting of acute inflammation, neutrophils are the first white blood cells to migrate across activated endothelium.[82] After an acute inflammatory stimulus, neutrophils roll along post-capillary venules at velocities distinctly below that of average blood flow. Extravasation of neutrophils into the extravascular milieu is a multistep process where each step requires the upregulation or activation of a distinct sets of CAM.[38] In addition, CAM expression is important because cross-linking of

some of the endothelial CAM stimulates signals that are consistent with a potential for increased endothelial cell basal surface attachment or induction of gene expression.

The selectin family of adhesion molecules mediates the initial trapping of neutrophils from the rapidly flowing bloodstream to the blood vessel endothelium, before their firm adhesion and diapedesis at sites of tissue injury and inflammation.[38] The selectin family consists of three closely related cell-surface molecules: L-selectin, E-selectin, and P-selectin. One important property of the selectins is that they promote leukocyte attachment and rolling at shear stresses characteristic of post-capillary venules.[39] P-selectin rapidly increases on endothelial cells after exposure to reactive oxygen, and appears to play a more important role that E-selectin in neutrophil extravasation with cardiac IR injury.[40]

Firm adhesion of neutrophils is dependent primarily on the leukocyte β_2 (CD11/CD18) integrins and endothelial ICAM-1.[40] ICAM-1 is constitutively expressed at low levels on the endothelial surface and is markedly upregulated by cytokine stimulation.[40] Recent studies have also shown cardiac myocyte ICAM-1 protein expression within 6 h of reperfusion.[40] The rapid induction of ICAM-1 occurs in viable myocytes immediately adjacent to nonviable myocardial cells, which coincides with the region of maximal neutrophil infiltration.[40]

Interestingly, no one has examined the dependence of ventricular dyssynchrony induced inflammatory responses on the upregulation of CAM. To gain further insight in the possible role that CAM may play in triggering LV pacing

induced inflammation, a transgenic mouse model was considered. CAM comprise a large family of important members. Published literature documented critical roles for ICAM-1 and p-selectin in the developmental role of myocardial inflammation following IR injury.[40] In a mouse model of IR injury, results demonstrated that the genetic deficiency of ICAM-1 significantly attenuated myocardial necrosis in mice in association with reductions in myocardial neutrophil infiltration, following either brief or extended periods of reperfusion.[40, 83, 84] In another study it was demonstrated that p-selectin expression was upregulated with IR in the coronary.[40, 83, 84] Conversely, neutrophil accumulation and myocardial injury were attenuated in p-selectin deficient mice following IR.[40, 83, 84] Thus, the major objectives of this study are to assess the role played by CAM (specifically, ICAM-1 and p-selectin) in the development of dyskinesis induced inflammation. For this purpose, we used a mouse model of ventricular dyssynchrony to determine if myocardial inflammatory responses are mitigated in ICAM-1 or p-selectin null mice.

6.2 Methods

6.2.1 Surgical Preparation

C57BL/6 male mice (22-26 g) were anesthetized with ketamine (100mg/kg) and xylazine (10mg/kg) IP, intubated, and mechanically ventilated with room air (Kent Scientific Respirator). The heart was exposed via a thoracotomy through the fifth intercostal space. After the pericardial dissection, a 36-gauge dual-insulated magnet wire (Belden CDT, Richmond, IN) with a hook on the end was inserted into the LV anterior wall via a 27-gauge needle to serve as a unipolar electrode. The chest was then closed with 6-0 silk prior to pacing. Another unipolar electrode was introduced into the abdominal muscles to serve as a ground. Surface electrocardiograms were recorded throughout the study. Wildtype mice served as controls in this study.

6.2.2 Study Groups and Study Design

To assess the effects of anesthesia and electrode insertion on myocardial inflammatory markers, a group of wildtype mice (n=18) were instrumented but not paced. A second group of wildtype mice (n= 24) underwent instrumentation and LV pacing to determine if dyssynchrony induces inflammatory responses as seen in the canine model of LV pacing. To examine the effect of dyssynchrony on CAM and inflammatory responses, mice deficient in specific cellular adhesion molecules (ICAM-1 $^{-/-}$ or p-selectin $^{-/-}$ mice) were used. For both null models, one group of animals served as controls in order to study the effects of

anesthesia and instrumentation on the inflammatory markers (n= 16). The second group (n=19) was instrumented and underwent LV pacing.

LV pacing was initiated by the use of a square-wave, constant-voltage electronic stimulator (Grass Instruments, Quincy, MA) at a frequency 10-20% above baseline heart rate to suppress native sinus rhythm. LV pacing induced electromechanical dyssynchrony was verified by the widening of the QRS complex on the ECG or by the analysis of echocardiography images. LV dyssynchrony was maintained for 40 min (this time point was calculated so that the number of beats of a murine heart is the same as the number of beats of a canine heart during 4 h).

In the control group, recordings took place immediately after instrumentation (beginning atrial), at 40 min, and immediately after (late atrial). In the paced group, recordings took place immediately after instrumentation (beginning atrial), 40 min under LV pacing, and then immediately after under normal sinus rhythm (late atrial). Additional recordings took place in all animals between the beginning atrial and 40 min timepoints. Data from selected timepoints are shown.

6.2.3 Sacrifice Protocol and tissue collection

After 40 min of ventricular dyssynchrony, the electrical stimulator was turned off. Animals were euthanized with pentobarbital sodium (200 mg/kg), and hearts excised. Tissue samples were taken from the early activated region

and late activated region, as indicated by 2D echo images (Figure 1) and stored at -80°C. In control animals, regions surrounding the pacing electrode were classified as early activated region and the opposite wall as the late activated region. Given the limited amount of tissue available for biochemical assays, a select group of tests were performed in animal subgroups.

6.2.4 Ventricular function

In a subgroup of animals, mechanical dyssynchrony was documented by echocardiography (Vevo 770, Visual Sonics, RMV 700-Series scanhead). A closed chest preparation was utilized to optimize echocardiography images. Animals were anesthetized with isoflurane at 5% and maintained at 1-1.5% throughout the study. The unipolar electrode was inserted through the chest wall at the fifth intercostal space. A grounding unipolar electrode was introduced into the abdominal muscles. Successful placement of the electrode was visualized using echo images (Figure 6.6.1). Ventricular dyssynchrony was documented by the visual inspection of dyssynchronous wall motion using the EKV mode.

Additional documentation of ventricular dyssynchrony was generated by analysis of M-mode echo recordings of LV anterior and posterior wall thickness in Image J. Briefly, the image pixels were calibrated with the scale within the echo image. Measurements (20-30) of the anterior wall thickness and posterior wall thickness were taken throughout one cardiac cycle (Figure 6.6.1).

6.2.5 Myeloperoxidase activity

Tissue samples were homogenized in ice-cold buffer (50mM KH_2PO_4 and 0.5% hexadecyltrimethylammonium bromide, pH 6.0). Homogenates were incubated on ice for 30 min and centrifuged at 4°C for 5 min. Following centrifugation, the supernatants were reacted with 0.8mM tetramethylbenzidine (Sigma; St. Louis, MO) and 0.006% H_2O_2 in 50mM KH_2PO_4.Kinetic absorbance measurements of MPO activity were immediately monitored at 655 nm (readings every 40s for ~20 min). Substrate cleavage rates were determined from the linear regions of the kinetic curve. Data were normalized to protein concentrations determined the BCA protein assay kit (Pierce, Rockford, IL).

6.2.6 Glutathione Assay

Reduced and oxidized glutathione, GSH and GSSG respectively, levels were determined as previously described.[78] Briefly, tissue samples were homogenized in ice cold homogenization buffer (154mM KCL, 5mM diethylenetriaminepentaacetic acid (DPTA), and 0.1M potassium phosphate, pH 6.8). After centrifugation, an aliquot was removed for protein determination using the BCA protein assay kit. Immediately after an aliquot was taken, one volume of cold acid buffer (40mM HCl, 10mM DPTA, 20mM ascorbic acid, and 10% trichloroacetic acid (TCA) was added to the homogenate. The suspension was centrifuged and the resulting supernatant solution was centrifuged through a 0.45m microcentrifuge filter (Millipore Corp., Bedford, MA). GSH and GSSG levels were determined using the fluorophore *o*-

phtaladehyde.

6.2.7 Gelatin Zymography

Samples were homogenized in 10mM HEPES, pH 7.5, 150mM NaCl, 0.2mM EDTA, 25% glycerol, with protease inhibitor cocktail (Sigma). Samples (10g of protein) was loaded onto a 10% SDS-PAGE gel substituted with 0.1% gelatin and then stained with 0.5% coomassie blue. Bands of MMP-2 and/or MMP-9 gelatinolytic activity were digitally quantified with Image J.

6.2.9 Data analyses and statistics

Results were expressed as mean ± SEM. Comparisons between means were analyzed, as appropriate, by student's *t*-test, one-way ANOVA, or two-way ANOVA followed by Bonferroni post-hoc analysis. A value of $p<0.05$ was considered statistically significant.

6.3 Results

6.3.1 Ventricular function

Figure 6.6.2 is a representative M-mode echocardiography image and a corresponding wall thickness analysis during the beginning atrial period and at the 40 min LV pace period. The analysis of LV wall thickness before and during LV pacing showed the anterior wall and posterior wall contracting simultaneously during normal sinus rhythm. In contrast, there is early thickening in the anterior wall and early thinning in the posterior wall (as indicated by the arrows) with LV pacing. Ventricular dyssynchrony was also documented in the LV using EKV mode.

In animals that did not undergo echocardiography, the effects of LV pacing were documented by the widening of the QRS on the ECG. QRS duration was significantly greater during LV pace compared to normal sinus rhythm (67±5 vs. 24±2; $p<0.001$; paired t-test).

6.3.2 Inflammatory responses

As seen in Figure 6.6.3.A, there was a significant three-fold increase in MPO activity in the early activated region of paced vs. control animals (0.45±0.06 vs. 0.17±0.03; $p<0.002$). This increase in MPO activity correlated with a significant two-fold increase in oxidative stress in the early activated regions of paced animals (2.9 ± 0.49 paced vs. 1.60±0.14 control; $p<0.05$;

Figure 6.6.3.B). Gelatin zymography (Figure 6.6.3.C) revealed a significant 3-fold increase in 92 kDa MMP-9 activity in the early activated regions of animals that underwent LV pacing (42.9±11.7 control vs. 150.2±34.3 paced; $p<0.02$; Figure 6.6.3.D).

As seen in Figure 6.6.4, LV pacing failed to significantly increase MPO activity in the early activated region in the paced vs. control group for both ICAM-1 null (0.045±0.02 AU control vs. 0.11±0.05 AU paced; p=NS; Figure 6.6.4.A) and p-selectin null animals (0.07±0.04 AU control vs. 0.08±0.04 paced; p=NS; Figure 6.6.4.B). No significant increases were observed in 92 kDa MMP-9 activity in the control vs. paced ICAM-1 null mice (64.5±29.3 vs. 96.6±29.9 ADU; p=NS; Figure 6.6.4.C).

6.4 Discussion

Results from this study demonstrate that a mouse model could be used to study the inflammatory responses associated with ventricular dyssynchrony. We were able to show significant increases in neutrophil infiltration, ROS generation, and MMP-9 activity in early activated regions of paced wildtype mice. These inflammatory responses were mitigated in ICAM-1 or p-selectin null mice.

To gain insight into the mechanism responsible for the inflammatory responses and the possible dependence on a vascular event, we implemented a mouse model of local dyskinesis using wildtype and CAM null animals. The upregulation of CAM allows for the physical interaction between inflammatory cells and the vascular endothelium needed for neutrophil transmigration to occur.[40] Given the development of the inflammatory process only in the canine epicardial layer of early activated myocardium, a local triggering event must occur. On the basis of the alterations noted with LV pacing in transmural strain patterns, there is a possibility that alterations in epicardial microvascular flow patterns induced epicardical LV pacing may trigger the expression of CAM, and lead to an acute inflammatory response.

The effects that mechanical forces exert on endothelial cell (EC) CAM gene expression and protein production have gained vast attention due to its relationship with atherogenesis [47-49, 51]. It has been shown that endothelial CAM expression can be modulated by mechanical stimuli, which is recognized through "stress-sensitive promoter elements".[85] Hemodynamic forces, such as fluid shear stress, are known to

regulate vascular wall structure/function including EC cell shape, nitric oxide and prostacycin production, EC proliferation, and CAM expression [47-49, 51]. Studies have demonstrated that exposure of EC to "normal" laminar flow patterns produce low levels of CAM and enhance the production of anti-adhesive factors [47-49, 51]. However, when EC are exposed to altered patterns of flow, CAM expression/production significantly increases [47-49, 51].This perturbed flow induced increase in CAM expression/production can then become the trigger for inflammation. Studies are warranted to examine the possibility that epicardial venular flow patterns may be perturbed in the setting of LV pacing, in a manner in which they trigger inflammation. The examination of vascular flow patterns has been performed in beating canine myocardium using intravital microscopy [36, 86]. These studies also allow the examination of neutrophil rolling and adhesion. However, studies are needed to examine epicardial venular flows in the setting of ventricular dyskinesis in early activated sites and neutrophil adhesion.

There is precedent for the use of mice to study ventricular dyssynchrony. A recent study evaluated the influence of non-failing ventricular dyssynchrony on regional cardiac gene expression in mice.[87] For this purpose, a custom miniature implantable mouse pacemaker capable of stimulating the murine heart at varying rates was used. In this study, they employed right ventricular free wall stimulation to generate ventricular dyssynchrony for a period of 1 week. Results demonstrated that LV pacing led to significant regional heterogeneity of gene expression involved in extracellular matrix remodeling, stem cell differentiation, myocardial stress responses,

and hypertrophy. This study proved that ventricular dyssynchrony generates a complexity of acute and chronic responses, which ultimately may be responsible for changes in cardiac structure/function.

We utilized a unipolar electrode implanted into the free wall to pace the LV. Using echocardiography, we were able to document the early activation of the LV free wall. Most importantly, in the mouse model, we managed to recapitulate the inflammatory response seen in dogs by subjecting wildtype mice to 40 min of LV pacing. In the mouse model, we documented significant upregulation of MPO, oxidative stress, and MMP-9 activity in presumably early activated regions. The use of ICAM-1 or p-selectin null mice blocked the development of inflammatory responses in early activated regions. The differences seen in neutrophil infiltration in these types of null mice compared to wildtype mice in our model of local dyskinesis is comparable to that of the IR model,[40, 83, 84] thus confirming the importance of ICAM-1 and p-selectin in the induction of the myocardial inflammatory responses associated with LV pacing.

In conclusion, results demonstrate that CAM expression plays a critical role in the triggering of the LV pacing induced inflammation, thus providing evidence of a vascular mechanism for inflammation associated with local dyskinesis. The mechanisms that trigger an upregulation of epicardial inflammation await further investigation as they suggest a specific involvement of vascular events solely in the outer layers of the myocardium.

6.5 Acknowledgements

Chapter 6, in part, has been submitted for publication as it may appears as Yamazaki KG, Covell JW, Ihm SH, Roth D, Villarreal FJ. *Circulation*. 2009. The dissertation author was the primary author on this manuscript.

Figure 6.6.1. Pacing preparation and experimental protocol. A: Experimental design for mouse model of ventricular dyssynchrony. Briefly, a unipolar pacing electrode was inserted into the LV of the mouse. Successful implantation of the electrode was visualized by the 2-D echo images (B) and ventricular dyssynchrony was determined by M-mode echocardiography wall thickness analysis of the anterior and posterior wall (C). Tissue samples were collected from the early activated region and late activated regions (B) from all hearts and used for biochemical analysis.

A


TIMELINE FOR MOUSE MODEL
Instrumentation
Beginning Atrial
40 min LV pacing
Late Atrial

B

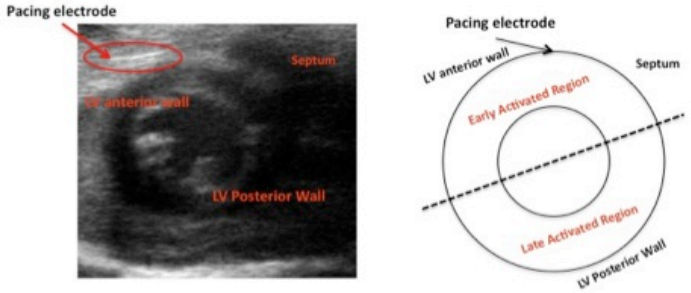
Pacing electrode
Septum
LV anterior wall
LV Posterior Wall
Pacing electrode
LV anterior wall
Septum
Early Activated Region
Late Activated Region
LV Posterior Wall

C

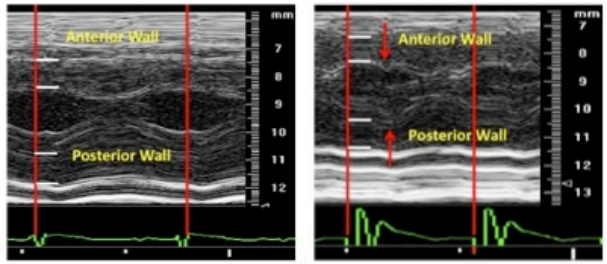
Anterior Wall
Posterior Wall
mm
7
8
9
10
11
12
Anterior Wall
Posterior Wall
mm
7
8
9
10
11
12
13

Figure 6.6.2. . Representative M-mode echocardiogram in a mouse during normal sinus rhythm (row A) and LV free wall pacing (row B). Dyssynchrony is demonstrated during LV free wall pacing by the presence of early anterior wall thickening and early posterior wall thinning (arrows). AWT=anterior wall thickness; PWT=posterior wall thickness; WT=wall thickness.

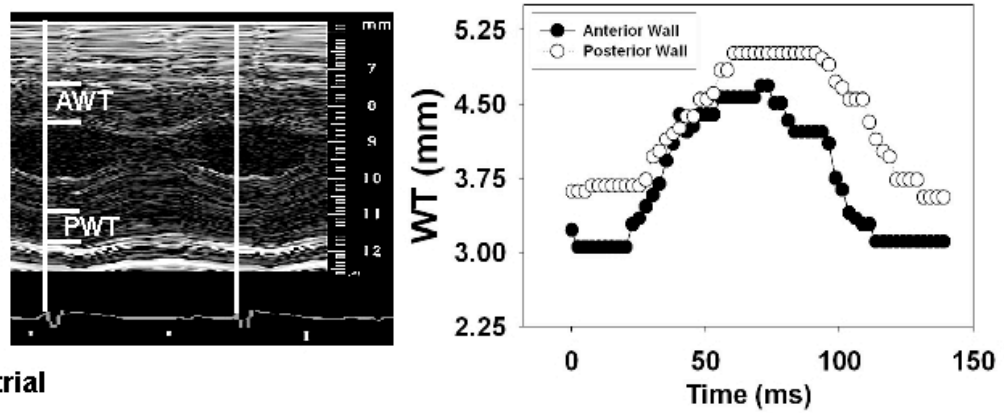

A: Beginning Atrial

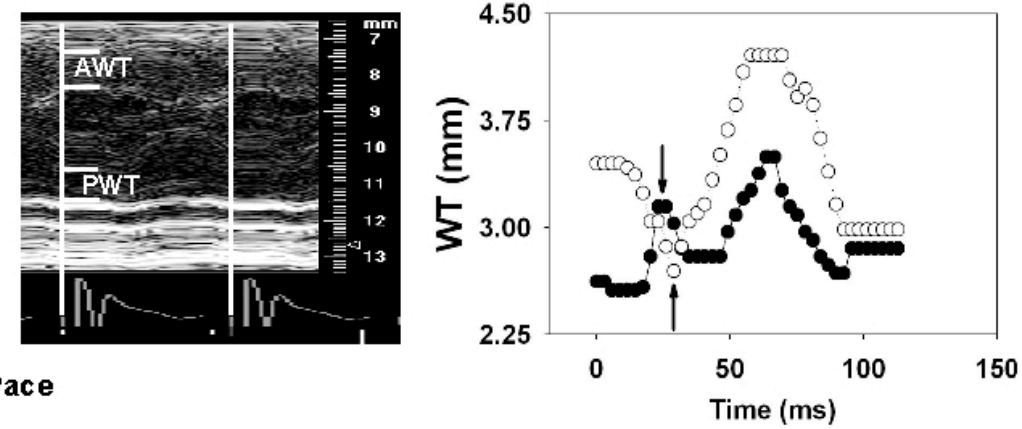

B: 40 min LV Pace

Figure 6.6.3. Myocardial inflammatory responses induced by ventricular dyssynchrony in early activated regions of wildtype C57BL/6 mice. *A*: myeloperoxidase (MPO) activity in control (n=8) and LV paced (n=12) hearts. *B*: Oxidative stress (GSSG/GSH) in control (n=5) and LV paced (n=6) hearts. *C*: Representative gelatin zymogram of myocardial MMP-2 and MMP-9 levels in a control and LV paced heart. 'Std'=human MMP-2/MMP-9 as standards. *D*: Densitometric analysis of 92 kDa MMP-9 zymographic activity in control hearts (n=5) and paced hearts (n=6). Values are mean ± sem.

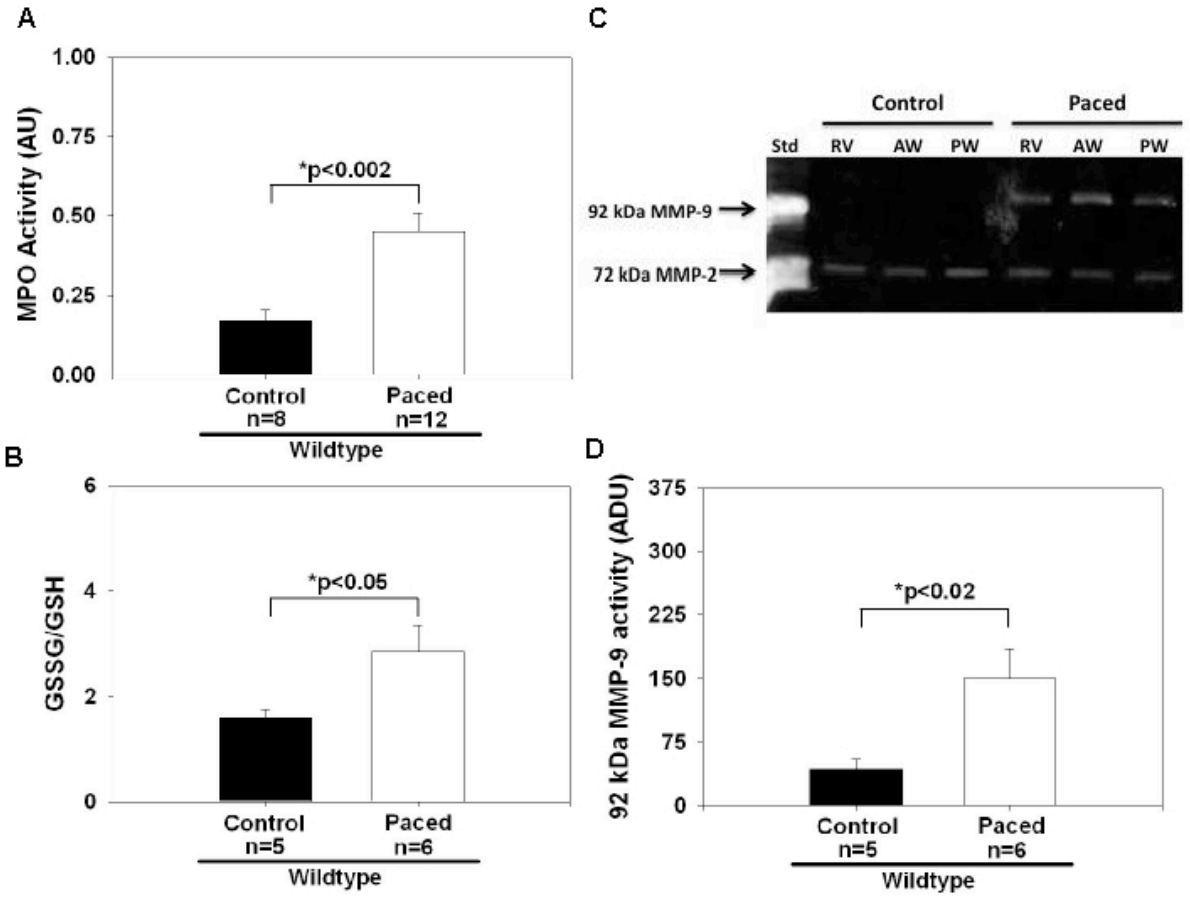
A
1.00
0.75
0.50
0.25
0.00
MPO Activity (AU)
*p<0.002
Control
n=8
Paced
n=12
Wildtype
C
Control
Paced
Std
RV
AW
PW
RV
AW
PW
92 kDa MMP-9
72 kDa MMP-2
B
6
4
2
0
GSSG/GSH
*p<0.05
Control
n=5
Paced
n=6
Wildtype
D
375
300
225
150
75
0
92 kDa MMP-9 activity (ADU)
*p<0.02
Control
n=5
Paced
n=6
Wildtype

Figure 6.6.4 Inflammatory responses induced by ventricular dyssynchrony in early activated regions of ICAM-1 or p-selectin null mice. *A*: myeloperoxidase (MPO) activity in control (n=5) and LV paced (n=7) ICAM-1 null hearts. *B*: myeloperoxidase (MPO) activity in control (n=5) and LV paced (n=6) p-selectin null hearts. *C*: Densitometric analysis of 92 kDa MMP-9 zymographic activity in control (n=5) and LV paced (n=6) ICAM-1 null hearts (n=6). Values are mean ± sem.

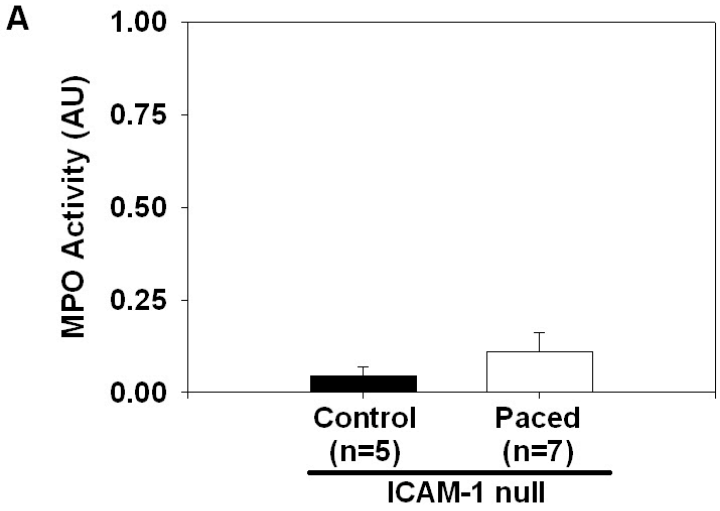
A
1.00
0.75
0.50
0.25
0.00
MPO Activity (AU)
Control
(n=5)
Paced
(n=7)
ICAM-1 null

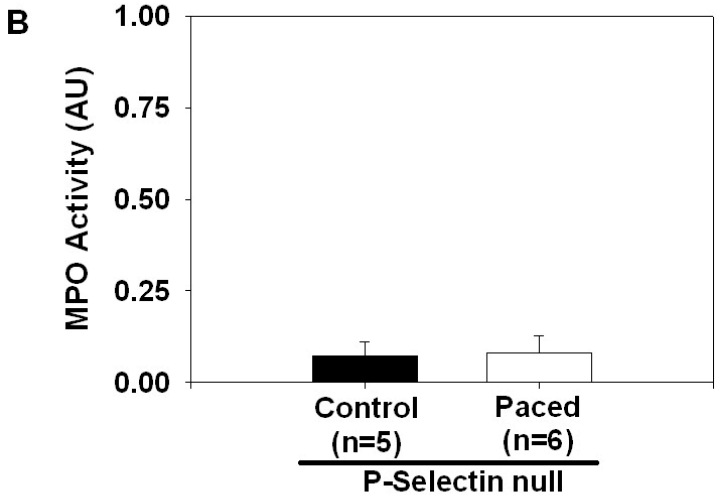
B
1.00
0.75
0.50
0.25
0.00
MPO Activity (AU)
Control
(n=5)
Paced
(n=6)
P-Selectin null

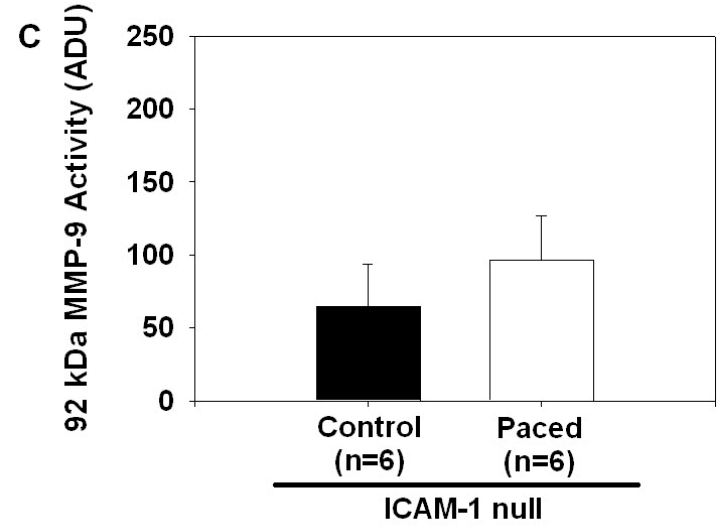
C
250
200
150
100
50
0
92 kDa MMP-9 Activity (ADU)
Control
(n=6)
Paced
(n=6)
ICAM-1 null

Chapter 7. Discussion

7.1 Main Findings of Dissertation

The goals of this dissertation were to investigate the effects of pacing on 2D and 3D myocardial deformation, as well as on regional and transmural myocardial inflammatory responses associated with ventricular dyskinesis. We also wanted to evaluate the involvement of vascular mediated events (via CAM) in the upregulation of dyskinesis induced inflammation.

Using epicardial bead arrays to map the spread of mechanical activation, i.e. 2D myocardial deformation, in animals undergoing 4 h of LV pacing demonstrated that the pace site and regions surrounding the pace site undergo early shortening. Results from these studies also demonstrate that all of the early shortening sites demonstrate significant increases in MPO, and 92 kDa MMP-9 activity, which, interestingly, are localized to the epicardial half of the LV. These regional and transmural differences in myocardial inflammatory responses were blunted in the studies were animals were anesthetized with the preconditioning agent propofol, even in the presence of early shortening.

In studies investigating the effects of bead implantation on LV function and myocardial inflammatory responses, results demonstrated that bead implantation on the day of the terminal study mitigated the inflammatory responses in the bead set site. Animals that underwent 4 h of LV pacing in the presence of a chronic bead set, or in the absence of beads demonstrated significant upregulation of inflammatory responses

at the bead set/pace site. Results also showed that there were significant increases in MPO activity, oxidative stress, and MMP-9 activity in regions around the bead set in both the acute and chronic/no bead groups. These regions are known to undergo early shortening as demonstrated in the first studies using epicardial bead arrays. These findings validated our decision to sample away from the bead set site in studies investigating 3D myocardial deformation and inflammation in the presence of dyskinesis.

Results from studies investigating the effects of pacing on 3D myocardial deformation and transmural myocardial inflammatory responses demonstrated that 4 h of local epicardial activation induced local dyskinesis at the site of early activation and progressively depressed endocardial wall thickening over time, which did not recover upon discontinuation of LV pacing. An inflammatory response was localized to the epicardium in all early shortening regions. Furthermore, results from these studies in animals subjected to LV anterior wall pacing indicated that the inflammatory response is likely a vascular (CAM) mediated event since inflammation was abrogated in animals anesthetized with propofol, as well as in ICAM-1 or p-selectin null animals.

7.2 Significance of Dissertation

Although it has been known for some time that dyssynchronous contraction reduces LV function and alters myocardial energetics, it has only been recently appreciated that long standing abnormal wall motion is associated with chamber remodeling in both non-failing and failing human hearts[21, 25]. Although the

mechanisms that trigger the development of chamber remodeling associated with dyssynchrony are unknown, our findings indicate that an inflammatory response induced at regions of early shortening may be a contributing cause. These findings are unique in that no previous work has linked the presence of abnormal LV wall motion with inflammation. Furthermore, as our data indicates the inflammatory response induced by epicardial LV pacing is localized to the outer layers of the LV and would predict that the long-term remodeling response will also be limited to this region. If substantiated, these findings may open new potential approaches to the therapy of dyssynchrony associated remodeling.

7.3 Discussion of Results

Our previously published study evidenced ventricular dyskinesis induced inflammation early after LV pacing.[32] To our knowledge, there have been no other studies investigating the mechanisms of inflammation involved in non heart failure ventricular dyssynchrony-induced LV remodeling. Results from this study demonstrated that short term dyskinesis induced by epicardial LV pacing is associated with increases in neutrophil infiltration as measured by MPO, which correlated with increases in nitrotyrosine levels (a marker for oxidative stress), and enhanced 92 kDa MMP-9 activity. Results also revealed increases in local collagen degradation. These results indicate that ventricular dyskinesis triggers an inflammatory response, which may ultimately induce LV remodeling. If acute inflammatory responses are associated

with long-term structural changes in the remodeled LV, it is reasonable to speculate that the remodeling of the ventricular wall is to differ transmurally.

Because in our initial study pairs of sonomicrometer crystals assessed ventricular function and inflammation was evaluated by utilizing transmural samples of myocardium, a detailed assessment of 3D LV function over time is required (short and long-term) to further understand the nature of ventricular dyssynchrony. Similarly, in order to identify the molecular mechanism possibly involved in the development of structural changes, a detailed transmural assessment of inflammatory responses is required. Although ventricular dyssynchrony is known to induce adverse changes in LV diastolic and systolic function, most of the published studies have focused on changes occurring over the long term. Thus in this study, we wish to focus on the acute changes induced by ventricular dyskinesis on 3D LV function and transmural distribution of inflammatory responses as a means to gain insight into their possible role in long term changes in structure/function.

Unique observations derived from the large animal study demonstrated that 4 h of dyskinesis significantly depressed endocardial wall thickening over time and induced an inflammatory response localized to the epicardial layers of the LV. The transmural differences in wall thickening and inflammatory responses seen in our study may be explained by different possible mechanisms relating to regional alterations in blood flow, shear stresses, and/or transient ischemia.

A study by Prinzen and Reneman indicated that timing of electrical activation is an important determinant for the distribution of fiber strain and blood flow in the left ventricular wall.[16] Previous investigations indicate that the direction of electromechanical activation matches and maintains a synchrony between the timing and direction of activation and blood flow.[23] At the tissue level, isovolumic intervals are associated with asynchronous movements of the subendocardial and subepicaridal regions. During LV isovolumic contraction, the subendocardial fibers that form a right-handed helix shorten, whereas the left-handed helically-oriented subepicardial fibers lengthen simultaneously. Conversely, during isovolumic relaxation, the subepicardial fibers that from the left-handed helix lengthen, and the right-handed helically-directed subendocardial fibers shorten briefly. This pattern of normal contraction likely defines the pattern of normal myocardial flow. Ventricular dyskinesis may thus yield a "flow-redirecting feature" that perturbs the normal patterns of flow. Indeed, Sengupta et al found that an altered sequence of electromechanical activation prolongs the pre-ejection period and disrupts the organized sequence of blood flow redirection.[23] Thus, the loss of endocardial function in our study may be secondary to perturbations in flow patterns, which translate into hypoperfusion of the subendocardium.

It is well known that the subendocardium is the most vulnerable area of the LV to the effects of hypoperfusion. However, the underlying mechanisms accounting for transmural differences of vulnerability and susceptibility to coronary hypoperfusion are still unresolved.[88] Many factors have been speculated as contributing to this

difference. Goto et al showed that cardiac compression predominantly affects subendocardial vessels and impedes subendocardial flow more than subepicardial flow regardless of LV pressure.[80] Data from other studies demonstrated regional differences in the distribution of capillaries in the subepicardial and subendocardial microcirculations[86, 89], which may also explain this transmural difference in blood flow. Bolli and Marbán reported that myocardial stunning leads to both systolic and diastolic dysfunction and that it is a nonuniform phenomenon that is most severe in the subendocardium.[90] It can be speculated that early contraction of the myocardium further exacerbates the time of endocardial hypoperfusion, subjecting the subendocardium to repetitive episodes of ischemic insult during early contraction followed by stunning that eventually create a sustained depression of contractile function.[81]

In a model of reversible ischemia, the investigators hypothesized that myocardial stunning triggers the coordinated expression of different sets of genes acting to protect the myocardium against irreversible damage. Results from this study demonstrated that 30% of the genes upregulated in stunned myocardium are involved in different mechanisms of cell survival, including anti-apoptosis, cytoprotection ("stress response") and cell growth. In particular, they found genes that participate in the development and growth of different forms of tumors are expressed in stunned, but not normal myocardium. Interestingly, they showed all the gene responses to be of higher amplitude in the subendocardium, where the flow reduction is the most important.[81] Therefore, there exists a gradient of gene response that matches the

gradient of flow reduction, which suggests that the nuclear response is proportional to the intensity of the initial stimulus. If, indeed, the loss of endocardial contractile function in the absence of an inflammatory response is due to endocardial stunning plus ischemic preconditioning, the mechanisms involved in the genesis of ischemic preconditioning with ventricular dyssynchrony need to be determined.

In this regard, a study has demonstrated that pacing-induced ventricular dyssynchrony preconditions that rabbit myocardium against ischemia/reperfusion injury.[91] Results from this study indicated that cardioprotection achieved by ventricular dyssynchrony is not due to myocardial ischemia since LV pacing coronary flow and lactate release did not change.[91] They suggested that stretch-mediated signaling resulting from the increased mechanical loading ("stretch") occurring in regions remote from the pacing site is a more likely trigger for ventricular dyssynchrony-induced preconditioning. Other studies have shown that stretch-activated channels might participate in the osmotic and volume regulation of cells.[92] Ovize et al proposed the idea that stretch induced by rapid volume overload could precondition the canine myocardium via stretch-activated ion channels.[92] A follow-up study by this group showed that cardioprotection through myocardial stretch is mediated by cardiac receptors sensitive to mechanical stress, which may interact with K^{+}_{ATP} channels and/or adenosine receptors via activation of PKC.[93] Because the rate of recovery from myocardial stunning is faster in the subepicardium than in the subendocardium[90], these observations may explain why a loss of function and no

inflammatory responses are seen in the endocardial layers of the myocardium in our study.

Another possible mechanism for the epicardial localization of inflammatory responses may be due to perturbations in blood flow in the epicardial microvasculature. It has been speculated that alterations in regional myocardial perfusion associated with ventricular pacing can be associated with abnormalities of microvascular flow.[42] Smith and Kassab demonstrated that as heart rate increases, small-vessel epicardial flow increases due to higher average arterial inflow pressure, whereas intramyocardial vessels show a decrease in flow particularly in the LV endocardium.[43] These hemodynamic changes may potentially decrease shear stress in the coronary microvasculature system and therefore lead to an inflammatory response.

It follows that for an inflammatory response to be triggered, it is essential for an upregulation of CAM to occur in the venular vascular compartment.[40] CAM allows for the physical interaction between inflammatory cells and the vascular endothelium. Given the development of the inflammatory process only in the epicardial layer of early activated myocardium, a local triggering event must occur. On the basis of the alterations noted with ventricular dyskinesis in transmural strain patterns, there is a possibility that alterations in epicardial microvascular flow patterns with ventricular dyskinesis may trigger the expression of CAM, and lead to inflammation. The effects that mechanical forces exert on EC gene expression and protein production have gained vast attention due to its relationship with atherogenesis. It has been shown that

endothelial CAM expression can be modulated by mechanical stimuli, which is recognized through "stress-sensitive promoter elements".[85] Hemodynamic forces, such as fluid shear stress, are known to regulate vascular wall structure/function including EC cell shape, NO and prostacycin production, EC proliferation, and CAM expression.[45, 47, 48, 51] Studies have demonstrated that exposure of EC to "normal" laminar flow patterns produce low levels of CAM and enhance the production of anti-adhesive factors.[45] However, when EC are exposed to altered patterns of flow, CAM expression/production significantly increases.[51] This increase in CAM expression/production can then lead to the triggering of an inflammatory response, Further studies are warranted to examine the possibility that epicardial venular flow patterns may be perturbed in the setting of ventricular dyssynchrony, such that they trigger an inflammatory response.

The other major finding of this study was that in mice subjected to ventricular dyssynchrony the inflammatory response is largely mediated by the expression of CAM, as inflammation was abrogated in ICAM-1 or p-selectin null animals. These results suggest that inflammatory response is likely a vascular mediated event. This hypothesis is further supported by the amelioration of the dyskinesis-induced inflammatory responses in propofol anesthetized dogs undergoing 4 h of LV pacing, where propofol is known to decrease CAM.

A prerequisite for rigorously testing the role of CAM in ventricular dyssynchrony required the implementation of an acute mouse model of ventricular

dyskinesis. A recent study evaluated the influence of chronic non-failing ventricular dyssynchrony on regional cardiac gene expression in mice.[87] For this purpose, a custom miniature implantable mouse pacemaker capable of stimulating the murine heart at varying rates was used. This study employed right ventricular free wall stimulation to generate ventricular dyssynchrony for a period of 1 week. Results demonstrated that ventricular dyssynchrony led to significant regional heterogeneity of gene expression involved in extracellular matrix remodeling, stem cell differentiation, myocardial stress responses, and hypertrophy. Thus, this study proved that ventricular dyssynchrony has a complexity of acute and chronic responses, which ultimately may be responsible for changes in cardiac structure/function.

In our acute model of ventricular dyssynchrony, we were able to properly document the early activation of the LV free wall using echocardiography. We documented a significant upregulation of MPO, oxidative stress, and 92 kDa MMP-9 activity in early activated regions, thus replicating the observations taken from the large animal study. The implementation of ventricular dyssynchrony in ICAM-1 or p-selectin null mice yielded a mitigation of the inflammatory responses in the early activated regions, thus confirming a critical role of CAM in triggering early ventricular dyssynchrony induced inflammatory responses. Possible mechanisms for the role of ICAM-1 or p-selectin in mediating ventricular dyssynchrony-induced inflammation need to be evaluated.

P-selectin and ICAM-1 are important mediators of leukocyte extravasation. The initial step is the transition from rapid flow of neutrophils to neutrophil rolling, which is mediated by members of the selectin family present on leukocytes (l-selectin) and endothelial cells (p-selectin and e-selectin).[40] P-selectin, the largest member of the selectin family, is translocated to the surface of the endothelium within minutes of stimulation.[94, 95] Studies have reported that p-selectin may play a more important role than e-selectin in neutrophil extravasation since it is expressed within minutes of stimulation compared to several hours as in the case with e-selectin.[40, 94] Binding of selectins on leukocytes stimulates "outside-in" signals in leukocytes, increasing the affinity of the integrin family of receptors, which then bind to immunoglobulin endothelial cell adhesion molecules such as ICAM-1 and VCAM-1.[82] ICAM-1 and VCAM-1 expression is thus needed to mediate the firm adhesion of leukocytes to the endothelium and transmigration of leukocytes out of blood vessels and into tissues.[40, 96]

Recent work in molecular and cellular biology has uncovered a set of complex interactions between the various components of the blood vessel including endothelium, smooth muscle, matrix and blood-borne elements such as platelets and leukocytes.[45] Recent work on the effects of fluid shear stress classified patterns of gene expression responses into three categories: a transient increase with return to baseline (type I), a sustained increase (type II), and a biphasic response consisting of an early transient increase of varying extent followed by a pronounced and sustained decrease (type III).[45] Malek et al reported that ICAM-1 surface expression is increased

with increases in fluid shear stress and that its mRNA levels remain elevated 2 and 8 h after stimulation.[45] They found that ICAM-1 falls within the type II category of sustained increase, whereas VCAM-1 is in the type III category, which is characterized by a transient early upregulation, subsiding back to basal levels, and is followed by a sustained decrease in gene expression at longer time points.[45]

The capability of ICAM-1 to transduce signals "outside-in" was identified several years ago and may also explain the importance of this particular molecule in mediating the inflammatory responses seen in our study. It has been reported that the cytoplasmic tail of ICAM-1 contains a tyrosine residue that can be phosphorylated and lead to a signaling cascade that upregulates proinflammatory cytokines, such as TNF-α, and NFκB, as well as lead to upregulation of VCAM-1 on the cell surface.[96] These findings further support the idea that ICAM-1 and p-selectin predominantly mediates the inflammatory responses seen in our model of ventricular dyssynchrony.

Indeed many studies have used p-selectin or ICAM-1 null mice in a setting of myocardial ischemia and reperfusion (IR) to determine the role of leukocyte-endothelial interaction in the development of myocardial injury.[40, 83, 84, 97] P-selectin and ICAM-1 mediate early interaction and adhesion of neutrophils to the coronary endothelial cells and cardiac myocytes after an injury to the myocardium. In a model of IR, results demonstrated that genetic deficiency of ICAM-1 significantly attenuated myocardial necrosis in mice in association with reductions in myocardial neutrophil infiltration, following both brief and extended periods of reperfusion.[83, 84, 97] Another

study showed that p-selectin expression was upregulated in the IR coronary circulation and that neutrophil infiltration was enhanced in wildtype mice.[83, 98] Conversely, neutrophil accumulation and myocardial injury were attenuated in p-selectin deficient mice following IR.[83, 98]

7.4 Conclusions

In conclusion, our results demonstrate that local dyskinesis causes an acute loss in endocardial function over time. More importantly, our results show an epicardial localization of inflammatory responses. Results also demonstrate that CAM expression plays a critical role in the triggering of the LV pacing induced inflammation, thus providing evidence of a vascular mechanism for inflammation associated with local dyskinesis. If the inflammatory events were responsible for localized remodeling, then long-term studies assessing the transmural distribution of LV remodeling would anticipate that the thinning of the LV wall would be mostly localized to the outer half of the chamber. This issue awaits further investigation. Further studies are also needed to examine the likely epicardial nature of perturbations in vascular flow patterns, which may trigger the upregulation of CAM and thus, induce inflammation.

References

1. Spragg DD, Kass DA. Pathobiology of left ventricular dyssynchrony and resynchronization. Prog Cardiovasc Dis. 2006;49(1):26-41.

2. Vernooy K, Verbeek XA, Peschar M, Prinzen FW. Relation between abnormal ventricular impulse conduction and heart failure. J Interv Cardiol. 2003;16(6):557-562.

3. Duzenli MA, Ozdemir K, Soylu A, Aygul N, Yazici M, Tokac M. The effect of isolated left bundle branch block on the myocardial velocities and myocardial performance index. Echocardiography. 2008;25(3):256-263.

4. Ozdemir K, Altunkeser BB, Danis G, Ozdemir A, Uluca Y, Tokac M, Telli HH, Gok H. Effect of the isolated left bundle branch block on systolic and diastolic functions of left ventricle. J Am Soc Echocardiogr. 2001;14(11):1075-1079.

5. Kass DA. Cardiac resynchronization therapy. J Cardiovasc Electrophysiol. 2005;16 Suppl 1:S35-41.

6. Cleland JG, Daubert JC, Erdmann E, Freemantle N, Gras D, Kappenberger L, Tavazzi L. The effect of cardiac resynchronization on morbidity and mortality in heart failure. N Engl J Med. 2005;352(15):1539-1549.

7. Prinzen FW, Peschar M. Relation between the pacing induced sequence of activation and left ventricular pump function in animals. Pacing Clin Electrophysiol. 2002;25(4 Pt 1):484-498.

8. Aaronson P, Ward J. The Cardiovascular system at a glance. Second ed. King's College, London: Blackwell Publishing; 1999.

9. Kyriakides ZS, Manolis AG, Kolettis TM. The effects of ventricular asynchrony on myocardial perfusion. Int J Cardiol. 2007;119(1):3-9.

10. Wetzel G, Knecht K. Bundle Branch Block, Right. emedicine. 2008.

11. van Hemel N. Left is worse than right: the outcome of bundle branch in middle-aged men. European Heart Journal. 2005;26:2222-2223.

12. Kakavand B. Bundle Branch Block, Left. emdicine. 2009.

13. Jain AC, Mehta MC. Etiologies of left bundle branch block and correlations with hemodynamic and angiographic findings. Am J Cardiol. 2003;91(11):1375-1378.

14. Waldman LK, Covell JW. Effects of ventricular pacing on finite deformation in canine left ventricles. Am J Physiol. 1987;252(5 Pt 2):H1023-1030.

15. van Oosterhout MF, Prinzen FW, Arts T, Schreuder JJ, Vanagt WY, Cleutjens JP, Reneman RS. Asynchronous electrical activation induces asymmetrical hypertrophy of the left ventricular wall. Circulation. 1998;98(6):588-595.

16. Prinzen FW, Augustijn CH, Arts T, Allessie MA, Reneman RS. Redistribution of myocardial fiber strain and blood flow by asynchronous activation. Am J Physiol. 1990;259(2 Pt 2):H300-308.

17. Coppola BA, Covell JW, McCulloch AD, Omens JH. Asynchrony of ventricular activation affects magnitude and timing of fiber stretch in late-activated regions of the canine heart. Am J Physiol Heart Circ Physiol. 2007;293(1):H754-761.

18. Badke FR, Boinay P, Covell JW. Effects of ventricular pacing on regional left ventricular performance in the dog. Am J Physiol. 1980;238(6):H858-867.

19. Hotta S. The sequence of mechanical activation of the ventricle. Jpn Circ J. 1967;31(11):1568-1572.

20. Prinzen FW, Hunter WC, Wyman BT, McVeigh ER. Mapping of regional myocardial strain and work during ventricular pacing: experimental study using magnetic resonance imaging tagging. J Am Coll Cardiol. 1999;33(6):1735-1742.

21. Kerwin WF, Paz O. Cardiac resynchronization therapy: overcoming ventricular dyssynchrony in dilated heart failure. Cardiol Rev. 2003;11(4):221-239.

22. Fuster V, RW A, RA OR. Hurst's The Heart. Tenth Edition ed: McGraw-Hill; 2001.

23. Sengupta PP, Khandheria BK, Korinek J, Jahangir A, Yoshifuku S, Milosevic I, Belohlavek M. Left ventricular isovolumic flow sequence during sinus and paced rhythms: new insights from use of high-resolution Doppler and ultrasonic digital particle imaging velocimetry. J Am Coll Cardiol. 2007;49(8):899-908.

24. Prinzen F, Arts T, McVeigh E, Hunter W, Reneman R. Contraction and blood flow patterns in the left ventricle during abnormal electrical activation. 1996.

25. Spragg DD, Leclercq C, Loghmani M, Faris OP, Tunin RS, DiSilvestre D, McVeigh ER, Tomaselli GF, Kass DA. Regional alterations in protein expression in the dyssynchronous failing heart. Circulation. 2003;108(8):929-932.

26. Prinzen FW, Cheriex EC, Delhaas T, van Oosterhout MF, Arts T, Wellens HJ, Reneman RS. Asymmetric thickness of the left ventricular wall resulting from asynchronous electric activation: a study in dogs with ventricular pacing and in patients with left bundle branch block. Am Heart J. 1995;130(5):1045-1053.

27. Adomian GE, Beazell J. Myofibrillar disarray produced in normal hearts by chronic electrical pacing. Am Heart J. 1986;112(1):79-83.

28. van Oosterhout MF, Arts T, Bassingthwaighte JB, Reneman RS, Prinzen FW. Relation between local myocardial growth and blood flow during chronic ventricular pacing. Cardiovasc Res. 2002;53(4):831-840.

29. Spragg DD, Akar FG, Helm RH, Tunin RS, Tomaselli GF, Kass DA. Abnormal conduction and repolarization in late-activated myocardium of dyssynchronously contracting hearts. Cardiovasc Res. 2005;67(1):77-86.

30. Chakir K, Daya SK, Tunin RS, Helm RH, Byrne MJ, Dimaano VL, Lardo AC, Abraham TP, Tomaselli GF, Kass DA. Reversal of global apoptosis and regional stress kinase activation by cardiac resynchronization. Circulation. 2008;117(11):1369-1377.

31. Yu CM, Gorcsan J, 3rd, Bleeker GB, Zhang Q, Schalij MJ, Suffoletto MS, Fung JW, Schwartzman D, Chan YS, Tanabe M, Bax JJ. Usefulness of tissue Doppler velocity and strain dyssynchrony for predicting left ventricular reverse remodeling response after cardiac resynchronization therapy. Am J Cardiol. 2007;100(8):1263-1270.

32. Garcia RA, Brown KL, Pavelec RS, Go KV, Covell JW, Villarreal FJ. Abnormal cardiac wall motion and early matrix metalloproteinase activity. Am J Physiol Heart Circ Physiol. 2005;288(3):H1080-1087.

33. Brown L. Cardiac extracellular matrix: a dynamic entity. Am J Physiol Heart Circ Physiol. 2005;289(3):H973-974.

34. Pope AJ, Sands GB, Smaill BH, LeGrice IJ. Three-dimensional transmural organization of perimysial collagen in the heart. Am J Physiol Heart Circ Physiol. 2008;295(3):H1243-H1252.

35. May-Newman K, Mathieu-Costello O, Omens JH, Klumb K, McCulloch AD. Transmural distribution of capillary morphology as a function of coronary perfusion pressure in the resting canine heart. Microvasc Res. 1995;50(3):381-396.

36. Kajiya F, Yada T, Matsumoto T, Goto M, Ogasawara Y. Intramyocardial influences on blood flow distributions in the myocardial wall. Ann Biomed Eng. 2000;28(8):897-902.

37. Edwards S. Biochemistry and physiology of the neutrophil. Vol 1: New York: Press syndicate of the University of Cambridge; 1994.

38. Frangogiannis NG. Chemokines in the ischemic myocardium: from inflammation to fibrosis. Inflamm Res. 2004;53(11):585-595.

39. Frangogiannis NG, Smith CW, Entman ML. The inflammatory response in myocardial infarction. Cardiovasc Res. 2002;53(1):31-47.

40. Briaud SA, Ding ZM, Michael LH, Entman ML, Daniel S, Ballantyne CM. Leukocyte trafficking and myocardial reperfusion injury in ICAM-1/P-selectin-knockout mice. Am J Physiol Heart Circ Physiol. 2001;280(1):H60-67.

41. Bloch EH. Principles of the microvascular system. Invest Ophthalmol. 1966;5(3):250-255.

42. Skalidis EI, Kochiadakis GE, Koukouraki SI, Chrysostomakis SI, Igoumenidis NE, Karkavitsas NS, Vardas PE. Myocardial perfusion in patients with permanent ventricular pacing and normal coronary arteries. J Am Coll Cardiol. 2001;37(1):124-129.

43. Mittal N, Zhou Y, Linares C, Ung S, Kaimovitz B, Molloi S, Kassab GS. Analysis of blood flow in the entire coronary arterial tree. Am J Physiol Heart Circ Physiol. 2005;289(1):H439-446.

44. Brooks AR, Lelkes PI, Rubanyi GM. Gene expression profiling of vascular endothelial cells exposed to fluid mechanical forces: relevance for focal susceptibility to atherosclerosis. Endothelium. 2004;11(1):45-57.

45. Malek AM, Izumo S. Control of endothelial cell gene expression by flow. J Biomech. 1995;28(12):1515-1528.

46. Levesque MJ, Nerem RM. The elongation and orientation of cultured endothelial cells in response to shear stress. J Biomech Eng. 1985;107(4):341-347.

47. Bongrazio M, Baumann C, Zakrzewicz A, Pries AR, Gaehtgens P. Evidence for modulation of genes involved in vascular adaptation by prolonged exposure of endothelial cells to shear stress. Cardiovasc Res. 2000;47(2):384-393.

48. Braddock M, Schwachtgen JL, Houston P, Dickson MC, Lee MJ, Campbell CJ. Fluid Shear Stress Modulation of Gene Expression in Endothelial Cells. News Physiol Sci. 1998;13:241-246.

49. Shyy JY, Chien S. Role of integrins in endothelial mechanosensing of shear stress. Circ Res. 2002;91(9):769-775.

50. Papadaki M, Eskin SG. Effects of fluid shear stress on gene regulation of vascular cells. Biotechnol Prog. 1997;13(3):209-221.

51. Dancu MB, Berardi DE, Vanden Heuvel JP, Tarbell JM. Asynchronous shear stress and circumferential strain reduces endothelial NO synthase and cyclooxygenase-2 but induces endothelin-1 gene expression in endothelial cells. Arterioscler Thromb Vasc Biol. 2004;24(11):2088-2094.

52. Borregaard N, Cowland JB. Granules of the human neutrophilic polymorphonuclear leukocyte. Blood. 1997;89(10):3503-3521.

53. Faurschou M, Borregaard N. Neutrophil granules and secretory vesicles in inflammation. Microbes Infect. 2003;5(14):1317-1327.

54. Badwey JA, Curnutte JT, Robinson JM, Lazdins JK, Briggs RT, Karnovsky MJ, Karnovsky ML. Comparative aspects of oxidative metabolism of neutrophils from human blood and guinea pig peritonea: magnitude of the respiratory burst, dependence upon stimulating agents, and localization of the oxidases. J Cell Physiol. 1980;105(3):541-545.

55. Feuerstein G. Inflammation and Cardiac Diseases. West Point, PA: Bertelsmann Springer Publishing Group.

56. Spinale FG, Coker ML, Bond BR, Zellner JL. Myocardial matrix degradation and metalloproteinase activation in the failing heart: a potential therapeutic target. Cardiovasc Res. 2000;46(2):225-238.

57. Edwards DR, Murphy G. Cancer. Proteases--invasion and more. Nature. 1998;394(6693):527-528.

58. Shapiro SD. Matrix metalloproteinase degradation of extracellular matrix: biological consequences. Curr Opin Cell Biol. 1998;10(5):602-608.

59. Benbow U, Schoenermark MP, Mitchell TI, Rutter JL, Shimokawa K, Nagase H, Brinckerhoff CE. A novel host/tumor cell interaction activates matrix metalloproteinase 1 and mediates invasion through type I collagen. J Biol Chem. 1999;274(36):25371-25378.

60. Creemers EE, Cleutjens JP, Smits JF, Daemen MJ. Matrix metalloproteinase inhibition after myocardial infarction: a new approach to prevent heart failure? Circ Res. 2001;89(3):201-210.

61. Ramos-DeSimone N, Hahn-Dantona E, Sipley J, Nagase H, French DL, Quigley JP. Activation of matrix metalloproteinase-9 (MMP-9) via a converging plasmin/stromelysin-1 cascade enhances tumor cell invasion. J Biol Chem. 1999;274(19):13066-13076.

62. Opdenakker G, Van den Steen PE, Dubois B, Nelissen I, Van Coillie E, Masure S, Proost P, Van Damme J. Gelatinase B functions as regulator and effector in leukocyte biology. J Leukoc Biol. 2001;69(6):851-859.

63. Delhaas T, Arts T, Prinzen FW, Reneman RS. Relation between regional electrical activation time and subepicardial fiber strain in the canine left ventricle. Pflugers Arch. 1993;423(1-2):78-87.

64. Wyman BT, Hunter WC, Prinzen FW, McVeigh ER. Mapping propagation of mechanical activation in the paced heart with MRI tagging. Am J Physiol. 1999;276(3 Pt 2):H881-891.

65. Tapuria N, Kumar Y, Habib MM, Abu Amara M, Seifalian AM, Davidson BR. Remote ischemic preconditioning: a novel protective method from ischemia reperfusion injury--a review. J Surg Res. 2008;150(2):304-330.

66. Kato R, Foex P. Myocardial protection by anesthetic agents against ischemia-reperfusion injury: an update for anesthesiologists. Can J Anaesth. 2002;49(8):777-791.

67. Balakumar P, Rohilla A, Singh M. Pre-conditioning and postconditioning to limit ischemia-reperfusion-induced myocardial injury: what could be the next footstep? Pharmacol Res. 2008;57(6):403-412.

68. Schultz JE, Rose E, Yao Z, Gross GJ. Evidence for involvement of opioid receptors in ischemic preconditioning in rat hearts. Am J Physiol. 1995;268(5 Pt 2):H2157-2161.

69. Kahraman S, Demiryurek AT. Propofol is a peroxynitrite scavenger. Anesth Analg. 1997;84(5):1127-1129.

70. Murphy PG, Myers DS, Davies MJ, Webster NR, Jones JG. The antioxidant potential of propofol (2,6-diisopropylphenol). Br J Anaesth. 1992;68(6):613-618.

71. Lim KH, Halestrap AP, Angelini GD, Suleiman MS. Propofol is cardioprotective in a clinically relevant model of normothermic blood cardioplegic arrest and cardiopulmonary bypass. Exp Biol Med (Maywood). 2005;230(6):413-420.

72. Corcoran TB, Engel A, Shorten GD. The influence of propofol on the expression of intercellular adhesion molecule 1 (ICAM-1) and vascular cell adhesion molecule 1 (VCAM-1) in reoxygenated human umbilical vein endothelial cells. Eur J Anaesthesiol. 2006;23(11):942-947.

73. Feng CS, Ma HC, Yue Y, Zhang YQ, Qu XD. [Effect of propofol on the activation of nuclear factor-kappa B and expression of inflammatory cytokines in cerebral cortex during transient focal cerebral ischemia-reperfusion: experiment with rats]. Zhonghua Yi Xue Za Zhi. 2004;84(24):2110-2114.

74. Hu XM, Lu Y, Yao SL. [Propofol reduces intercellular adhesion molecular-1 expression in lung injury following intestinal ischemia/reperfusion in rats.]. Zhongguo Wei Zhong Bing Ji Jiu Yi Xue. 2005;17(1):53-56.

75. Ashikaga H, Omens JH, Ingels NB, Jr., Covell JW. Transmural mechanics at left ventricular epicardial pacing site. Am J Physiol Heart Circ Physiol. 2004;286(6):H2401-2407.

76. Costa KD, Takayama Y, McCulloch AD, Covell JW. Laminar fiber architecture and three-dimensional systolic mechanics in canine ventricular myocardium. Am J Physiol. 1999;276(2 Pt 2):H595-607.

77. Ashikaga H, Criscione JC, Omens JH, Covell JW, Ingels NB, Jr. Transmural left ventricular mechanics underlying torsional recoil during relaxation. Am J Physiol Heart Circ Physiol. 2004;286(2):H640-647.

78. Senft AP, Dalton TP, Shertzer HG. Determining glutathione and glutathione disulfide using the fluorescence probe o-phthalaldehyde. Anal Biochem. 2000;280(1):80-86.

79. Kerckhoffs RC, McCulloch AD, Omens JH, Mulligan LJ. Effects of biventricular pacing and scar size in a computational model of the failing heart with left bundle branch block. Med Image Anal. 2009;13(2):362-369.

80. Goto M, Flynn AE, Doucette JW, Jansen CM, Stork MM, Coggins DL, Muehrcke DD, Husseini WK, Hoffman JI. Cardiac contraction affects deep myocardial vessels predominantly. Am J Physiol. 1991;261(5 Pt 2):H1417-1429.

81. Depre C, Vatner SF. Cardioprotection in stunned and hibernating myocardium. Heart Fail Rev. 2007;12(3-4):307-317.

82. Cook-Mills JM, Deem TL. Active participation of endothelial cells in inflammation. J Leukoc Biol. 2005;77(4):487-495.

83. Jones SP, Trocha SD, Strange MB, Granger DN, Kevil CG, Bullard DC, Lefer DJ. Leukocyte and endothelial cell adhesion molecules in a chronic murine model of myocardial reperfusion injury. Am J Physiol Heart Circ Physiol. 2000;279(5):H2196-2201.

84. Entman ML, Michael L, Rossen RD, Dreyer WJ, Anderson DC, Taylor AA, Smith CW. Inflammation in the course of early myocardial ischemia. FASEB J. 1991;5(11):2529-2537.

85. Methe H, Balcells M, Alegret Mdel C, Santacana M, Molins B, Hamik A, Jain MK, Edelman ER. Vascular bed origin dictates flow pattern regulation of endothelial adhesion molecule expression. Am J Physiol Heart Circ Physiol. 2007;292(5):H2167-2175.

86. Chilian WM. Microvascular pressures and resistances in the left ventricular subepicardium and subendocardium. Circ Res. 1991;69(3):561-570.

87. Bilchick KC, Saha SK, Mikolajczyk E, Cope L, Ferguson WJ, Yu W, Girouard S, Kass DA. Differential regional gene expression from cardiac dyssynchrony induced by chronic right ventricular free wall pacing in the mouse. Physiol Genomics. 2006;26(2):109-115.

88. Toyota E, Ogasawara Y, Hiramatsu O, Tachibana H, Kajiya F, Yamamori S, Chilian WM. Dynamics of flow velocities in endocardial and epicardial coronary arterioles. Am J Physiol Heart Circ Physiol. 2005;288(4):H1598-1603.

89. Gerdes AM, Callas G, Kasten FH. Differences in regional capillary distribution and myocyte sizes in normal and hypertrophic rat hearts. Am J Anat. 1979;156(4):523-531.

90. Bolli R, Marban E. Molecular and cellular mechanisms of myocardial stunning. Physiol Rev. 1999;79(2):609-634.

91. Vanagt WY, Cornelussen RN, Poulina QP, Blaauw E, Vernooy K, Cleutjens JP, van Bilsen M, Delhaas T, Prinzen FW. Pacing-induced dys-synchrony preconditions rabbit myocardium against ischemia/reperfusion injury. Circulation. 2006;114(1 Suppl):I264-269.

92. Ovize M, Kloner RA, Przyklenk K. Stretch preconditions canine myocardium. Am J Physiol. 1994;266(1 Pt 2):H137-146.

93. Gysembergh A, Margonari H, Loufoua J, Ovize A, Andre-Fouet X, Minaire Y, Ovize M. Stretch-induced protection shares a common mechanism with ischemic preconditioning in rabbit heart. Am J Physiol. 1998;274(3 Pt 2):H955-964.

94. Kakkar AK, Lefer DJ. Leukocyte and endothelial adhesion molecule studies in knockout mice. Curr Opin Pharmacol. 2004;4(2):154-158.

95. Polgar J, Matuskova J, Wagner DD. The P-selectin, tissue factor, coagulation triad. J Thromb Haemost. 2005;3(8):1590-1596.

96. Lawson C, Wolf S. ICAM-1 signaling in endothelial cells. Pharmacol Rep. 2009;61(1):22-32.

97. Sligh JE, Jr., Ballantyne CM, Rich SS, Hawkins HK, Smith CW, Bradley A, Beaudet AL. Inflammatory and immune responses are impaired in mice deficient in intercellular adhesion molecule 1. Proc Natl Acad Sci U S A. 1993;90(18):8529-8533.

98. Palazzo AJ, Jones SP, Anderson DC, Granger DN, Lefer DJ. Coronary endothelial P-selectin in pathogenesis of myocardial ischemia-reperfusion injury. Am J Physiol. 1998;275(5 Pt 2):H1865-1872.